



HAL
open science

Influence of stress and structural parameters on the hydrothermal ageing of zirconia-based ceramics

Chong Wei

► **To cite this version:**

Chong Wei. Influence of stress and structural parameters on the hydrothermal ageing of zirconia-based ceramics. Materials. Université de Lyon, 2017. English. NNT : 2017LYSEI091 . tel-01973959

HAL Id: tel-01973959

<https://theses.hal.science/tel-01973959>

Submitted on 8 Jan 2019

HAL is a multi-disciplinary open access archive for the deposit and dissemination of scientific research documents, whether they are published or not. The documents may come from teaching and research institutions in France or abroad, or from public or private research centers.

L'archive ouverte pluridisciplinaire **HAL**, est destinée au dépôt et à la diffusion de documents scientifiques de niveau recherche, publiés ou non, émanant des établissements d'enseignement et de recherche français ou étrangers, des laboratoires publics ou privés.



N°d'ordreNNT : 2017LYSEI091

THESE de DOCTORAT DE L'UNIVERSITE DE LYON
opérée au sein de
INSA Lyon

Ecole Doctorale N° 34
Matériaux de Lyon

Spécialité/ discipline de doctorat : Matériaux

Soutenue publiquement le 20/10/2017, par :

Chong WEI

***Influence of stress and structural
parameters on the hydrothermal ageing
of zirconia-based ceramics***

Devant le jury composé de :

ANGLADA, Marc	Professeur	UPC Barcelone	Rapporteur
DJURADO, Elisabeth	Professeur	Université Grenoble-Alpes	Rapporteuse
CHEVALIER, Jérôme	Professeur	INSA-LYON	Examineur
VLEUGELS, Jozef	Professeur	Université Catholique de Leuven	Examineur
LIAO, Hanlin	Professeur	UTBM	Examineur
GREMILLARD, Laurent	Directeur de recherches	INSA-Lyon	Directeur de thèse

Département FEDORA – INSA Lyon - Ecoles Doctorales – Quinquennal 2016-2020

SIGLE	ECOLE DOCTORALE	NOM ET COORDONNEES DU RESPONSABLE
CHIMIE	<p>CHIMIE DE LYON http://www.edchimie-lyon.fr</p> <p>Sec : Renée EL MELHEM Bat Blaise Pascal 3^e étage secretariat@edchimie-lyon.fr Insa : R. GOURDON</p>	<p>M. Stéphane DANIELE Institut de Recherches sur la Catalyse et l'Environnement de Lyon IRCELYON-UMR 5256 Equipe CDFA 2 avenue Albert Einstein 69626 Villeurbanne cedex directeur@edchimie-lyon.fr</p>
E.E.A.	<p>ELECTRONIQUE, ELECTROTECHNIQUE, AUTOMATIQUE http://edeea.ec-lyon.fr</p> <p>Sec : M.C. HAVGOUDOUKIAN Ecole-Doctorale.eea@ec-lyon.fr</p>	<p>M. Gérard SCORLETTI Ecole Centrale de Lyon 36 avenue Guy de Collongue 69134 ECULLY Tél : 04.72.18 60.97 Fax : 04 78 43 37 17 Gerard.scorletti@ec-lyon.fr</p>
E2M2	<p>EVOLUTION, ECOSYSTEME, MICROBIOLOGIE, MODELISATION http://e2m2.universite-lyon.fr</p> <p>Sec : Sylvie ROBERJOT Bât Atrium - UCB Lyon 1 04.72.44.83.62 Insa : H. CHARLES secretariat.e2m2@univ-lyon1.fr</p>	<p>M. Fabrice CORDEY CNRS UMR 5276 Lab. de géologie de Lyon Université Claude Bernard Lyon 1 Bât Géode 2 rue Raphaël Dubois 69622 VILLEURBANNE Cédex Tél : 06.07.53.89.13 cordev@univ-lyon1.fr</p>
EDISS	<p>INTERDISCIPLINAIRE SCIENCES-SANTE http://www.ediss-lyon.fr</p> <p>Sec : Sylvie ROBERJOT Bât Atrium - UCB Lyon 1 04.72.44.83.62 Insa : M. LAGARDE secretariat.ediss@univ-lyon1.fr</p>	<p>Mme Emmanuelle CANET-SOULAS INSERM U1060, CarMeN lab, Univ. Lyon 1 Bâtiment IMBL 11 avenue Jean Capelle INSA de Lyon 696621 Villeurbanne Tél : 04.72.68.49.09 Fax : 04 72 68 49 16 Emmanuelle.canet@univ-lyon1.fr</p>
INFOMATHS	<p>INFORMATIQUE ET MATHÉMATIQUES http://infomaths.univ-lyon1.fr</p> <p>Sec : Renée EL MELHEM Bat Blaise Pascal, 3^e étage Tél : 04.72. 43. 80. 46 Fax : 04.72.43.16.87 infomaths@univ-lyon1.fr</p>	<p>M. Luca ZAMBONI Bâtiment Braconnier 43 Boulevard du 11 novembre 1918 69622 VILLEURBANNE Cedex Tél : 04 26 23 45 52 zamboni@maths.univ-lyon1.fr</p>
Matériaux	<p>MATERIAUX DE LYON http://ed34.universite-lyon.fr</p> <p>Sec : Marion COMBE Tél: 04-72-43-71-70 -Fax : 87.12 Bat. Direction ed.materiaux@insa-lyon.fr</p>	<p>M. Jean-Yves BUFFIERE INSA de Lyon MATEIS Bâtiment Saint Exupéry 7 avenue Jean Capelle 69621 VILLEURBANNE Cedex Tél : 04.72.43 71.70 Fax 04 72 43 85 28 Ed.materiaux@insa-lyon.fr</p>
MEGA	<p>MECANIQUE, ENERGETIQUE, GENIE CIVIL, ACOUSTIQUE http://mega.universite-lyon.fr</p> <p>Sec : Marion COMBE Tél: 04-72-43-71-70 -Fax : 87.12 Bat. Direction mega@insa-lyon.fr</p>	<p>M. Philippe BOISSE INSA de Lyon Laboratoire LAMCOS Bâtiment Jacquard 25 bis avenue Jean Capelle 69621 VILLEURBANNE Cedex Tél : 04.72 .43.71.70 Fax : 04 72 43 72 37 Philippe.boisse@insa-lyon.fr</p>
ScSo	<p>ScSo* http://recherche.univ-lyon2.fr/scso/ Sec : Viviane POLSINELLI Brigitte DUBOIS Insa : J.Y. TOUSSAINT Tél : 04 78 69 72 76 viviane.polsinelli@univ-lyon2.fr</p>	<p>M. Christian MONTES Université Lyon 2 86 rue Pasteur 69365 LYON Cedex 07 Christian.montes@univ-lyon2.fr</p>

*ScSo : Histoire, Géographie, Aménagement, Urbanisme, Archéologie, Science politique, Sociologie, Anthropologie

Acknowledgments

For thanks, here there are many words to say to my supervisor Laurent Gremillard, because he helped me open the door to scientific research. He is one of the most patient of my encounter with me. I am very grateful to his patience to let me see the hope of my research work. In the past few years, his teachings, his dedication, his rigor, his seriousness always inspired me. Now I want to tell him that I grew up, maybe not very mature, but I will be brave to create my own future. In the future, I will try my best to explore the material world, to discover the law of the world, to prove it, and to apply it.

I would like to thank everyone in the ceramic team.

In addition, I would like to thank the each member of jury. Their presence is my pleasure.

Finally, I would like to thank my family, for their understanding and support.

Résumé

Cette thèse explore l'influence des contraintes et des paramètres structuraux sur la sensibilité au vieillissement de la céramique à base de zircon. Elle traite d'abord de l'influence des contraintes externes (appliquées) et des contraintes internes (résiduelles). Des contraintes extérieures sont appliquées par des tests de flexion in situ, tandis que des contraintes internes sont obtenues en contrôlant la microstructure des composites d'alumine renforcés à la zircon. Le comportement au vieillissement de différents matériaux (3Y-TZP, 4Y-TZP et ZTA) est étudié par diffraction des rayons X (XRD) et spectroscopie Micro-Raman. Le résultat principal est l'influence principale des contraintes résiduelles sur les contraintes appliquées, principalement dans les matériaux de zircon.

Elle discrimine ensuite l'effet de différents paramètres microstructuraux sur la cinétique du vieillissement. Des échantillons de 3Y-TZP de même composition nominale mais de microstructures différentes (caractérisées par leur taille de grain, la teneur en Y_2O_3 de la phase quadratique et la proportion de phase cubique) sont obtenues en utilisant différents procédés de frittage (frittage en deux étapes ou frittage normal pour différents temps et à différentes températures). En utilisant deux modèles semi-empiriques, on peut d'abord quantifier la relation entre la microstructure et les paramètres de traitement, puis la relation entre la cinétique du vieillissement et la microstructure.

Enfin, elle qualifie différents traitements de surface pour améliorer la résistance au vieillissement de la 3Y-TZP. Les échantillons 3Y-TZP sont recuits sur des poudres de différentes compositions (TZ3YE, TZ4YS, 12CeTZP) et leur comportement au vieillissement est comparé. Les résultats montrent qu'une amélioration significative de la résistance au vieillissement peut être atteinte à 134 °C, sans compromettre la ténacité, mais ce gain n'est pas toujours valable à température ambiante ou corporelle.

Étant donné que cette thèse traite de nombreux matériaux et des temps de vieillissement très long (jusqu'à plusieurs milliers d'heures), il était essentiel d'accélérer les tests de vieillissement et de réduire le nombre d'échantillons. Ainsi, nous avons mis en place une méthode rapide permettant d'accéder à l'énergie d'activation du vieillissement, avec une réduction de dix fois de la durée des études vieillissantes (présenté en annexe).

Abstract

This thesis explores the influence of stresses and structural parameters on the sensitivity to ageing of zirconia-based ceramics. It first addresses the influence of both external (applied) stresses and internal (residual) stresses. External stresses are applied by in-situ bending tests, while internal stresses are obtained by controlling the microstructure of zirconia-toughened alumina composites. The ageing behavior of different materials (3Y-TZP, 4Y-TZP and ZTA) is investigated by X-ray diffraction (XRD) and Micro-Raman spectroscopy. The main result is the primary influence of residual stresses over applied stresses, mainly in zirconia materials.

It then discriminates the effect of different microstructural parameters on the ageing kinetics. 3Y-TZP samples of identical nominal composition but different microstructures (characterized by their grain sizes, content of Y_2O_3 in tetragonal phase and proportion of cubic phase) are obtained by using different sintering processes (two step sintering or normal sintering for different times and at different temperatures). Using two semi-empirical models, we are first able to quantify the relation between microstructure and processing parameters, and then the relation between ageing kinetics and microstructure.

Finally it qualifies different surface treatments to improve the ageing resistance of 3Y-TZP. 3Y-TZP samples are annealed by placing on powders of different compositions (TZ3YE, TZ4YS, 12CeTZP) and their ageing behavior are compared. The results show that a significant improvement of the ageing resistance can be reached at 134°C, without compromising the toughness, however this gain is not always valid at room or body temperature.

Since this thesis deals with many materials and very long ageing times (up to several thousand hours), it was crucial to accelerate ageing tests and reduce the number of samples. Thus we set up a fast method enabling access to the activation energy of ageing, with a tenfold reduction in the duration of the ageing studies (presented in the appendix).

Contents

Acknowledgments.....	4
Résumé.....	5
Abstract.....	6
Contents.....	7
General Introduction.....	10
Chapter 1:.....	13
Background.....	13
Chapter 1. Background.....	14
Introduction.....	14
Introduction.....	14
1.1 A short history of bio-ceramics.....	14
1.2 Problems and future of zirconia-based bioceramics.....	15
1.3 Scientific aspects of zirconia ceramics:.....	16
1.3.1 Crystal structures of zirconia.....	16
1.3.2 Martensitic Transformation (T→M) of tetragonal zirconia.....	17
References.....	32
Chapter 2:.....	37
Influence of applied and internal stresses on zirconia hydrothermal ageing.....	37
Chapter 2. Influence of applied and internal stresses on zirconia hydrothermal ageing.....	38
2.1 Common Introduction.....	38
2.2 The influence of applied and residual stresses on hydrothermal ageing of 3Y- and 4Y- stabilized zirconia.....	39
Abstract.....	39
Résumé.....	39
2.2.1 Introduction.....	40
2.2.2 Materials and methods.....	40
2.2.3. Results.....	43
2.2.4 Discussions.....	50
2.2.5 Conclusion.....	53
2.3 The influence of internal stresses on ZTA hydrothermal ageing.....	54
Abstract.....	54
Résumé.....	54

2.3.1 Introduction	54
2.3.2. Materials and methods	55
2.3.3 Results and discussions	58
2.3.4. Conclusion	69
2.4 Common conclusion.....	70
References	71
Chapter 3:.....	73
Influence of structural parameters on zirconia hydrothermal ageing	73
Chapter 3. Influence of structural parameters on zirconia hydrothermal ageing.....	74
Abstract	74
3.1 Introduction.....	75
3.2 Materials and methods	75
3.2.1. Material preparation	75
3.2.2 Microstructural analyses: grain size, proportion of cubic phase, yttria content	77
3.2.3 Assessment of ageing kinetics parameters.	78
3.3 Results	79
3.3.1 Microstructural analyses	79
3.3.2 Ageing kinetics.....	81
3.4 Discussion	84
3.4.1 Correlation analysis of structural parameters and sintering cycle	84
3.4.2 Prediction of ageing kinetics parameters from micro structural parameters	86
3.4.3 Predictive ability of the phenomenological models	88
3.4.4 Influence of the microstructure on ageing kinetics of zirconia	90
3.5 Conclusions	90
References	92
Chapter 4:.....	94
Surface treatment methods for hydrothermal ageing mitigation	94
Chapter 4. Surface treatment methods for hydrothermal ageing mitigation	95
Abstract	95
Résumé.....	95
4.1 Introduction.....	95
4.2 Experimental materials and methods	96
4.2.1 Experimental samples	96
4.2.2 Microstructural analyses: proportion of cubic phase, yttria content.....	96
4.2.3 Hardness analysis and crack propagation threshold	97
4.2.4 Assessment of ageing kinetics.....	97
4.3 Results of preliminary experiments.....	98
4.3.1 Surface topography	98

4.3.2 Ageing kinetic	98
4.4 Results on commercial samples	99
4.4.1 Microstructural analyses	99
4.4.2 Mechanical properties	100
4.4.3 Analysis of ageing kinetics	100
4.5 Discussions.....	102
4.5.1 The relationship between microstructure and doping with ceria and yttria.....	102
4.5.2 Influence on ageing kinetic	103
4.5.3 The ageing resistance feasibility of this post-sintering treatment (the surface treatment method of the formation of zirconia containing cerium on the surface of Y-TZP).....	103
4.6 Conclusions and future work.....	104
References	105
General Conclusions	107
Appendix:.....	108
A fast, stepwise procedure to extrapolate hydrothermal ageing of zirconia-based materials to low temperatures	108
Appendix A fast, stepwise procedure to extrapolate hydrothermal ageing of zirconia-based materials to low temperatures.....	109
Abstract	109
Résumé.....	109
Introduction.....	109
Materials and methods	111
Results.....	115
Conclusion	120
References.....	121

General Introduction

Zirconia-based Ceramics are generally produced by sintering. They are used in several fields (aeronautics, nuclear, microelectronics, fuel cells or even biomedical) thanks to their varied properties (high toughness and strength, ionic conductivity, color, low thermal conductivity...). This work focuses on the biomaterials application of zirconia-based ceramics. In the 1970s, Garvie and Nicholson discovered that alloying zirconia with oxides such as yttria, calcia, magnesia and others made it possible to stabilize its tetragonal modification thus halting the structurally and mechanically deleterious uncontrolled phase transition from the tetragonal to the monoclinic phase. This discovery allowed using the so-called transformation toughening of zirconia to produce ceramics with unsurpassed crack resistance ('ceramic steel') [1-3]. In the 1980s, besides structural and mechanical investigations of zirconia, studies on its biocompatibility moved into the limelight as evidenced [4-6]. Subsequently, these works have attracted a large number of researchers. Therefore zirconia ceramics has been increasingly extensively used as biomaterials, in particular stabilized in their tetragonal phase, for example as heads for total hip replacement or as dental implants. In the orthopedic field, one of the most important and common surgical procedure is the total hip arthroplasty, in fact the number of implanted hip prostheses has constantly increased and the demand will be driven by growing geriatric population across the world. In France, more than 120,000 prostheses are implanted per year; In Europe, approximately 1,300,000 patients are affected annually. In the United States, 325,000 people had total hip replacement surgery in 2015. In China, the official report points out that Chinese orthopedic implant market size reached 16.6 billion yuan (2.3 billion euro) in 2015, is expected to grow to 21.8 billion yuan (3 billion euro) by 2021. Global market for hip and knee orthopedic surgical implants was valued at USD 17 billion in 2015. It is projected to grow to USD 33 billion by 2022[7, 8]. Meanwhile in dentistry the importance of dental implants is growing. In response to an increasingly demanding aesthetic demand, 3Y-TZP zirconia appears to be an extremely promising material: it combines biocompatibility with a satisfactory aesthetic appearance and has mechanical properties far superior to other ceramics.

Zirconia ceramics exhibit the best mechanical properties of oxide ceramics: this is the consequence of phase transformation toughening, which increases its crack propagation resistance. Their high mechanical properties as compared to other monolithic oxide ceramics, and their good optical properties are their main advantages. On the other hand, they may suffer from an ageing phenomenon known as "hydrothermal ageing" or "Low Temperature Degradation" (LTD). This phenomenon is a phase transformation on the surface of the devices, triggered by the presence of water, and accelerated by temperature. It results in micro-cracking and roughening of the surface, both potentially decreasing the lifetime of implants. LTD came suddenly under the spotlights when hundreds of Y-TZP femoral heads failed in a very short time after surgery in the year 2001. The failure origin is now associated to an accelerated ageing in two particular batches of the leader Prozyr® product in which a defect in the manufacturing process dramatically increased the consequences of ageing. Since the premature failure of zirconia hip implants, the ageing phenomenon of zirconia has been considered by many researchers and has become a hot topic. The ageing phenomenon has been shown to be modulated by grain size, yttria content, grain orientation to the surface, residual surface stresses, and the content of cubic phase [9]. Although the T-M transformation is martensitic, the ageing progresses by a nucleation and growth process, well described by Mehl-Avrami-Johnson laws[10].

Although LTD becomes well known and extensively studied now, it is far from being fully characterized. My PhD study is to explore the influence of stresses and structural parameters on the sensitivity to ageing of zirconia-based bio-ceramics. This manuscript is divided into four main parts. The work about the influence of stresses on the ageing kinetics of zirconia-based ceramics is present in chapter 2. The stress effects are studied by considering both external, applied stresses and internal, residual stresses. External stresses are applied by *in-situ* bending tests, and the ageing behavior of different types of stresses surfaces of different samples (3Y-TZP, 4Y-TZP) was investigated by X-ray diffraction (XRD). The internal stresses are obtained by making a composite of alumina and zirconia, and the ageing kinetics behavior of zirconia aggregates of different sizes was investigated by XRD and Micro-Raman spectroscopy. The main goal is to explain the influence of stresses on the ageing kinetics behavior, in order to predict the ageing kinetics of zirconia ceramics under different stresses. In the chapter 3, it is to explore the effect of different microstructures on the ageing kinetics of zirconia ceramics,

including grain sizes, the content of Y_2O_3 in tetragonal phase and the content of cubic phase. Here 3Y-TZP samples of the same nominal composition but different microstructures are obtained by using different sintering processes (two step sintering and normal sintering), and their ageing behavior is characterized, quantified and related to the microstructures. In the chapter 4, it is to study how to obtain a better ageing resistant surface of 3Y-TZP. The zirconia 3Y-TZP samples were placed in different powders (TZ3YE, TZ4YS, 12CeTZP) for annealing. Then, we compare the ageing behavior of the annealed samples to expect to find a way which prevent the ageing of zirconia ceramics in the human body. A preliminary study was performed in order to accelerate the determination of the ageing parameters. Indeed, since this thesis deals with many materials, it was crucial to have access to a fast method. The one we set up, that can allow an up to tenfold reduction in the duration of the ageing studies, is presented in the appendix.

- [1] R.C. Garvie, P.S. Nicholson, Structure and Thermomechanical Properties of Partially Stabilized Zirconia in the CaO-ZrO₂ System, *Journal of the American Ceramic Society* 55(3) (1972) 152-157.
- [2] R.C. Garvie, Stabilization of the tetragonal structure in zirconia microcrystals, *The Journal of Physical Chemistry* 82(2) (1978) 218-224.
- [3] R.C. Garvie, R.H. Hannink, R.T. Pascoe, Ceramic steel?, *Nature* 258(5537) (1975) 703-704.
- [4] R.C. Garvie, C. Urbani, D.R. Kennedy, J.C. McNeuer, Biocompatibility of magnesia-partially stabilized zirconia (Mg-PSZ) ceramics, *Journal of Materials Science* 19(10) (1984) 3224-3228.
- [5] P. Christel, A. Meunier, M. Heller, J.P. Torre, C.N. Peille, Mechanical properties and short-term in vivo evaluation of yttrium-oxide-partially-stabilized zirconia, *Journal of Biomedical Materials Research* 23(1) (1989) 45-61.
- [6] K. Hayashi, N. Matsuguchi, K. Uenoyama, Y. Sugioka, Re-evaluation of the biocompatibility of bioinert ceramics in vivo, *Biomaterials* 13(4) (1992) 195-200.
- [7] Hip and Knee Orthopedic Surgical Implants Market Shares, Strategies, and Forecasts, Worldwide, 2016 to 2022, *Pharmaceuticals & Healthcare*, Jan 21, 2016
- [8] <http://www.morningpost.com.cn/2016/1118/1560279.shtml>.
- [9] J. Chevalier, What future for zirconia as a biomaterial?, *Biomaterials* 27(4) (2006) 535-543.
- [10] J. Chevalier, B. Cales, J.M. Drouin, Low-Temperature Ageing of Y-TZP Ceramics, *Journal of the American Ceramic Society* 82(8) (1999) 2150-2154.

Chapter 1:

Background

Chapter 1. Background

Introduction

Since this paper mainly focuses on the biomaterials application of zirconia-based ceramics, we firstly made a simple playback of the history of bioceramic materials. Secondly, a summary description of the problems and future of zirconia-based ceramics as bioceramics is made. Finally, the scientific aspects of zirconia-based ceramics were reviewed in detail by summing up previous studies, including the crystal structure of zirconia, and the two ways of martensitic transformation (transformation toughening and low temperature degradation). Here the process, mechanisms studies and influence parameters of low temperature degradation are highlighted. Low temperature degradation, also called hydrothermal ageing phenomenon, is a very slow transformation at the surface of zirconia ceramics in the presence of water or water vapour at low temperatures (from room temperature up to about 400 °C). This transformation process which is very sensitive to the parameters (stabilizer type, stabilizer content, porosity, surface finish and stresses, grain size, grain boundaries, cubic phase content, etc.), leads to the emergence of macro-cracks, which in turn leads to brittle fracture of zirconia ceramics. And it is also the root cause of the lifetime reduction of zirconia bioceramic devices.

Introduction

Étant donné que cet article se concentre principalement sur l'application des biomatériaux céramique à base de zircon, nous avons d'abord fait une lecture simple de l'histoire des matériaux biocéramiques. Deuxièmement, une description sommaire des problèmes et de l'avenir des biocéramique à base de zircon est réalisée. Enfin, les aspects scientifiques des céramiques à base de zircon ont été revus en détail en résumant des études antérieures, y compris la structure cristalline de la zircon, et les deux aspects de la transformation martensitique (renforcement par transformation de phase et dégradation à basse température). Ici, le processus, les études de mécanismes et les paramètres influençant la dégradation à basse température sont mis en évidence. La dégradation à basse température, également appelée phénomène de vieillissement hydrothermal, est une transformation très lente à la surface de la zircon en présence d'eau ou de vapeur d'eau à basse température (de la température ambiante jusqu'à environ 400 °C). Ce processus de transformation, très sensible aux paramètres microstructuraux (type de stabilisant et teneur, porosité, finition de surface et contraintes, taille des grains, nature des joints de grains, proportion de phase cubique, etc.) conduit à l'émergence de micro-fissures qui, à leur tour, conduisent à une rupture fragile. Et c'est aussi une cause majeure limitant la durée de vie des dispositifs en zircon.

1.1 A short history of bio-ceramics

Ceramics are generally defined as “inorganic, non-metallic materials”. Biomaterials are defined as “natural or synthetic materials suitable for introduction into living tissue especially as part of a medical device”. In clinical practice, the controlled implantation of bio-ceramics started late 18th century in dentals with the use of porcelain for crowns and late 19th in orthopedics with the use of Plaster of Paris, or gypsum (calcium sulfate dihydrate) for bone filling. With the rapid development of ceramic technology, more and more ‘high-tech’ceramics are available for medical purpose from the 20th century[1]. Tricalcium phosphate was first proposed in 1920 as a bioresorbable substance to fill bone gaps. However, tricalcium phosphate (TCP) and plaster are weak ceramics, unable to sustain significant loading. The need for tough and strong ceramics was not met before 1965, when the first alumina (Al_2O_3) material dedicated to hip joints was patented. Synthetic calcium phosphate ceramics (together with calcium and/or phosphorus containing ceramics and glasses) and zirconia were then proposed as alternatives to TCP and alumina, respectively. Fig 1.1 summarizes these 100 years of history of modern bio-ceramics.

Zirconia was identified as such in 1789 by the German chemist Martin Heinrich Klaproth in the reaction product obtained after heating some gems, and was used for a long time blended with rare-earth oxides as pigment for ceramics[2].The first paper[3] concerned the use of zirconia to manufacture ball heads for Total Hip

Replacements (THR), which is the current main application of this ceramic biomaterial. Biomedical grade zirconia was introduced to solve the problem of alumina brittleness and the consequent potential failure of implants. In the early stages of the development, several solid solutions (ZrO_2 -MgO, ZrO_2 -CaO, ZrO_2 - Y_2O_3) were tested for biomedical applications. But in the subsequent years the research efforts appeared to be more focused on yttria zirconia ceramics, characterized by fine-grained microstructures known as tetragonal zirconia polycrystals (TZP). Yttria-stabilized zirconia has excellent mechanical properties (high toughness and strength), but its lack of long-term stability is a major issue for medical use. Current research aims at developing zirconia based ceramics and composites that should benefit from phase transformation toughening without suffering surface degradation in the presence of water or body fluid.

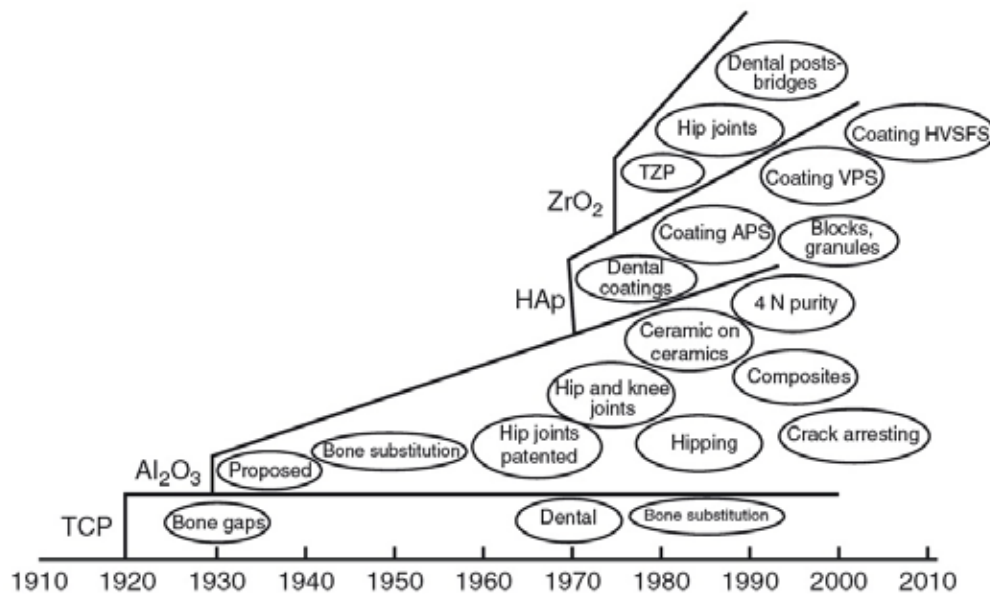


Fig 1.1 Application of bioceramics in medical devices: 100 years of history.[4]

1.2 Problems and future of zirconia-based bioceramics

The failure events of Prozyr® femoral heads in 2001–2002 magnify the biggest problem of zirconia ceramics in biomaterial applications: its sensitivity to a surface degradation in the presence of water, called hydrothermal ageing or Low Temperature Degradation (LTD). Since then, the use of monolithic zirconia for orthopaedic implants has ceased in Europe and in the US, although it does continue in China and Japan. These events triggered a lot of scientific studies to understand the ageing behaviour of zirconia. Current studies clearly indicate that the strong variability of zirconia to *in vivo* degradation is a consequence of the strong influence of processing conditions on ageing process. Therefore, in order to ensure a more accurate assessment and prediction of the lifetime of the zirconia implants, the role of each factor of zirconia ceramics processing on the ageing kinetics has to be studied in depth.

The main problem with zirconia-based bioceramic materials is how to prevent or delay the hydrothermal ageing process, while maintaining their superior mechanical properties.

- 1) Zirconia-based composites[1]. For example some ZTA materials (zirconia toughened alumina) may not be sensitive to ageing. Indeed, the stabilization of zirconia grains in such composites can be achieved thanks to the presence of a stiff alumina matrix. Moreover, for sufficiently low zirconia content (below the percolation threshold) and sufficiently good dispersion, zirconia grains are isolated and propagation of the transformation from one grain to another is avoided. Some alumina-zirconia composites are already implanted or developed by companies (Biolog delta® by Ceramtec being an improved version of these composites, with Cr_2O_3 additions and strontium aluminate grains with platelet-like morphology). They show significant improvement in ageing resistance as compared to Y-TZP, and excellent crack resistance. Furthermore, Micro-nano-alumina-zirconia composites and nano-nano-ceria

doped zirconia–alumina composites will also be more and more applied to bioceramics. However, these composites are often used for Total Hip Replacements and not preferred for dental restorations from the aesthetic point of view, because they are opaque. So zirconia doping with a small amount of other oxides are also being studied for trying to find better dental restoration materials.

- 2) Zirconia doping with a small amount of other oxides. For example most commercially available biomedical grade Y-TZP powders (i.e. TZ3Y-E, with a very small – less than 0.5 wt.% – alumina content, which exhibits improved ageing resistance), more efficient answers to the ageing issue lie in stabilization mechanisms minimizing the quantity of oxygen vacancies and/or minimizing nucleation and growth kinetics by avoiding contact between zirconia grains. Meanwhile other oxides have been studied, such as SiO₂[5], La₂O₃[6, 7], Sc₂O₃, Nd₂O₃[7].

The fear of the failure event of Prozyr® femoral heads has disappeared; the use of zirconia for dental applications is booming. However it is still necessary to fully understand its shortcomings, in order to further improve it, rather than abandon it. This dissertation also contributes to this goal.

1.3 Scientific aspects of zirconia ceramics:

1.3.1 Crystal structures of zirconia

From low temperature to high temperature, pure zirconia has three stable phases: monoclinic zirconia phase (the room temperature stable phase), tetragonal phase (transforms at 1170 °C), and cubic phase (between 2370 °C and the melting point, 2680°C). The monoclinic phase can be described in the P21/c space group, with the Zr atoms in sevenfold coordination with the O-sublattice. The tetragonal phase presents a distorted calcium fluorite structure (P42/nmc). The cubic phase is a calcium fluorite type structure (face centered cubic, Fm3m), with the O atoms displaced from the (1/4, 1/4, 1/4) position toward a higher z (around 0.28), which may be due to the tendency of the Zr atoms to form a sevenfold coordination [8-12].

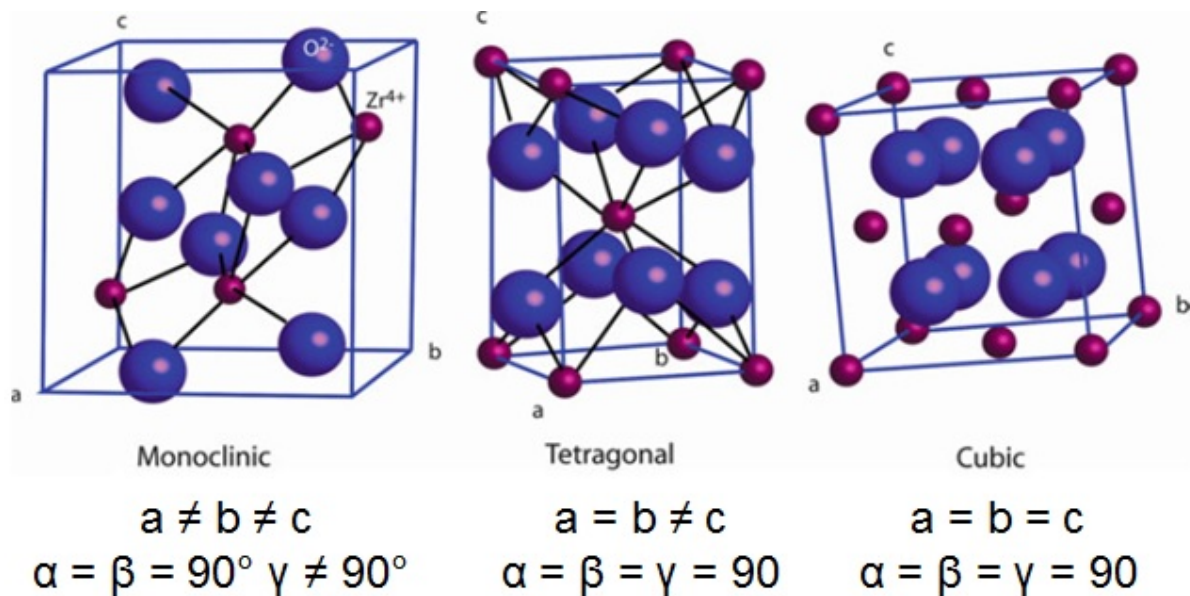


Fig 1.2 Crystallographic structures of zirconia. From left to right: monoclinic (*m*-ZrO₂, tetragonal (*t*-ZrO₂) and cubic (*c*-ZrO₂) [12]

Pure zirconia has a monoclinic crystal structure at room temperature. But its structure can be modified by doping with a few percent of other oxides (called “stabilizer”), such as Y₂O₃, CeO₂, MgO, CaO and so on, and the cubic phase or tetragonal phase can be retained at room temperature. Three different forms of stabilized zirconia ceramics are PSZ, FSZ and TZP (respectively for Fully Stabilized Zirconia, Partially Stabilized Zirconia and Tetragonal Zirconia Polycrystal) [10]. In the FSZ, zirconia is fully cubic phase. FSZ are generally obtained with large amounts of stabilizers (above 8% Y₂O₃) and used widely for oxygen sensors and solid oxide fuel cell

(SOFC) electrolytes. PSZ consist of a cubic matrix containing nanometric precipitates of tetragonal or monoclinic phase and are generally obtained by the addition of calcium or magnesium. TZP, for example 3 mol% yttria-doped zirconia (3Y-TZP), are composed of metastable tetragonal phase with a few cubic grains in accordance with phase diagram at sintering temperature. (The exact cubic–tetragonal phase partitioning depends on the sintering thermal cycle). Although only 3Y-TZP is used in clinical application currently, TZP and their composites will be increasingly used as biomaterials, for example Ce-TZP composites studied in European Long-life project. Fig1.3 is the Phase Diagrams of ZrO_2 - Y_2O_3 System and ZrO_2 - CeO_2 System.

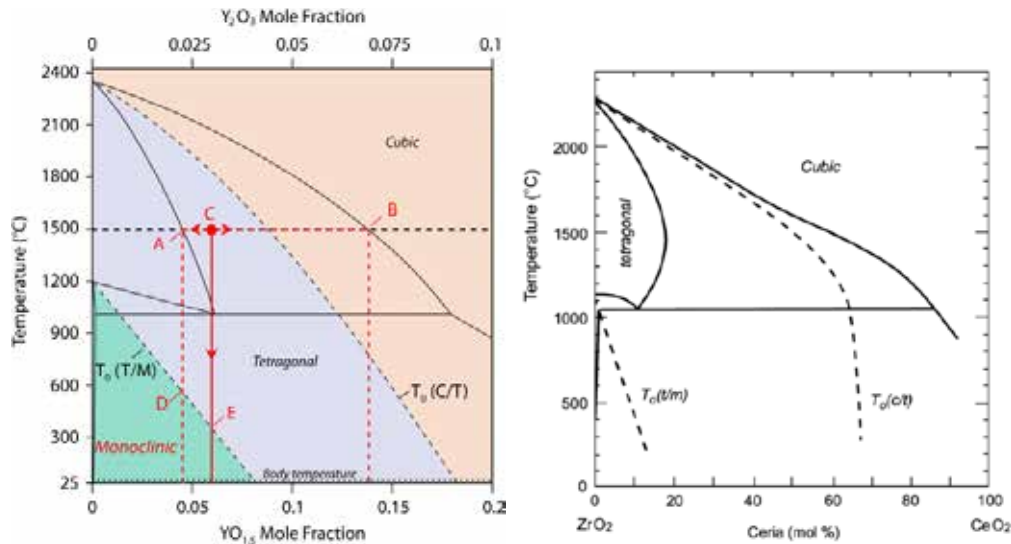


Fig 1.3 Phase Diagrams of ZrO_2 - Y_2O_3 System and ZrO_2 - CeO_2 System [8, 13]

1.3.2 Martensitic Transformation (T→M) of tetragonal zirconia

A thermodynamics description of T→M transformation in zirconia was proposed by Lange [14]:

$$\Delta G_{T \rightarrow M} = -\Delta G^c + \Delta U_{SE} + \Delta U_s$$

Here, $\Delta G_{T \rightarrow M}$ is the total free energy change during T-M transformation, ΔG^c is the chemical free energy (dependent on temperature and composition) and has a linear relationship with temperature, ΔU_{se} is the strain energy associated with the transformed particle, ΔU_s is the change in energy associated with the surface of the inclusion. The addition of Y_2O_3 in zirconia decreases ΔG^c . ΔG^c is also directly influenced by applied or internal stresses: tensile hydrostatic stress will act to reduce ΔU_{SE} , destabilizing the tetragonal phase. Patrick M. Kelly et al.'s work [15, 16] indicate that the Tetragonal to Monoclinic transformation in zirconia is stress-induced martensitic transformation accompanied by a volume expansion like other transformation toughening materials. Sylvain Deville et al. also described the T-M transformation process by an extensive atomic force microscopy study [17, 18] that evidenced its martensitic nature and crystallographic characteristics.

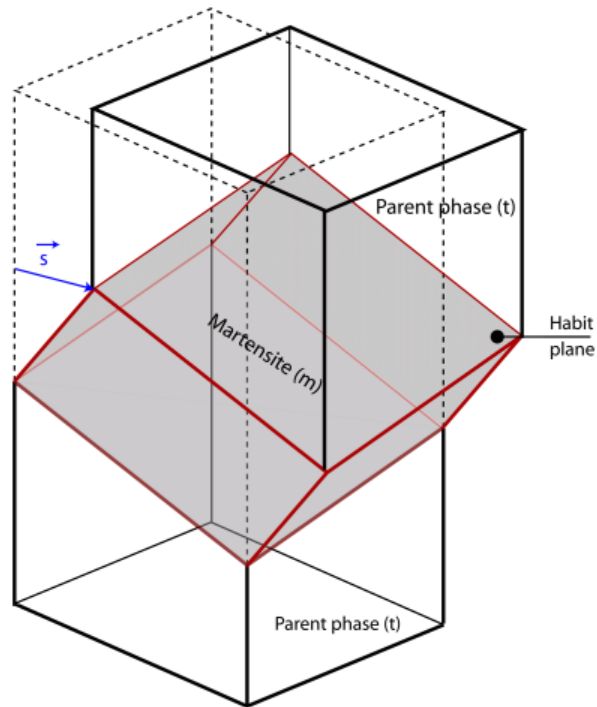


Fig 1.4 Schematic of martensitic Transformation (T→M) in zirconia [8]

The two different forms of the transformation (T→M) of tetragonal zirconia is crack-tip-induced transformation without water molecule (transformation toughening) and low temperature degradation with water molecule.

1.3.2.1 Transformation toughening

Zirconia ceramics have several advantages over other ceramic materials, due to the transformation toughening mechanisms operating in their microstructure that can give to components made out of them very interesting mechanical properties. In particular, yttria-stabilized zirconia ceramics present the highest strength (tensile strength up to 1,200 MPa), toughness (up to 6 MPa·m^{1/2}) of all single-phase oxide ceramics, although it can still suffer of slow crack growth and delayed fracture phenomenon[12]. Fig. 1.5 shows a schematic of transformation toughening (T→M) of zirconia during crack propagation [9, 12]. When tensile stress is applied to tetragonal grains, in the presence of a crack a large tensile stress at the crack tip is generated (stress concentration) and triggers the T-M transformation. The transformation is accompanied by a volume expansion. The volumetric expansion is constrained by the surrounding grains, which results in superimposing a compressive stress field to the one existing around the crack being propagated. Energy of the advancing crack is dissipated in phase transformation and in overcoming the matrix constraint by transforming grains.

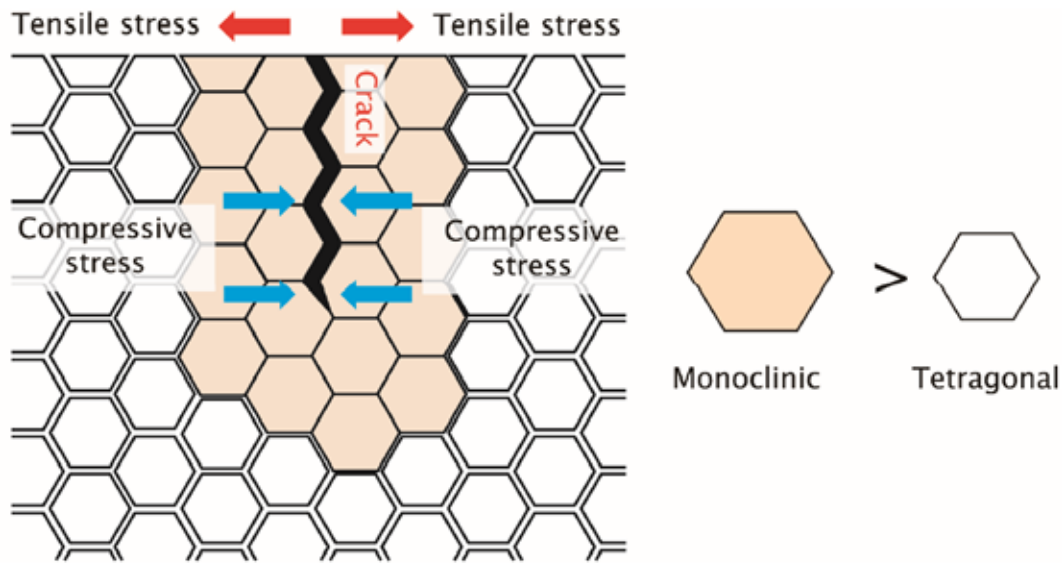


Fig 1.5 Schematic of transformation toughening (T→M) in crack propagation process of zirconia [8]

Features of the transformation at the surface, in the presence of a stress field

In the presence of a stress field, the net driving energy for the transformation can be modified. This change depends both on the nature and the magnitude of the stress field and on the orientation of the potential habit plane with respect to the stress field. Grains with their c_r -axis perpendicular to the surface and their junction planes parallel to the maximum tensile stress are the most likely to transform [8, 17]. Fig 1.6. shows an AFM picture of a transformed zone around a propagating crack. Large stresses around the crack favor the transformation, and this occurs first for the grains subjected to the largest tensile stresses, with an adequate orientation.

Features of the transformation in the bulk

T→M transformation in the bulk [8], in the presence of a stress field, is the main source of toughening in zirconia systems at room temperature. Transmission electron microscopy (TEM) images are so far the only way to obtain the features of the transformation in the bulk and the majority of TEM studies have been performed in Mg-PSZ. Lenticular tetragonal precipitates transform into a stack of monoclinic variants, which accommodate the shear component of the transformation. Therefore, in first good approximation, only the dilatant component of the transformation contributes to toughening.

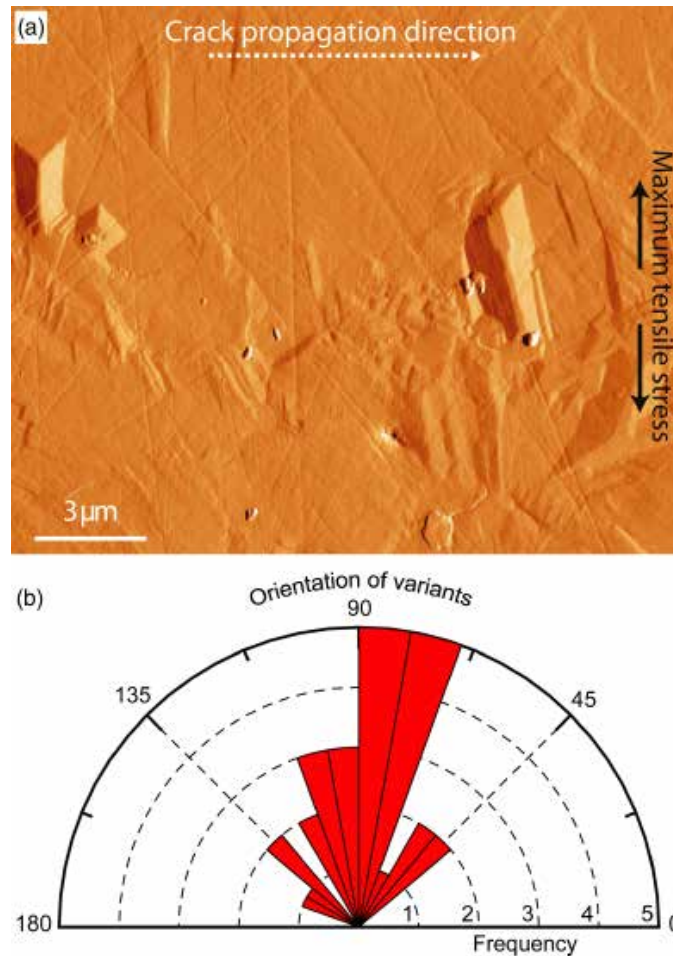


Fig1.6 Surface uplifts associated to the onset of transformation in a ceria-stabilized zirconia. [8, 17]

In the 1980s, McMeeking and Evans [12] developed a model to describe the transformation toughening in the crack propagation process.

$$K_{I_{tip}} = K_I - K_{I_{sh}} \quad (1)$$

$K_{I_{tip}}$ is the real stress intensity factor at the crack tip, K_I is the applied stress intensity factor. $K_{I_{sh}}$ is a shielding stress intensity factor. Now the theoretical model has been perfected by many researchers, and crack propagation mechanisms have been well known.

1.3.2.2 Low Temperature Degradation (LTD)

Hydrothermal ageing phenomenon

Compared to the phase transformation ($T \rightarrow M$) in crack propagation, that is almost instantaneous, hydrothermal ageing is a very slow transformation at the surface of zirconia ceramic in the presence of water or water vapour at low temperatures (from room temperature up to about 400 °C). During this process, water-derived species diffuse through the network of oxygen vacancies [8, 19] and occupy the vacancies. This results in ionic rearrangements, thus internal stresses, around the vacancies that can trigger the T-M transformation. It means that the transformation firstly occurs on the less stable grains (for example, the ones with lower yttrium content) of the zirconia ceramic surface. This transformation leads then to a cascade of events occurring neighbor to neighbor: the transformation of one grain leads to a volume increase stressing up the neighboring grains and to microcracking. Then, the microcracks allow the access of water in deeper and deeper layer of the material, allowing the transformed layer to progress into the bulk. Therefore the transformation process is described by a nucleation and growth process, and well fitted by Mehl–Avrami–Johnson laws [20]. The transformation process is shown in Fig1.7.

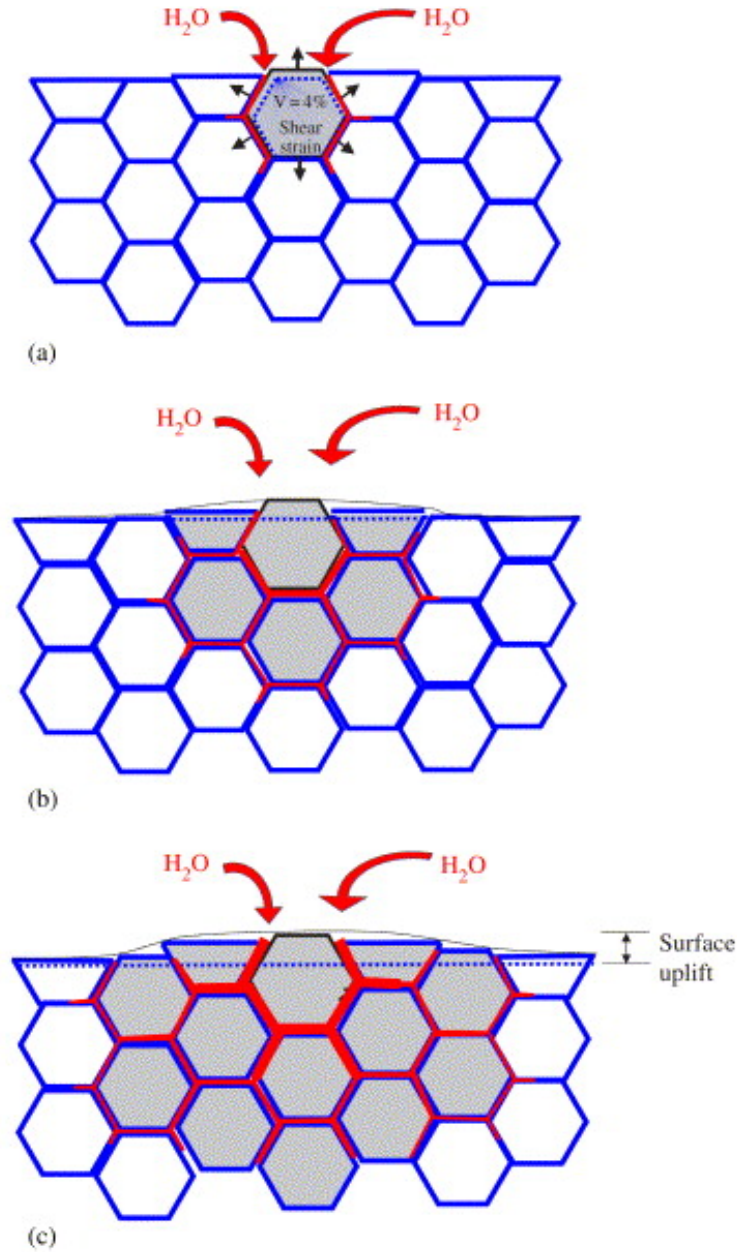


Fig1.7 Scheme of the ageing process occurring in a cross section, showing the transformation neighbor to neighbor. (a) Nucleation on a particular grain at the surface, leading to microcracking and stresses to the neighbors. (b) Growth of the transformed zone, leading to extensive microcracking and surface roughening. Transformed grains are gray. Red path represents the penetration of water due to microcracking around the transformed grains.[21]

Based on the above description, ageing kinetics are usually studied by the Mehl–Avrami–Johnson equation:

$$\frac{V_m - V_0}{V_{max} - V_0} = 1 - \exp(-(b \cdot t)^n) \quad (2)$$

In this equation, the parameter b is thermally activated: $b = b_0 \exp\left(\frac{-Q}{RT}\right)$ (3)

V_m is the monoclinic phase content after ageing during a duration t at absolute temperature T , V_0 and V_{max} are the initial and saturation levels of monoclinic phase content, and R is the gas constant. Q is the activation energy, typically around 100 kJ/mol [20, 22, 23]. The value of the parameter n is related to nucleation rate and growth rate, typically between 0.3 and 3.5 [24]. Meanwhile many factors such as nature, amount and distribution

(partitioning) of stabilizer, grain size, density, proportion of cubic phase, doping with more than one oxide, applied or residual stresses, all contribute towards the ageing process [8, 21, 25].

Effect of LTD on zirconia bioceramics

Hydrothermal ageing can lead to zirconia ceramic surface roughness, the generation of microcracks, decreased mechanical properties, and finally to brittle fracture. In 1980, Kobayashi [26] pointed out firstly that t-m transformation could take place on the surface of zirconia ceramics at relatively low temperatures (150–400 °C), and results in a decrease of the mechanical properties. In fact, the first real warning of the possible impact of ageing on zirconia prostheses came from the Food and Drugs Administration (FDA). In 1997, the FDA warned that the surgeon should not use the steam sterilization method on the zirconia implants [27]: this method has been shown to make the surface rough and to increase the wear of the cup made of polyethylene. More importantly, recent clinical studies have shown that polyethylene inclusions increase the wear rate of zirconia heads compared to alumina heads [28]. This increased wear rate resulted in increased risks of aseptic loosening of the hip prostheses, thus making shorter the lifetime of implants. In the years following 2001, LTD impact on the lifetime of the zirconia implants was once again amplified. Several hundreds of zirconia Prozyr® hip heads fractured in vivo around 2 years after implantation [29]. It was then demonstrated that a slight decrease in the density of the heads (although the density is much higher than the legal threshold) was sufficient to provide residual pores and to allow water molecules to penetrate into the head material, where ageing took place [30]. However, does not always lead to a decrease in mechanical properties. In some cases, the phase transformation (T→M) by LTD can put the surface in compression, thus increase the apparent strength [31]. When the transformed region has not been microcracked, this may be effective for short ageing times. But as soon as microcracks appear, these zirconia bioceramics can expect a decrease of the strength and the lifetime. Therefore, if the ageing time necessary to start microcracking is longer than the expected lifetime of an zirconia device (as an order of magnitude, 50 years in the case of a biomedical implant), ageing is not necessary deleterious. However, short time ageing of zirconia ceramics must not be considered as an easy way to increase their strength. Potential effect of ageing on the integrity of zirconia devices is like Fig.1.8.

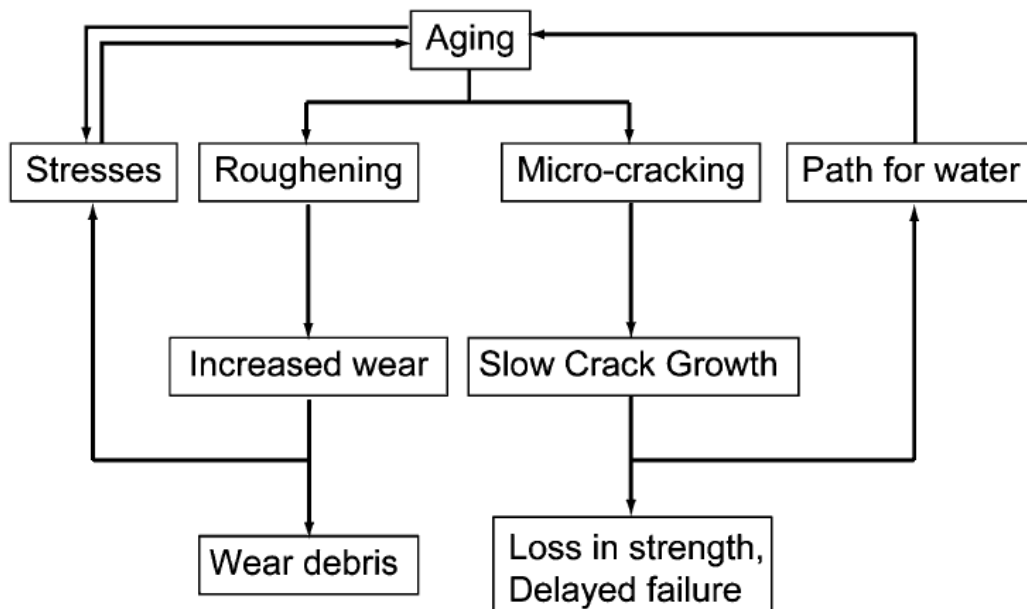


Fig.1.8 Scheme of potential effect of ageing on the integrity of zirconia devices. Arrows indicate coupling of ageing with crack propagation and wear mechanisms. [32]

The impact of ageing on zirconia bioceramics lifetime has been evaluated by some simple calculations based on two hypotheses: the surface monoclinic layer thickness is proportional to the ageing time, and this microcracked layer is assimilated to a defect (the thickness of the layer being the size of the defect). Under these assumptions, with growth rates of the monoclinic layer taken from the literature, one may calculate that the lifetime of a zirconia piece falls to a few years or a few tens of years, even under mechanical solicitations well below the

crack propagation threshold (and for which no crack propagation should ever occur). In fact, in this case the defects grow because of ageing, until they reach a size sufficient for crack propagation to occur. Once this stage is reached, the failure of the zirconia piece occurs in a matter of days or weeks[12].

Mechanism studies

Although zirconia ceramics have been studied for a long time, its low-temperature degradation mechanism is still not fully understood. In the degradation process, it was known that oxygen vacancies play a very important role in phase transformation process [33-43]. Now the major unresolved problem is the catalytic mechanism of water molecules on the ageing process. Here a few major mechanisms will be introduced.

1. SATO and SHIMADA indicated the tetragonal-to-monoclinic phase transformation in Y-TZP was greatly accelerated by low-temperature annealing in water. They thought that water molecules attack preferential sites (defects) and react with Zr-O-Zr bonds, as shown in Fig1.9 [44].

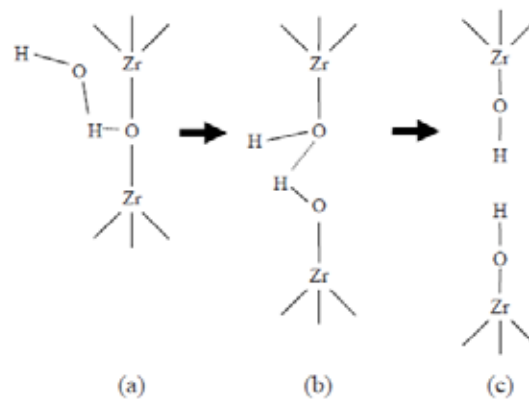


Fig.1.9 Ageing mechanism of model of SATO on the surface of the Y-TZP grain[44]

2. The formation of yttrium hydroxide crystallites ($a\text{-Y(OH)}_3$) by the reaction of water molecules with yttrium oxide on the ceramic surface, thereby reducing the content of Y_2O_3 , resulting in phase transformation [45, 46]. But soon it was suspected to be wrong, because the diffusion of yttrium in the zirconia structure is so slow that the hydroxide can't be formed in the corresponding ageing time (about 10^{29} s to diffuse 1 nm at 250 °C) [42] and there is no evidence for yttrium hydroxide formation during the period of phase transformation of the surface [35].

3. The mechanism proposed by Yoshimura (Fig 1.10) is relatively similar compared to model of SATO. The water is surface adsorbed, leading to the Zr-OH and Y-OH bond formation. This leads to the local appearance of stresses, which will then increase even more when OH^- anions migrate into the lattice and occupy the oxygen vacancies. When the accumulated stresses are sufficiently large, they trigger the transformation of the tetragonal phase. Microcracks are also formed which allow the propagation of water in the material. Yoshimura supports his theory on the observations by infrared spectroscopy of the penetration of hydroxyl ions into the lattice, ions disappearing after annealing. Moreover, the measured mass change shows that 60% of the oxygen vacancies are occupied by hydroxyl ions during ageing. However, the presence or absence of hydroxyl ions in the network is still widely disputed[35, 38].

It can also be noted that they do not have the same process compared Yoshimura model and SATO model: in one case he pointed to the role of oxygen vacancy in the lattice, meanwhile the creation of Zr-OH bonds leads to the increase of stresses which cause the transformation, whereas in the other case the creation of Zr-OH bonds leads to the stress relaxation but the whole process does not involve the participation of oxygen vacancies.

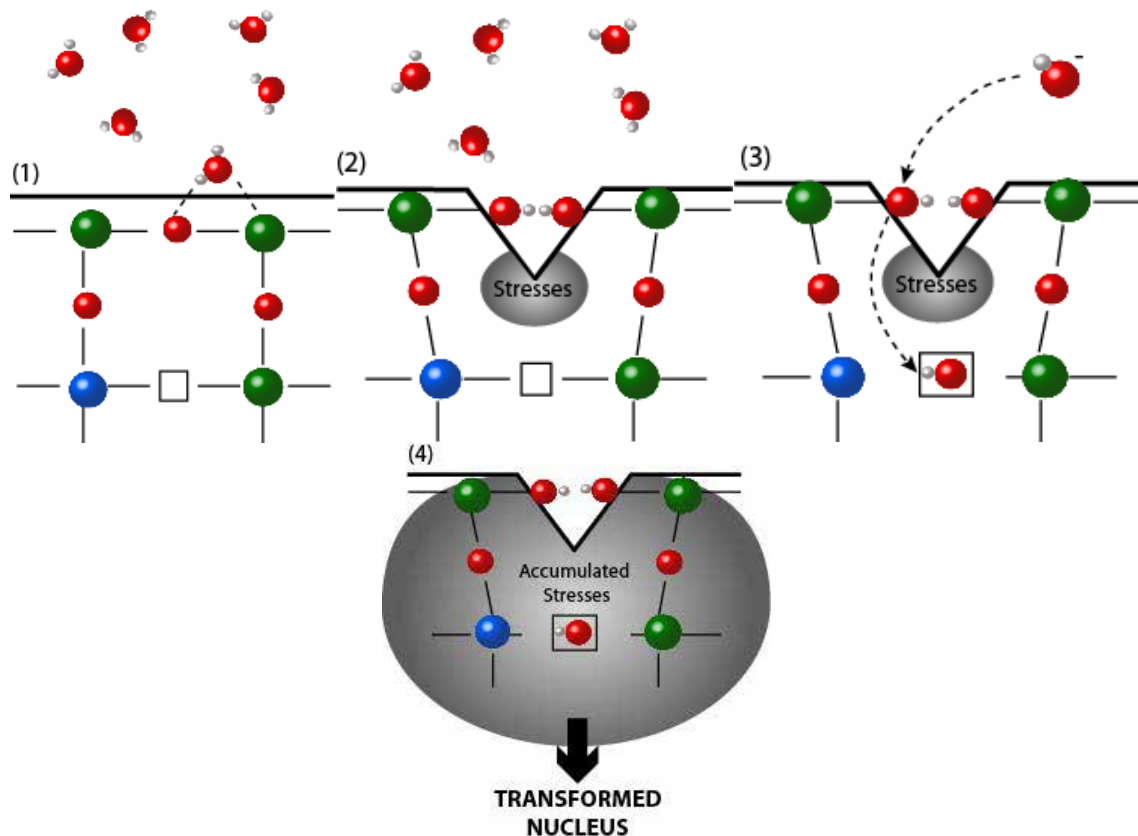


Fig.1.10 Ageing mechanism of model of Yoshimura[42]

4. The mechanism of hydrothermal ageing ($T \rightarrow M$) in the presence of stress was proposed by Schmauder and Schubert[47]. They observe that only unconstrained grains are resistant to ageing by studying the ageing behaviour of thin plates of TEM. They assume that the transformation ($T \rightarrow M$) is caused by stress corrosion by the water molecules (tensile or shear stresses are necessary, the compressive stresses producing a priori the opposite effect). Yttrium hydroxide formation would occur, not by diffusion of yttrium, but by diffusion of water into the zirconia matrix via oxygen vacancies or substitution between water and oxygen anions. Schubert calculated that the mobility of water in zirconia is substantially equivalent to that of yttrium hydroxide. Thus, corrosion under surface stress by water molecules results in the formation of crystallites of yttrium hydroxide and thus of a zone depleted in yttrium, which as in the case of the mechanism proposed by Lange serves as the germ for transformation to the monoclinic phase. Kim and Jung [36] also mention the role of internal stresses due to the anisotropy of the coefficient of thermal expansion. In this case, destabilization does not occur by migration of the yttrium. Indeed, the internal stresses are relaxed by a rearrangement of the dipoles (thermally activated), which also creates stress concentrations in small localized zones that will serve as a starting point for the transformation. Note that this mechanism implies that ageing can also occur under vacuum (the ageing medium does not intervene in the rearrangement of the dipoles), which nobody has been able to verify experimentally. This mechanism is therefore incomplete, but it explains the Sato mechanism by showing how a relaxation of the internal stresses can cause the transformation of the material.

5. The mechanism proposed by Schubert and Frey (Fig 1.11). They observe that during degradation water radicals are penetrating the lattice of the t-zirconia, and the profile showed a depth of penetration of about 500 nm, which is more than the size of nucleus for martensitic transformations. The concentrations of hydrogen and oxygen are similar and both are in the order of the vacancy concentration of this material. The penetration of water radical leads to a lattice contraction (a general contraction of both a and c parameters, hence, the “free” structural z (oxygen) parameter as well as the c/a -ratio are closer to the values of cubic zirconia) and is deep enough to reach the dimensions of a nucleus. In a strain hindered situation—such as the surface near region—the contraction leads to the formation of tensile stresses. And then tensile stresses induce the transformation $T \rightarrow M$ [41].

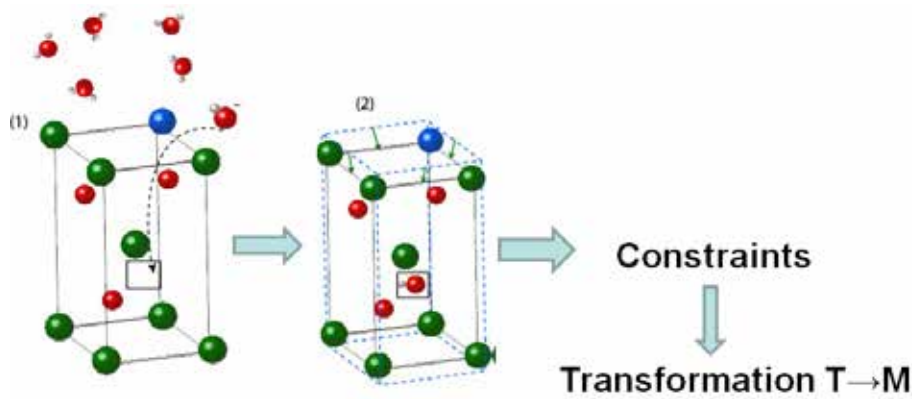


Fig 1.11 Ageing mechanism (model of Schubert)

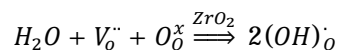
Now it is recognized by more and more scholars that the annihilation of oxygen vacancies during the ageing process in the presence of water molecules leading to the instability of the tetragonal zirconia phase [33, 39, 41, 43]. The scenario often proposed for the LTD of tetragonal ZrO_2 consists of the following steps [33]:

- (i) Chemical adsorption of H_2O on ZrO_2 surface,
- (ii) Reaction of H_2O with O^{2-} on the ZrO_2 surface to form hydroxyl ions OH^\bullet ,
- (iii) Penetration of OH^\bullet into the inner part by grain boundary diffusion,
- (iv) Filling of oxygen vacancies within the grains by OH^\bullet ions, and therefore formation of proton defects,
- (v) Occurrence of a $T \rightarrow M$ transformation when the oxygen vacancy concentration is reduced to the extent that the tetragonal phase is no longer stable.

The ageing mechanism based on the annihilation of oxygen vacancies indicates that the grain boundaries are susceptible to erosion by free radicals (OH^\bullet) because the depletion of oxygen vacancies in the space charge layer of grain boundaries [48], explaining the intergranular cracking induced by hydrothermal ageing. Meanwhile it explains why a higher content of stabilizer and a smaller grain size lead to a higher ageing resistance. In these cases, more oxygen vacancies need to be filled to destabilize the tetragonal phase. Here the excellent ageing resistance of Ce-TZP compared to Y-TZP is explained probably by the lack of oxygen vacancies.

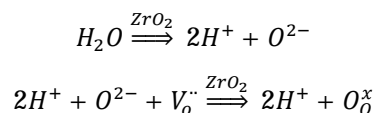
Penetration of “water-derived species” and filling of oxygen vacancies are also clearly established and these are generally accepted as the mechanism of hydrothermal ageing. However, some questions are still discussed.

a). The nature of the diffusing species and of the species filling the oxygen vacancies (including H^+ , O^{2-} , OH^\bullet and H_2O) are still under discussion. It is reported [19, 33, 37, 42, 49] that OH^\bullet diffuses and fills oxygen vacancies, and this is supported by XPS, FT-IR observations on polycrystals. In this case, the process of the oxygen vacancy annihilation can be written as:

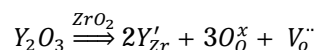


where $(OH)_o^\bullet$ represents an OH^\bullet ion on an oxygen site in the zirconia lattice.

However, a parallel but independent diffusion of both separated O^{2-} and H^+ ions was proposed consistent with SIMS results [50], and the process of oxygen vacancy annihilation should be written as:



where the reaction is buffered by the stabilizer charge compensation reaction:



If diffusion of water species alone were important, then one might expect that the higher the yttria stabilizer content, the larger the diffusional flux would be as there would be a greater number of diffusion paths. However, SIMS data indicate that neither H nor D ions diffuse in cubic YSZ (that contains high amounts of yttria) at the temperatures associated with LTD. There are two possible explanations for this contrary behavior of the hydrogen. The first possibility is that the kinetics of the surface decomposition reaction of water into hydrogen and oxygen are retarded at the surface of the higher yttria content zirconia, perhaps due to changes in surface structure or enhanced surface segregation of Y to the surface sites where the water decomposition occurs. The other possibility is that the higher yttria content alters the energy of the H (and D) in zirconia by altering the Fermi level, namely the electrochemical potential for H depends on the yttria concentration.

b). How the annihilation of oxygen vacancies results in T→M transformation is also still under discussion. It is reported [51, 52] that the stability of zirconia has a direct relationship with oxygen vacancy concentration. When the oxygen vacancy concentration decreased, the transformation of the tetragonal phase to the monoclinic phase (LTD) spontaneously occurs. Another point of view is also reported [41] that the filling of the oxygen vacancies with the penetration of water radical leads to a lattice contraction and the contraction leads to the formation of tensile stresses. Then the tensile stresses induce the transformation T→M.

Research on the influence parameters of LTD

From the current study [2, 17, 21, 32, 53, 54], the factors affecting the ageing process mainly include the stabilizer type, stabilizer content, porosity(density), surface finish and stresses, grain size, grain boundaries, cubic phase content, etc.

A). Stabilizer type

The zirconia materials with different stabilizer have different ageing kinetics processes as shown on Fig 1.12[1, 32, 55, 56]. Magnesia-stabilized zirconia (Mg-PSZ) and ceria-stabilized zirconia (Ce-TZP) have a better ageing resistance and a higher fracture toughness than yttria-stabilized zirconia(Y-TZP)[57]. For Ce-TZP, the ageing process was greatly delayed because the cerium ions are tetravalent and doesn't introduce oxygen deficiencies. And compared Ce-TZP and Y-TZP, more ceria content (typically 10-12 mol% > 3mol% of yttria) is required to stabilize the tetragonal phase. For Mg-PSZ, hydrothermal ageing behaviour don't occur because they are mainly composed of cubic phase.

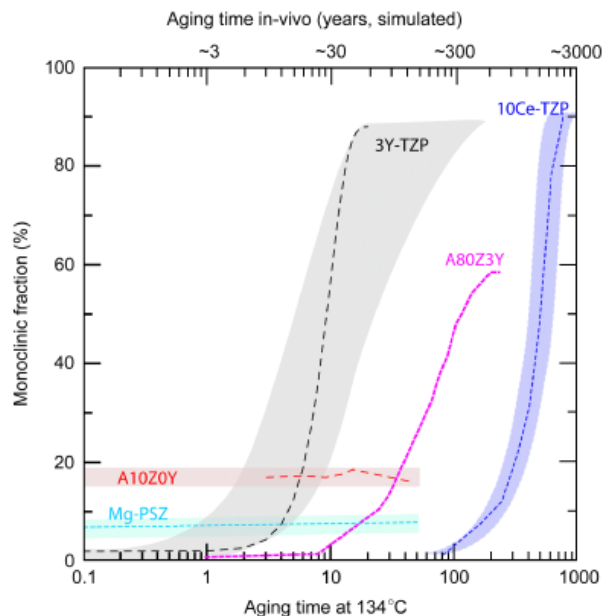


Fig 1.12 Low-temperature degradation kinetics of 10 mol% ceria-stabilized zirconia, 3 mol% yttria-stabilized zirconia, Magnesium partially stabilized zirconia, alumina-toughened zirconia (A80Z3Y), and zirconia-toughened alumina (A10Z0Y) measured at 134°C and expected in-vivo at 37°C (considering an activation energy of 106 kJ/mol for all materials, which is probably not completely accurate). The shadowed areas give uncertainty ranges when they can be evaluated [32].

However, Y-TZP was preferred for orthopedic applications thanks to its more excellent strength. These studies found the composites of alumina-toughened zirconia(Y-TZP) have a better ageing resistance than Y-TZP, meanwhile they also have excellent mechanical properties [1, 58]. So the study of hydrothermal ageing process of Y-TZP is very useful for the bioceramics.

B). Stabilizer content

Increasing the stabilizer content improves the ageing resistance of zirconia ceramics while also lowering their transformation threshold. Fig 1.13 shows that transformed monoclinic ZrO_2 fraction versus ageing time for different stabilizer content zirconia ceramics. With the increase of the stabilizer content, the threshold of transformation is obviously reduced, and ageing resistance is enhanced. However, when the content is high to a certain value, the zirconia material is completely cubic phase composition, which does not have excellent mechanical properties like 8YSZ.

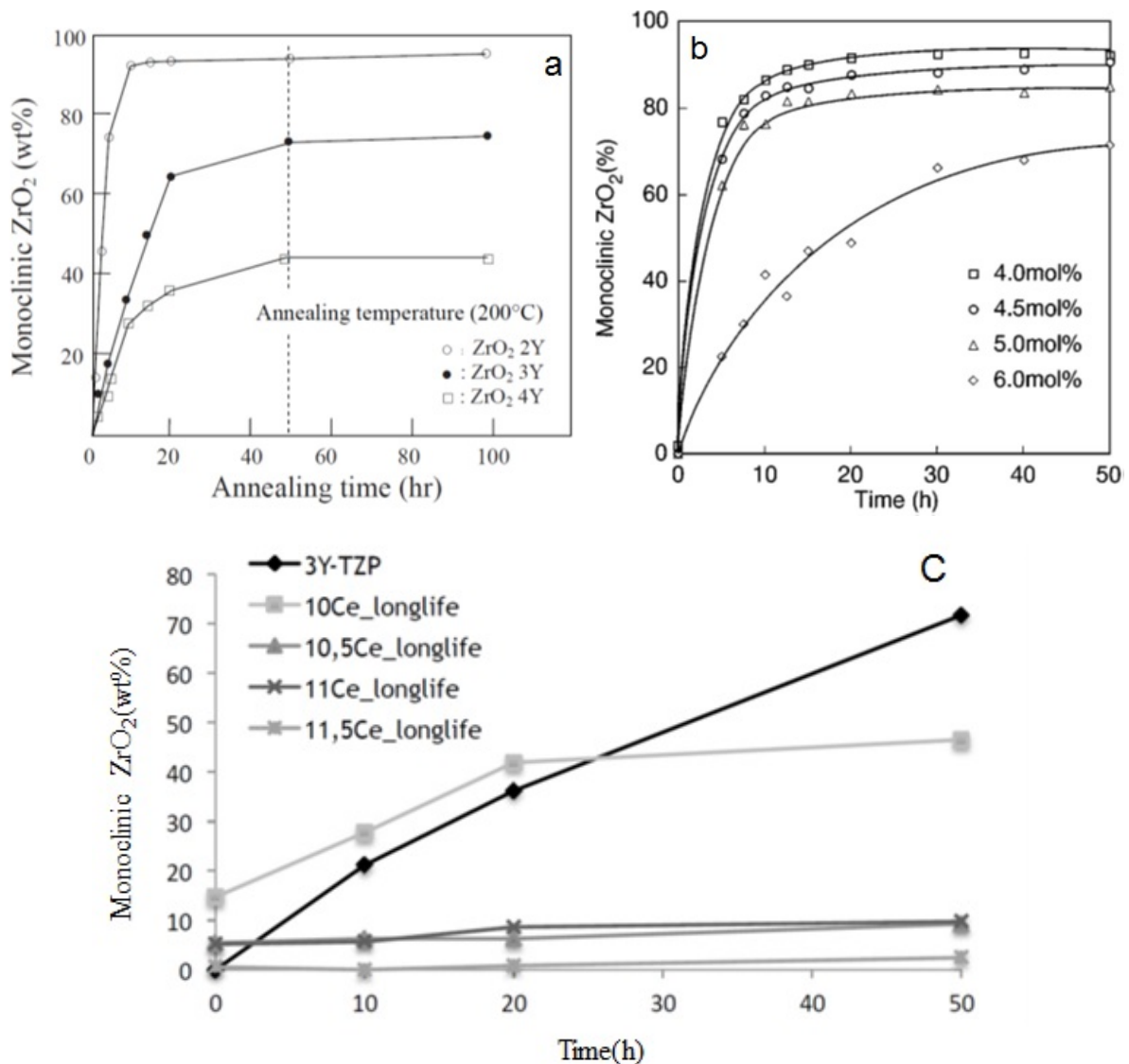


Fig.1.13 Scheme of transformed monoclinic ZrO_2 fraction versus ageing time for different stabilizer content zirconia ceramics: a. different content Y_2O_3 -doped zirconia ceramics ageing at 200°C [34, 59]; b. different content Sc_2O_3 -doped zirconia ceramics sintered at 1400 °C for 1h ageing at 180°C [60]; c. different content CeO_2 -doped zirconia composite ceramics ageing at 134°C [61]

C). Porosity

Porosity (density) has a certain effect on the ageing kinetics of zirconia ceramics. Fig 1.14 shows the ageing state of the different density regions of a 3Y-TZP sample with density gradient after 10 h ageing at 134 °C. In the low-density region, the pores in particular the presence of open porosities provide a channel for the diffusion of water molecules, so that the region suffers from severe ageing. Therefore, dense zirconia ceramics are selected as bioceramics.

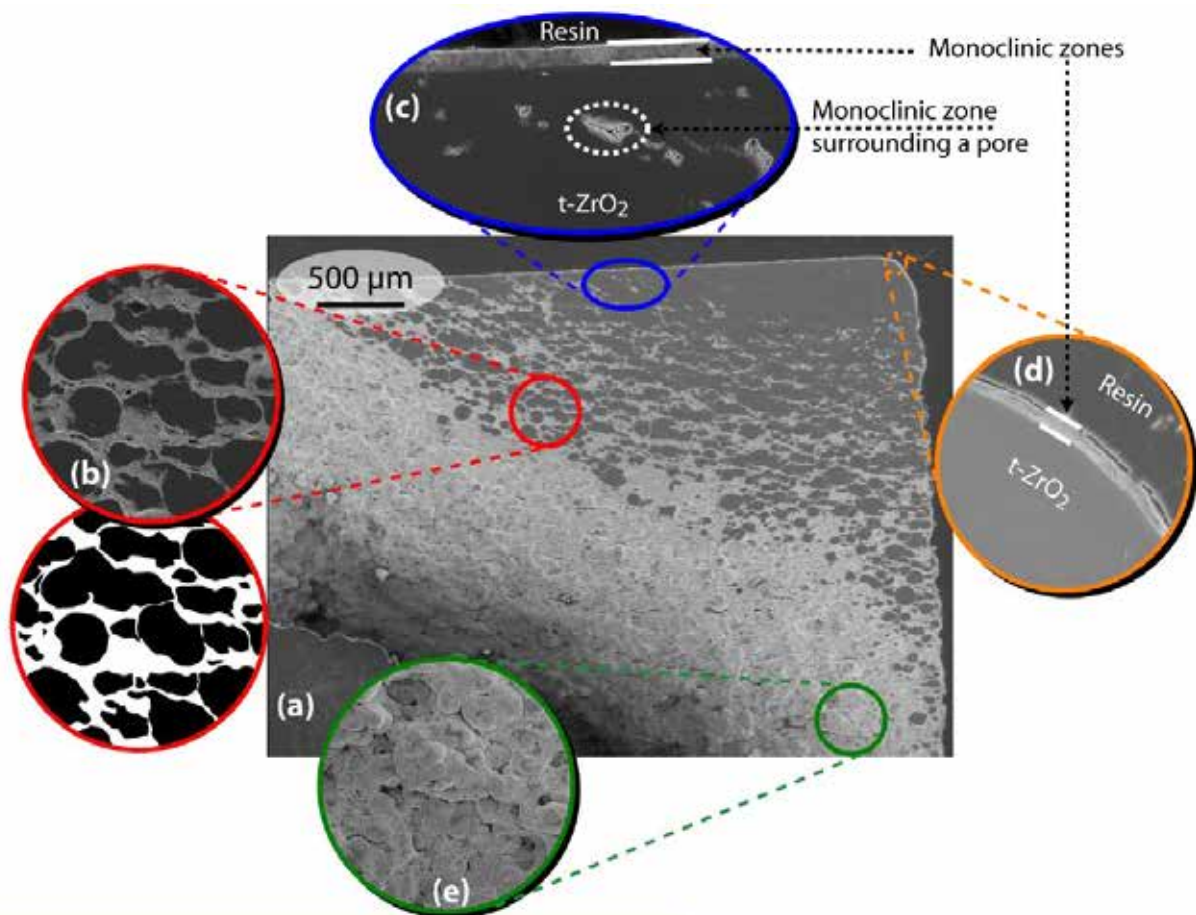


Fig1.14 (a) SEM images of cross-sectional of a sample of 3Y-TZP having a porosity gradient and accelerated ageing at 134 °C after 10h. (b) to (e) details of less dense areas, showing increasingly severe ageing as density decreases.[62]

D) Surface finish and stresses

Rough polishing produces a compressive surface stress layer beneficial for the ageing resistance, while smooth polishing produces preferential transformation nucleation around scratches, due to elastic/plastic damage tensile residual stresses [54]. Fig 1.15 indicate that preferential transformation occurs around scratches and areas with residual tensile stresses.

The stress has a significant effect on the ageing of each zirconia ceramic. SCHMAUDER [40] showed that the degradation does not occur in stress-free grains of zirconia, and starts at the surface of Y-TZP in the presence of water vapor and stresses. Sylvain Deville [54] indicated that the ageing sensitivity of zirconia ceramics is directly linked to the type of stress (compressive or tensile) and amount of residual stresses. Where the tensile stress has the effect of promoting the ageing process, and the compressive stress has no corresponding effect [63-65]. Schubert [41] thought that the microscopic tensile stress caused by the lattice shrinkage due to the infiltration of water molecules during the ageing process is the root cause of the T→M phase transformation. However, because the impact research of stress is more difficult, now only some qualitative conclusions are given.

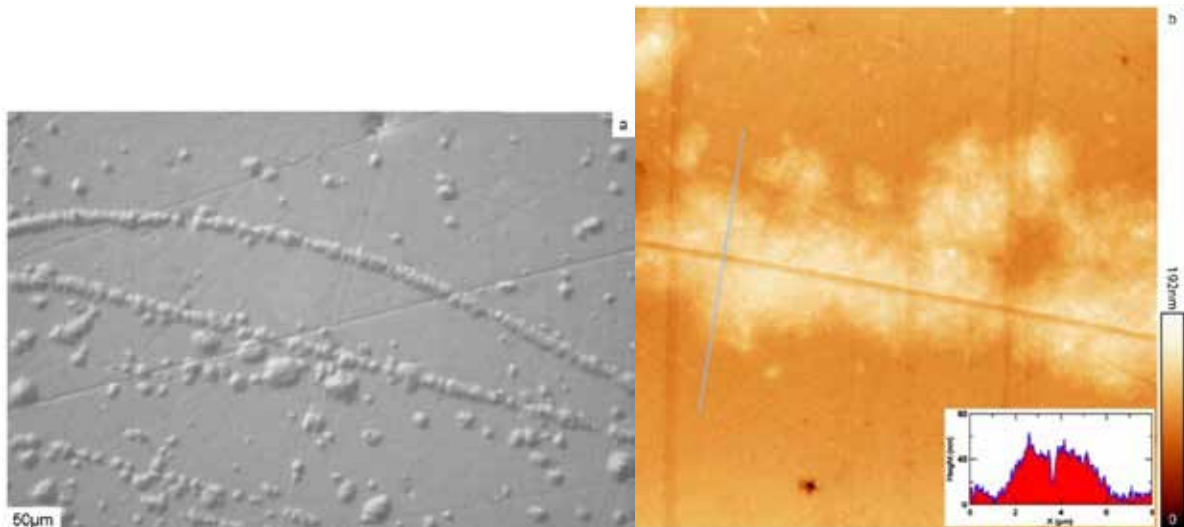


Fig 1.15 a) Optical microscopy observation (Normarski contrast) of a partially transformed surface after 75 min at 140°C; b) Atomic force microscopy observation (height image) of a partially transformed surface, showing the preferential transformation (bright areas) in the surrounding of a polishing scratch. The inset represents a line profile perpendicular to the scratch [54].

E). Grain size

The effect of grain size on the ageing process is also evident. Many researchers thought that the reduction of grain size can improve the ageing resistance ability of zirconia ceramics [66-69]. It is reported [68] that nano 3Y-TZP ceramics with <100 nm grain size don't exhibit degradation, whereas sub-micrometric 3Y-TZP ceramics undergo severe degradation. Some researches [66] point to a critical value of grain size around 300 nm, below which ageing processes do not occur, but later results showed that this critical value has no physical base [17] and may be dependent on other materials parameters [70]. S. R. Jansen et al. reported that doping with ceria or decreasing the grain size improved strongly the ageing resistance of Y-TZP [71].

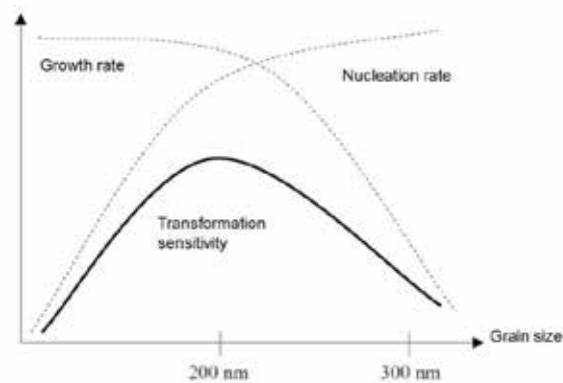


Fig 1.16 The relationship between ageing sensitivity and grain size[72]

However, Li and Watanabe [73] found that the sensitivity of ageing did not show a single change as the grain size increased from 0.51 to 0.96 µm, while ageing sensitivity is initially reduced and then enhanced for 2Y-TZP under the same polished condition. Deville [72] thought that the ageing sensitivity has a direct relationship with nucleation rate and growth rate, but the effect of grain size on these two speeds is just the opposite like Fig 1.16, and from his ageing results of different grain sizes (Fig 1.17), it is known that the most sensitive grain size for ageing is 200 nm.

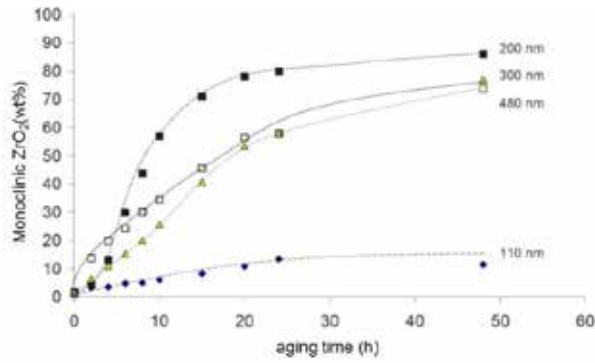


Fig 1.17 Scheme of transformed monoclinic ZrO_2 fraction versus ageing time for different grain sizes of 3Y-TZP samples under same polish conditions. [72]

F). Grain boundaries

The influence of grain boundary on the ageing process is also getting more and more attention. E. P. Butler and A. H. Heuer [74] studied grain-boundary regions in a ternary (Ca, Mg)-partially-stabilized ZrO_2 during ageing at $1400^\circ C$ and it is indicated that a liquid-phase analogue of diffusion-induced grain-boundary migration has a certain effect on the phase change in zirconia. Then it is reported that a silica glass phase only at triple grain junctions greatly improves the resistance to LTD of zirconia ceramics [75]. Guo pointed out that there are a large number of oxygen vacancies which play a very important role on the ageing process distributed around grain boundary for zirconia ceramics as shown Fig.1.18, and the alumina phase doping to the grain boundary can increase the Schottky barrier height of oxygen vacancy migration of the grain boundaries in the electrical properties study for zirconia ceramics [48]. Others have confirmed that the addition of alumina or other oxides at the grain boundary stabilizes oxygen vacancies, thereby enhancing the ageing resistance of zirconia [5, 7].

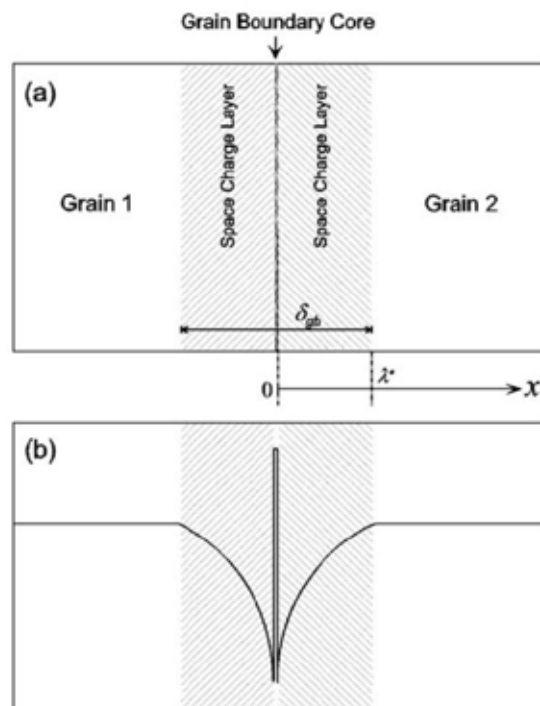


Fig 1.18 (a) Schematic representation of an “electrical grain boundary”, consisting of one grain-boundary core and two adjacent space-charge layers. At the interface between the space-charge layer and the grain-boundary core $x = 0$, while far into the bulk $x = \infty$. (b) Schematic representation of oxygen vacancy profiles in space-charge layers and grain-boundary core. [48]

G). Cubic phase

Although it has been reported that there is also a hydrothermal ageing phenomenon in the cubic phase [76], it is not within the scope of this work and only used for reference. Indeed, cubic grains grow faster than tetragonal grains, and suck yttrium from neighboring tetragonal grains during zirconia sintering process [53, 77, 78]. Higher sintering temperature or prolonged sintering time will increase the content of cubic phase. The cubic grains are enriched with yttrium, causing a depletion of yttria in the surrounding tetragonal grains, and these grains will act as nucleation sites for tetragonal-to-monoclinic transformation (Fig 1.19). Therefore, the presence of cubic grains has a detrimental impact on ageing resistance.

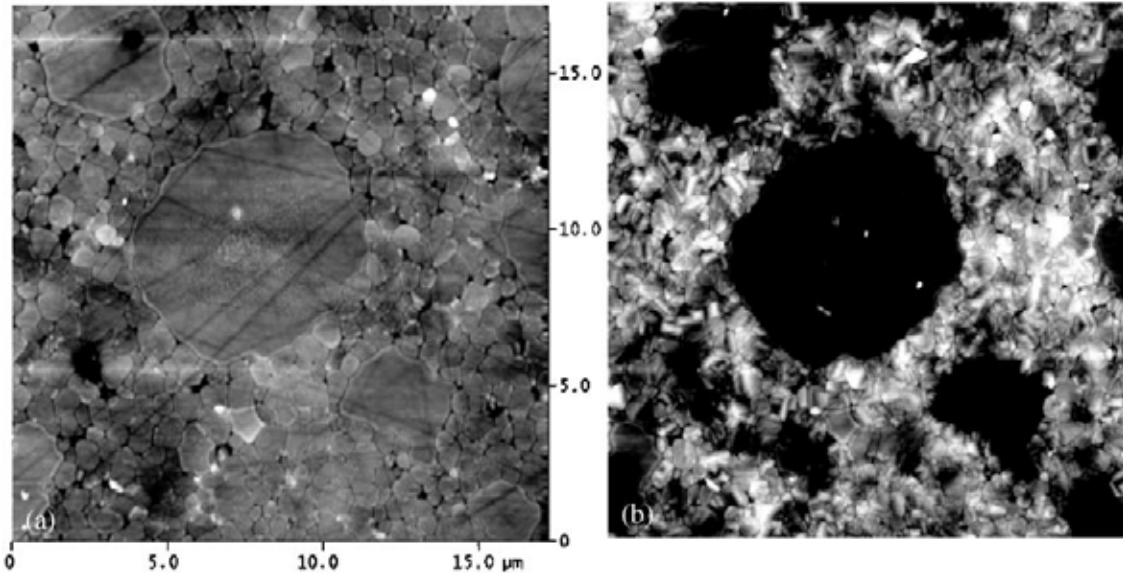


Fig.1.19 Atomic force microscopy images of the same zone, (a) before and (b) after 24 h ageing at 134°C, for a 3Y-TZP ceramic sintered at 1550°C for 5 h. [53]

H). What are the significant parameters that control ageing in a real 3Y-TZP?

As a conclusion, a few parameters have been identified as playing a role on ageing sensitivity of zirconia-based ceramics. However, up to now no study was able to separate these effects: for example, the easiest way to change the grain size of a given 3Y-TZP ceramic is to modify the sintering cycle. However, this also modifies yttrium partitioning and proportion of cubic phase, and also perhaps the nature of grain boundaries. Besides, ageing has proven to be very sensitive to residual stresses (arising from polishing procedures for example). Thus a small change in the polishing procedure (new polishing sheet, different applied pressure...) may greatly influence the ageing kinetics.

It is thus exceedingly difficult to conclude with certainty, from the literature, on the main parameters that directly influence ageing kinetics.

References

- [1] J. Chevalier, L. Gremillard, Ceramics for medical applications: A picture for the next 20 years, *Journal of the European Ceramic Society* 29(7) (2009) 1245-1255.
- [2] C. Piconi, G. Maccauro, Zirconia as a ceramic biomaterial, *Biomaterials* 20(1) (1999) 1-25.
- [3] P. Christel, A. Meunier, M. Heller, J.P. Torre, C.N. Peille, Mechanical properties and short-term in vivo evaluation of yttrium-oxide-partially-stabilized zirconia, *Journal of Biomedical Materials Research* 23(1) (1989) 45-61.
- [4] R.B. Heimann, H.D. Lehmann, *Bioceramic Coatings for Medical Implants: Trends and Techniques*, Wiley-VCH; 1 edition (May 26, 2015)2015.
- [5] A. Samodurova, A. Kocjan, M.V. Swain, T. Kosmač, The combined effect of alumina and silica co-doping on the ageing resistance of 3Y-TZP bioceramics, *Acta Biomaterialia* 11 (2015) 477-487.
- [6] A.A. Nogiwa-Valdez, W.M. Rainforth, P. Zeng, I.M. Ross, Deceleration of hydrothermal degradation of 3Y-TZP by alumina and lanthana co-doping, *Acta Biomaterialia* 9(4) (2013) 6226-6235.
- [7] F. Zhang, K. Vanmeensel, M. Batuk, J. Hadermann, M. Inokoshi, B. Van Meerbeek, I. Naert, J. Vleugels, Highly-translucent, strong and ageing-resistant 3Y-TZP ceramics for dental restoration by grain boundary segregation, *Acta Biomaterialia* 16 (2015) 215-222.
- [8] J. Chevalier, L. Gremillard, A.V. Virkar, D.R. Clarke, The Tetragonal-Monoclinic Transformation in Zirconia: Lessons Learned and Future Trends, *Journal of the American Ceramic Society* 92(9) (2009) 1901-1920.
- [9] D.J. Green, R.H. Hannink, M.V. Swain, *Transformation toughening of ceramics*, (1989).
- [10] L. GREMILLARD, *Biocéramiques : des monolithes aux composites*, 2009.
- [11] R.H.J. Hannink, P.M. Kelly, B.C. Muddle, Transformation Toughening in Zirconia-Containing Ceramics, *Journal of the American Ceramic Society* 83(3) (2000) 461-487.
- [12] N. Eliaz, *Degradation of implant materials*, Springer Science & Business Media2012.
- [13] M. Yashima, M. Kakihana, M. Yoshimura, Metastable-stable phase diagrams in the zirconia-containing systems utilized in solid-oxide fuel cell application, *Solid State Ionics* 86 (1996) 1131-1149.
- [14] F. Lang, Transformation toughening part 1 size effects associated with the thermodynamics of the constrained transformation, *J. Mater Sci* 17 (1982) 225-234.
- [15] P.M. Kelly, L.F. Rose, The martensitic transformation in ceramics—its role in transformation toughening, *Progress in Materials Science* 47(5) (2002) 463-557.
- [16] G.R. Hugo, *A Crystallographic Analysis of the Tetragonal to Monoclinic Transformation in ZrO₂-12 Mole% CeO₂*, Monash University, 1994.
- [17] S. Deville, G. Guénin, J. Chevalier, Martensitic transformation in zirconia, *Acta Materialia* 52(19) (2004) 5697-5707.
- [18] S. Deville, J. Chevalier, H. El Attaoui, Atomic Force Microscopy Study and Qualitative Analysis of Martensite Relief in Zirconia, *Journal of the American Ceramic Society* 88(5) (2005) 1261-1267.
- [19] X. Guo, Hydrothermal degradation mechanism of tetragonal zirconia, *Journal of Materials Science* 36(15) (2001) 3737-3744.
- [20] J. Chevalier, B. Cales, J.M. Drouin, Low-Temperature Ageing of Y-TZP Ceramics, *Journal of the American Ceramic Society* 82(8) (1999) 2150-2154.
- [21] J. Chevalier, What future for zirconia as a biomaterial?, *Biomaterials* 27(4) (2006) 535-543.

- [22] J. Chevalier, S. Grandjean, M. Kuntz, G. Pezzotti, On the kinetics and impact of tetragonal to monoclinic transformation in an alumina/zirconia composite for arthroplasty applications, *Biomaterials* 30(29) (2009) 5279-5282.
- [23] P. Fabbri, C. Piconi, E. Buresi, G. Magnani, F. Mazzanti, C. Mingazzini, Lifetime estimation of a zirconia–alumina composite for biomedical applications, *Dental Materials* 30(2) (2014) 138-142.
- [24] L. Gremillard, J. Chevalier, T. Epicier, S. Deville, G. Fantozzi, Modeling the ageing kinetics of zirconia ceramics, *Journal of the European Ceramic Society* 24(13) (2004) 3483-3489.
- [25] S. Lawson, Environmental degradation of zirconia ceramics, *Journal of the European Ceramic Society* 15(6) (1995) 485-502.
- [26] K. Kobayashi, H. Kuwajima, T. Masaki, Phase change and mechanical properties of ZrO₂-Y₂O₃ solid electrolyte after ageing, *Solid State Ionics* 3 (1981) 489-493.
- [27] *Degradation of Implant Materials*, Springer, New York, 2012.
- [28] P. Hernigou, T. Bahrami, Zirconia and alumina ceramics in comparison with stainless-steel heads, *Bone & Joint Journal* 85(4) (2003) 504-509.
- [29] G. Maccauro, C. Piconi, W. Burger, L. Pilloni, E. De Santis, F. Muratori, I. Learmonth, Fracture of a Y-TZP ceramic femoral head, *Bone & Joint Journal* 86(8) (2004) 1192-1196.
- [30] J. Chevalier, L. Gremillard, S. Deville, Low-temperature degradation of zirconia and implications for biomedical implants, *Annu. Rev. Mater. Res.* 37 (2007) 1-32.
- [31] J. Chevalier, J. Loh, L. Gremillard, S. Meille, E. Adolphson, Low-temperature degradation in zirconia with a porous surface, *Acta Biomaterialia* 7(7) (2011) 2986-2993.
- [32] J. Chevalier, L. Gremillard, A.V. Virkar, D.R. Clarke, The tetragonal-monoclinic transformation in zirconia: lessons learned and future trends, *Journal of the American Ceramic Society* 92(9) (2009) 1901-1920.
- [33] X. Guo, Property degradation of tetragonal zirconia induced by low-temperature defect reaction with water molecules, *Chemistry of Materials* 16(21) (2004) 3988-3994.
- [34] M.T. Hernandez, J.R. Jurado, P. Duran, J.L. Fierro, Subeutectoid Degradation of Yttria-Stabilized Tetragonal Zirconia Polycrystal and Ceria-Doped Yttria-Stabilized Tetragonal Zirconia Polycrystal Ceramics, *Journal of the American Ceramic Society* 74(6) (1991) 1254-1258.
- [35] A.E. Hughes, F.T. Ciacchi, S.P. Badwal, Role of O²⁻, OH⁻ and anion vacancies in the degradation of Y-TZP in moist environments, *Journal of Materials Chemistry* 4(2) (1994) 257-263.
- [36] D. Kim, H. Jung, Low temperature degradation of tetragonal zirconia: mechanism and prevention, *Presentado en Zirconia V, Australia* (1992).
- [37] Y. Kim, C. Jung, J. Park, Low temperature degradation of yttria-stabilized tetragonal zirconia polycrystals under aqueous solutions, *Journal of nuclear materials* 209(3) (1994) 326-331.
- [38] T. Lepistö, T. Mantyla, A Model for Structural Degradation of Y-TZP Ceramics in Humid Atmosphere, A Collection of Papers Presented at the 13th Annual Conference on Composites and Advanced Ceramic Materials, Part 1 of 2: Ceramic Engineering and Science Proceedings, Volume 10, Issue 7/8, Wiley Online Library, 1989, pp. 658-667.
- [39] G. Pezzotti, M.C. Munisso, A.A. Porporati, K. Lessnau, On the role of oxygen vacancies and lattice strain in the tetragonal to monoclinic transformation in alumina/zirconia composites and improved environmental stability, *Biomaterials* 31(27) (2010) 6901-6908.
- [40] S. Schmauder, H. Schubert, Significance of internal stresses for the martensitic transformation in Yttria-stabilized tetragonal zirconia polycrystals during degradation, *Journal of the American Ceramic Society* 69(7) (1986) 534-540.

- [41] H. Schubert, F. Frey, Stability of Y-TZP during hydrothermal treatment: neutron experiments and stability considerations, *Journal of the European Ceramic Society* 25(9) (2005) 1597-1602.
- [42] M. Yoshimura, T. Noma, K. Kawabata, S. Sōmiya, Role of H₂O on the degradation process of Y-TZP, *Journal of Materials Science Letters* 6(4) (1987) 465-467.
- [43] F. Zhang, M. Batuk, J. Hadermann, G. Manfredi, A. Mariën, K. Vanmeensel, M. Inokoshi, B. Van Meerbeek, I. Naert, J. Vleugels, Effect of cation dopant radius on the hydrothermal stability of tetragonal zirconia: grain boundary segregation and oxygen vacancy annihilation, *Acta Materialia* 106 (2016) 48-58.
- [44] T. SATO, M. SHIMADA, Transformation of Yttria-Doped Tetragonal ZrO₂ Polycrystals by Annealing in Water, *Journal of the American Ceramic Society* 68(6) (1985) 356-356.
- [45] F. Lange, G. Dunlop, B.I. Davis, Degradation During Ageing of Transformation-Toughened ZrO₂-Y₂O₃ Materials at 250 C, *Journal of the American Ceramic Society* 69(3) (1986) 237-240.
- [46] H. Schubert, Investigations on the stability of yttria stabilized tetragonal zirconia (YTZP), *Zirconia Ceramics* 7 (1986) 65-8.
- [47] S. Schmauder, H. Schubert, Significance of Internal Stresses for the Martensitic Transformation in Yttria-Stabilized Tetragonal Zirconia Polycrystals During Degradation, *Journal of the American Ceramic Society* 69(7) (1986) 534-540.
- [48] X. Guo, R. Waser, Electrical properties of the grain boundaries of oxygen ion conductors: acceptor-doped zirconia and ceria, *Progress in Materials Science* 51(2) (2006) 151-210.
- [49] X. Guo, On the degradation of zirconia ceramics during low-temperature annealing in water or water vapor, *Journal of Physics and Chemistry of Solids* 60(4) (1999) 539-546.
- [50] T. Duong, A.M. Limarga, D.R. Clarke, Diffusion of Water Species in Yttria-Stabilized Zirconia, *Journal of the American Ceramic Society* 92(11) (2009) 2731-2737.
- [51] S. Fabris, A.T. Paxton, M.W. Finnis, A stabilization mechanism of zirconia based on oxygen vacancies only, *Acta Materialia* 50(20) (2002) 5171-5178.
- [52] M. Raza, D. Cornil, J. Cornil, S. Lucas, R. Snyders, S. Konstantinidis, Oxygen vacancy stabilized zirconia (OVSZ); a joint experimental and theoretical study, *Scripta Materialia* 124 (2016) 26-29.
- [53] J. Chevalier, S. Deville, E. Münch, R. Jullian, F. Lair, Critical effect of cubic phase on ageing in 3mol% yttria-stabilized zirconia ceramics for hip replacement prosthesis, *Biomaterials* 25(24) (2004) 5539-5545.
- [54] S. Deville, J. Chevalier, L. Gremillard, Influence of surface finish and residual stresses on the ageing sensitivity of biomedical grade zirconia, *Biomaterials* 27(10) (2006) 2186-2192.
- [55] D. Gutknecht, J. Chevalier, V. Garnier, G. Fantozzi, Key role of processing to avoid low temperature ageing in alumina zirconia composites for orthopaedic application, *Journal of the European Ceramic Society* 27(2) (2007) 1547-1552.
- [56] J. Schneider, S. Begand, R. Kriegel, C. Kaps, W. Glien, T. Oberbach, Low-Temperature Ageing Behavior of Alumina-Toughened Zirconia, *Journal of the American Ceramic Society* 91(11) (2008) 3613-3618.
- [57] M. Nagl, L. Llanes, R. Fernandez, M. Anglada, The fatigue behaviour of Mg-PSZ and ZTA ceramics, *Fracture mechanics of ceramics*, Springer 1996, pp. 61-76.
- [58] R. Garvie, C. Urbani, D. Kennedy, J. McNeuer, Biocompatibility of magnesia-partially stabilized zirconia (Mg-PSZ) ceramics, *Journal of Materials Science* 19(10) (1984) 3224-3228.
- [59] T. Sato, S. Ohtaki, T. Endo, M. Shimada, CHANGES IN CRYSTALLINE PHASE AND MICROSTRUCTURE ON THE SURFACE OF YTTRIA-DOPED TETRAGONAL ZIRCONIA POLYCRYSTALS(Y-TZP) BY ANNEALING IN HUMID CONDITIONS, *Advances in ceramics* 24 (1986) 501-508.

- [60] M. Hirano, E. Kato, Preparation of tetragonal zirconia ceramics in ZrO₂-Sc₂O₃ system by hydrolysis and homogeneous precipitation and their phase stability, *Journal of the Ceramic Society of Japan* 105(1217) (1997) 37-42.
- [61] L. Preiss, Nouvelles prothèses intervertébrales en composite céramique : étude des matériaux, mise en place d'un test multiphysique in vitro et analyse de performances, INSA-Lyon, LYON, 2016.
- [62] L. Gremillard, Biocéramiques: des monolithes aux composites, INSA de Lyon; Université Claude Bernard-Lyon I, 2009.
- [63] J. Li, L. Zhang, Q. Shen, T. Hashida, Degradation of yttria stabilized zirconia at 370 K under a low applied stress, *Materials Science and Engineering: A* 297(1) (2001) 26-30.
- [64] V. Lughi, V. Sergo, Low temperature degradation -ageing- of zirconia: A critical review of the relevant aspects in dentistry, *Dental Materials* 26(8) (2010) 807-820.
- [65] F. Zhang, M. Inokoshi, K. Vanmeensel, B. Van Meerbeek, I. Naert, J. Vleugels, Lifetime estimation of zirconia ceramics by linear ageing kinetics, *Acta Materialia* 92 (2015) 290-298.
- [66] L. Hallmann, A. Mehl, P. Ulmer, E. Reusser, J. Stadler, R. Zenobi, B. Stawarczyk, M. Özcan, C.H. Hämmerle, The influence of grain size on low-temperature degradation of dental zirconia, *Journal of Biomedical Materials Research Part B: Applied Biomaterials* 100(2) (2012) 447-456.
- [67] M. Inokoshi, F. Zhang, J. De Munck, S. Minakuchi, I. Naert, J. Vleugels, B. Van Meerbeek, K. Vanmeensel, Influence of sintering conditions on low-temperature degradation of dental zirconia, *Dental Materials* 30(6) (2014) 669-678.
- [68] A. Paul, B. Vaidhyanathan, J.G. Binner, Hydrothermal Ageing Behavior of Nanocrystalline Y-TZP Ceramics, *Journal of the American Ceramic Society* 94(7) (2011) 2146-2152.
- [69] A. Suresh, M.J. Mayo, W.D. Porter, C.J. Rawn, Crystallite and Grain-Size-Dependent Phase Transformations in Yttria-Doped Zirconia, *Journal of the American Ceramic Society* 86(2) (2003) 360-362.
- [70] J. Eichler, J. Rödel, U. Eisele, M. Hoffman, Effect of Grain Size on Mechanical Properties of Submicrometer 3Y-TZP: Fracture Strength and Hydrothermal Degradation, *Journal of the American Ceramic Society* 90(9) (2007) 2830-2836.
- [71] S. Jansen, A.J. Winnubst, Y. He, H. Verweij, P.T. Van der Varst, G. De With, Effects of grain size and ceria addition on ageing behaviour and tribological properties of Y-TZP ceramics, *Journal of the European Ceramic Society* 18(5) (1998) 557-563.
- [72] S. Deville, Etude des mécanismes de renforcement et de dégradation des céramiques biomédicales à base de zircon: du macroscopique au nanoscopique: contribution de la microscopie à force atomique, Villeurbanne, INSA, 2004.
- [73] J.F. Li, R. Watanabe, Phase Transformation in Y₂O₃-Partially-Stabilized ZrO₂ Polycrystals of Various Grain Sizes during Low-Temperature Ageing in Water, *Journal of the American Ceramic Society* 81(10) (1998) 2687-2691.
- [74] E.P. Butler, A.H. Heuer, Grain-Boundary Phase Transformations During Ageing of a Partially Stabilized ZrO₂-A Liquid-Phase Analogue of Diffusion-Induced Grain-Boundary Migration (DIGM)(?), *Journal of the American Ceramic Society* 68(4) (1985) 197-202.
- [75] L. Gremillard, J. Chevalier, T. Epicier, G. Fantozzi, Improving the Durability of a Biomedical-Grade Zirconia Ceramic by the Addition of Silica, *Journal of the American Ceramic Society* 85(2) (2002) 401-407.
- [76] X. Guo, J. He, Hydrothermal degradation of cubic zirconia, *Acta Materialia* 51(17) (2003) 5123-5130.
- [77] K. Matsui, H. Horikoshi, N. Ohmichi, M. Ohgai, H. Yoshida, Y. Ikuhara, Cubic-Formation and Grain-Growth Mechanisms in Tetragonal Zirconia Polycrystal, *Journal of the American Ceramic Society* 86(8) (2003) 1401-1408.

[78] W. Zhu, Effect of cubic phase on the kinetics of the isothermal tetragonal to monoclinic transformation in ZrO_2 (3mol% Y_2O_3) ceramics, *Ceramics international* 24(1) (1998) 35-43.

Chapter 2:

Influence of applied and internal stresses on zirconia hydrothermal ageing

Chapter 2. Influence of applied and internal stresses on zirconia hydrothermal ageing

2.1 Common Introduction

Since the failure events of Prozyr® femoral heads in 2001–2002 occurred, the studies of the ageing behavior of zirconia ceramics has become the topic of many works. Hydrothermal ageing (also called LTD for Low Temperature Degradation) is a low temperature tetragonal-to-monoclinic phase transformation ($t \rightarrow m$) that occurs on the surface of zirconia ceramics in humid environment. This ageing process is strongly influenced by microstructural parameters (such as stabilizer nature and content, density, surface finish, grain size, cubic phase content, etc.) and mechanical stresses. This work focuses on the influence of both applied and internal stresses on the hydrothermal ageing behavior, which is not yet completely understood [1].

The present works study respectively the influence of residual stress, applied stress and internal stress on ageing process of zirconia ceramics. The applied stress is achieved by bending tests, and the ageing kinetics behavior of different types stress surfaces of different samples (3Y-TZP, 4Y-TZP) was investigated by XRD detection. The internal stress is obtained by making a composite ZTA of alumina and zirconia, and the ageing kinetics behavior of different sizes zirconia aggregates was investigated by XRD and Micro-Raman spectroscopy detection. The main goal is to explain the influence mechanism of stress on the ageing kinetics behavior, in order to predict the ageing life of zirconia ceramics under different stress.

2.2 The influence of applied and residual stresses on hydrothermal ageing of 3Y- and 4Y- stabilized zirconia

Influence des contraintes sur les cinétiques de vieillissement hydrothermal de zircons stabilisés à l'yttrium (3Y- et 4Y-)

This work was published in the Journal of the European Ceramic Society:

C. Wei, L. Gremillard, *The influence of stresses on ageing kinetics of 3Y- and 4Y- stabilized zirconia*, Journal of the European Ceramic Society, 2018, 38 (2), pp. 753-60, <https://doi.org/10.1016/j.jeurceramsoc.2017.09.044>

Abstract

Hydrothermal ageing is one of the most important limiting factors for the use of yttria-stabilized zirconia ceramics in contact with water-containing environments. It consists in the transformation of tetragonal phase to monoclinic phase, initiates on the surface of zirconia in the presence of water, and leads to roughening and potentially to micro-cracking and loss of integrity. The present work seeks to explore the influence of applied and residual mechanical stresses on the ageing kinetics of 3Y- and 4Y-TZP. Residual stresses were obtained by rough polishing, and removed on some samples by annealing. All samples were submitted to *in situ* 3-points bending tests in water vapour atmosphere inside an autoclave at 134°C, allowing surfaces with a mechanical stress gradient to be exposed to hydrothermal ageing. The evolution of the monoclinic fraction with time and stress was then analyzed using Mehl-Avrami-Johnson equation.

Résumé

Le vieillissement hydrothermal est un des facteurs les plus importants limitant l'utilisation des zircons stabilisés à l'yttrium en milieu humide. Il s'agit d'une transformation de la phase quadratique vers la phase monoclinique, sur les surfaces exposées à l'eau, et qui mène à une augmentation de la rugosité et potentiellement à l'apparition de microfissuration et une perte d'intégrité des pièces. Ce chapitre explore l'influence des contraintes appliquées et des contraintes internes sur les cinétiques de vieillissement de zircons (3Y-TZP et 4Y-TZP). Les contraintes résiduelles ont été obtenues par une rectification grossière, suivie d'un polissage léger. Sur une partie des échantillons, ces contraintes résiduelles ont été éliminées par recuit. Les échantillons ont ensuite été soumis à une sollicitation en flexion trois points sous atmosphère de vapeur d'eau (à l'intérieur d'un autoclave à 134°C), permettant le vieillissement de surfaces exposées à un gradient de contraintes. L'évolution du taux de phase monoclinique avec le temps a finalement été analysé en utilisant le formalisme de Mehl-Avrami-Johnson.

Nous avons conclu que les effets des contraintes sur le vieillissement de la zircone devaient être examinés en considérant trois types de contraintes :

- Les contraintes résiduelles (ici, des contraintes de traction en surface de l'ordre du GPa, et des micro-distorsions importantes) ;
- Les contraintes appliquées (ici, des contraintes uniaxiales (traction ou compression) entre -600 et +600 MPa, appliquées par le dispositif de flexion 3 points ;
- Les contraintes générées par la transformation quadratique-monoclinique (plusieurs MPa dans la littérature)

En général, les contraintes générées par la transformation et les contraintes résiduelles sont plus grandes que les contraintes appliquées. L'effet des contraintes appliquées n'en est pas moins mesurable : nous avons observé une accélération du vieillissement avec l'augmentation de la contrainte appliquée (qu'elle soit de traction ou de

compression). L'effet des contraintes résiduelles est aussi très marqué : en particulier, sur la 4YTZP, nous avons observé un très fort ralentissement du vieillissement lorsque les contraintes résiduelles sont éliminées par recuit. Enfin, nous avons montré que la vitesse de germination de la phase monoclinique augmente en présence de contraintes appliquées ou résiduelles, alors que la dépendance de la vitesse de croissance à la contrainte est beaucoup plus complexe.

2.2.1 Introduction

For the effect of stress on hydrothermal ageing, Schmauder and Schubert [2] showed that hydrothermal ageing does not occur in stress-free grains of zirconia, but starts at the surface of Y-TZP in the presence of water vapor and stresses. It is explained by Schubert and Frey [3] that when the water radicals penetrate into the oxygen vacancy present in the zirconia lattice, a lattice contraction occurs, causing tensile micro-stresses that lead to nucleation of the phase transformation. On the contrary, using DFT studies, Gebressilassie showed that the penetration of water in the zirconia lattice does not lead to lattice contraction, but rather to decrease of the energy barrier for the t-m transformation [4]. Both these studies hint to an influence of stresses on hydrothermal ageing, either directly [2] or through energetic considerations [4]. Indeed, Li et al. showed that a small applied tensile stress accelerates the ageing process of zirconia and a compressive stress has little effect on the degradation in hot water (97°C) [5]. However Lughì et Sergo [6] indicated that tensile stresses of the order of some hundreds MPa are sufficient to promote LTD. Deville[7] indicated that the ageing sensitivity of zirconia is directly linked to the type (compressive or tensile) and amount of residual stresses.

The present work seeks to relate the presence of residual and applied stresses to the ageing process of different zirconia ceramics (3Y and 4Y-TZP). In particular, since ageing proceeds by a nucleation and growth mechanism [8-11], the ageing kinetics are currently described using a Mehl-Avrami-Johnson (MAJ) equation. Previous works could relate some parameters of the MAJ equation to the nucleation rate and growth rate of the monoclinic phase [10, 11]. Thus by observing changes on these parameters, the present work will also seek to determine how the presence of mechanical stresses can influence the nucleation and growth rates.

2.2.2 Materials and methods

2.2.2.1. Material preparation

The experimental flowchart is summarized in figure 1. The samples were fabricated starting from three different ultra-pure Y-TZP powders (TZ3YS, TZ3YE, TZ4YS, Tosoh, Japan). TZ3YS and TZ3YE contain 3 mol.% yttria (in addition, TZ3YE contains 0.25 wt.% Al_2O_3). TZ4YS contains 4 mol.% yttria. The zirconia green bodies used in the present study were prepared by slip casting. The slurries were prepared by mixing the powders in water (70 wt.% solid content) using Darvan 821A as a dispersing agent (1.2 wt.% as compared to the weight of powder), and ball-milling with 3Y-TZP balls for 24 hours. They were then cast in a plaster mold, left to dry first in the mold for 24 hours then in air for at least one week. After drying, the cast green bodies were sintered in a programmable electrical furnace (sintering conditions chosen from previous experience to reach full density: debinding at 550 °C for 5h (heating rate 1°C/min); sintering at 1430°C for 5 h (heating and cooling rate 5°C/min)). The sintered samples were then shaped as plates (1.2×20×60 mm for $s_{max} \leq 300$ MPa, 1.2×20×25 mm for $s_{max} > 300$ MPa) and polished (using diamond abrasive decreasing in size down to 1 µm). Finally, half of the polished samples were annealed (1250°C for 0.5h at heating rate of 5°C/min according to a published procedure [12, 13]) in order to remove residual stresses. The “polished only” samples will be called xYzP, where x is 3 or 4 (mol% of yttria) and z is E or S (nature of the powder), while the annealed samples will be called xYZA, as shown in Table 2-1.

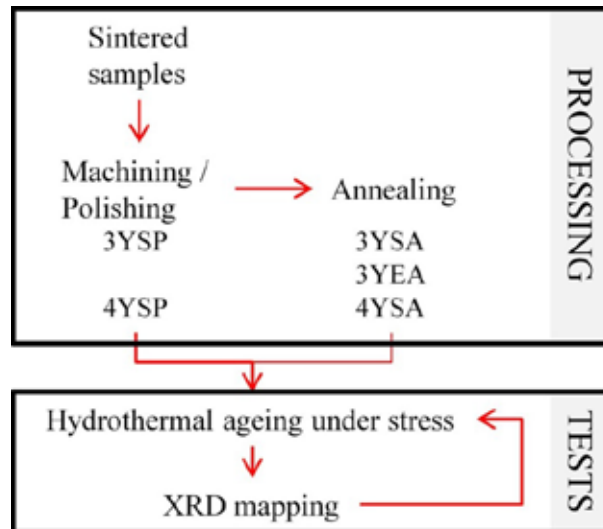


Fig.2-1 Experimental flow chart

2.2.2.2 Bending test

This study uses three-points bending test to apply a stress gradient on the zirconia plates. Dedicated sample holders were designed, able to perform 3-points bending tests under constant load inside an autoclave (Fig.2-2). The positioning accuracy of the sample in the sample holder is estimated to ± 1 mm. The load is applied manually through a screw, while the deflection is measured by an external LVDT sensor until the desired deflection is reached. The desired deflection is calculated after the desired maximum applied stress (s_{max} , between 100 and 600 MPa) using the following equation:

$$\sigma_{max} = E\varepsilon = \frac{6E\delta h}{l^2} \quad (2-1)$$

Where s_{max} is maximum stress of sample surface, E is flexural modulus of elasticity (200 GPa), ε is the maximum strain in the outer surface, δ is the deflection, h is the sample thickness, and l is distance between external rollers (50 mm for s_{max} up to 300 MPa, 20 mm for s_{max} 350 or 600 MPa).

The upper surface was in compression, the lower one in tension. The applied stress decreased linearly from $\pm s_{max}$ (in the center of the plate, under the central roller) to 0 (under the external rollers and further). Finally the stress distribution of each side of the sample under bending test is visualized in Fig. 2-3.

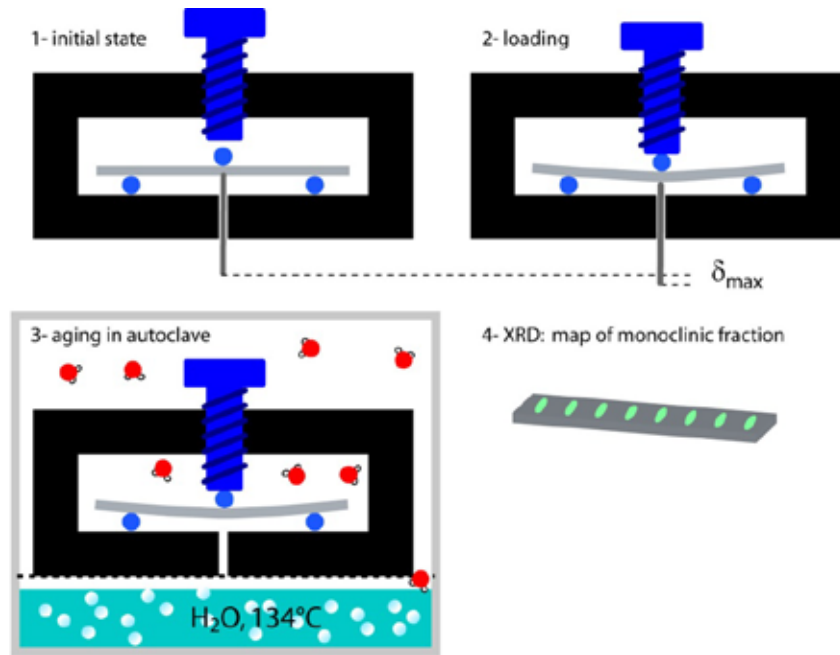


Fig.2-2 Experimental process for the study of applied stress

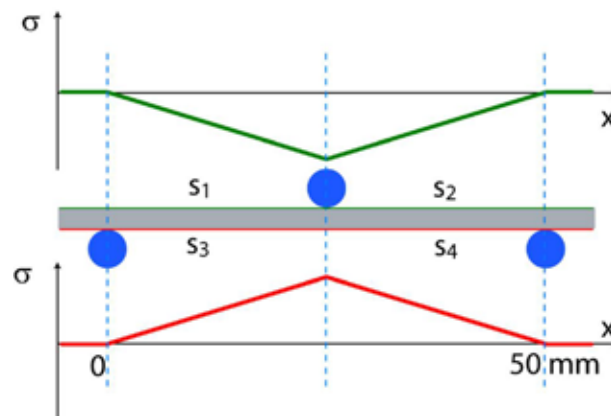


Fig.2-3 Applied stress distribution on both sides of the sample under bending

Table 2-1. Samples prepared for the study of applied stress

	Polished sample	Annealed sample
s_{\max} (MPa)	100	100, 300, 350 and 600
TZ3Y-S	3YSP	3YSA
TZ3Y-E		3YEA
TZ4Y-S	4YSP	4YSA

2.2.2.3 Microstructures and residual stresses

The residual stresses were quantified by x-ray diffraction (XRD, D8 advance Diffractometer (Bruker, Germany) with $K\alpha$ radiations, in Bragg-Brentano configuration), associated with Rietveld refinement (Topas 4.0 software, Bruker, Germany). Rietveld refinement was conducted with the fundamental parameters approach. This allowed

both the quantification of the different phases, the determination of their lattice parameters (from which the yttrium amount inside each phase was determined using Scott's calibration curves [14]), and the determination of crystallite size (parameter CrySize_L) and residual microstress s_m (calculated as: $\sigma_\mu = \frac{\pi \times E \times \text{strain}_G}{360}$, with E the Young modulus (taken here at 200 GPa)).

2.2.2.4 Assessment of the ageing kinetics

Every few hours, the samples were removed from the autoclave and unloaded. Then a cartography of the amount monoclinic phase was obtained by X-ray diffraction: the samples were mounted on an X-Y-Z moving stage, their long axis along the X axis. XRD measurements were performed every 2 mm along the X axis (at constant and adequate Y and Z), to get a determination of the monoclinic fraction versus position, thus versus applied load during ageing. To get a high enough signal/noise ratio, the width of the analyzed area was around 5 mm, preventing the detection of rapid changes. XRD patterns were recorded in the 27-33° (2 θ) range with a scan speed of 0.2 min⁻¹ and a step size of 0.05°. The monoclinic ZrO₂ phase content (V_m) was expressed after Toraya's equation [15]:

$$V_m = \frac{1.311X_m}{1 + 0.311X_m} \quad (2 - 2)$$

In which the value of X_m was calculated using Garvie and Nicholson method [16]:

$$X_m = \frac{I_m^{-111} + I_m^{111}}{I_m^{-111} + I_m^{111} + I_t^{101}} \quad (2 - 3)$$

Where I_p^{hkl} is the area of the diffraction peak related to the (hkl) plane of phase p (m for monoclinic and t for tetragonal).

For each sample, the knowledge of V_m versus time and stress allowed plotting ageing kinetics at different stress levels, further analyzed using the MAJ formalism.

2.2.3. Results

2.2.3.1 Determination of residual stresses

Fig. 2-4 shows details of the XRD measurements conducted on 3YSA, 3YSP, 4YSA and 4YSP samples. Only tetragonal and cubic phases were detected in the annealed samples. The XRD diagrams of the polished samples showed two main differences with the ones for annealed samples: apparition of monoclinic phase, and distortion of the highest peaks (shoulder indicated by an arrow at the left of the main peaks), which was interpreted as the presence of a distorted tetragonal phase [13] (no fit by orthorhombic phase was possible on these peaks). Unfortunately the angular resolution is not high enough to separate clearly the different convoluted peaks, thus to fit with absolute certainty the cubic and distorted tetragonal phases, but it seems the amount of cubic phase remains constant after annealing (~24% for 3YS, ~43% for 4YS), and while cubic phase gets slightly less distorted (lower second order strains after annealing). The distorted tetragonal phase presents lattice parameters between 1 and 2% larger than the tetragonal phase. An accurate analysis of its crystallite size and microstress is impossible.

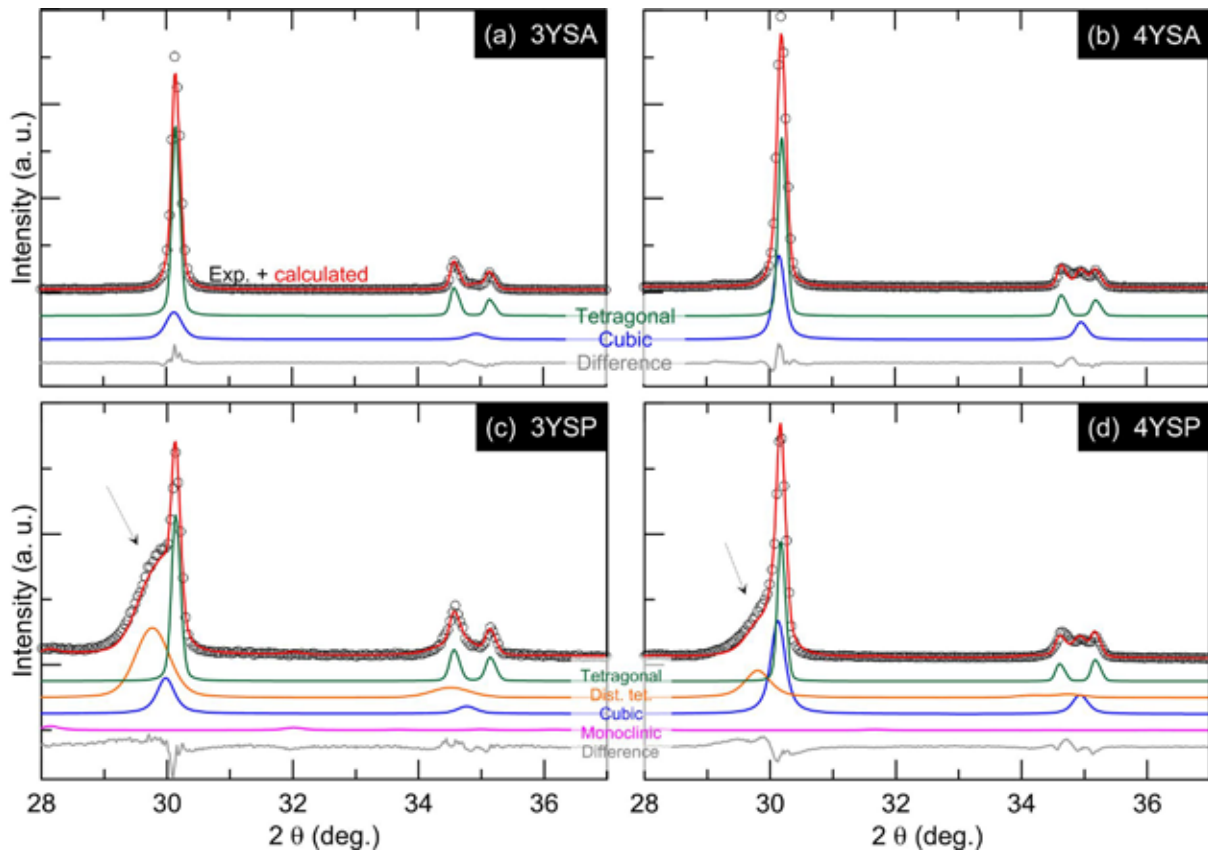


Fig. 2-4: XRD and Rietveld refinement of the different materials.

The tetragonal phase was hardly affected by annealing: the crystallite size remains identical (~300 nm for 3YS, ~600 nm for 4YS), the lattice parameters hardly change (a_t undergoes a slight increase (0.02%) while c_t undergoes a slight decrease (-0.01%) for both materials) and a small decrease of the microstress was seen (from ~600 MPa in polished zirconias to ~450 MPa in annealed ones). All these microstructural parameters are summarized in table 2-2 (it should be kept in mind that these measurements could be conducted on one location of one sample only for each material, thus their outcomes should be considered as order of magnitudes rather than precise values).

Table 2-2. Structural and microstructural parameters of 3YS and 4YS materials. Figures indicated are speculative due to the high convolution of the XRD peaks of the different phases (in particular Cubic and Distorted tetragonal)

parameter		3YSA	3YSP	4YSA	4YSP
Tetragonal phase	a_t (nm)	0.36044	0.36038	0.36054	0.36043
	c_t (nm)	0.51780	0.51786	0.51782	0.51781
	% Y_2O_3	2.50	2.40	2.70	2.48
	Cryst. Size (nm)	300	290	630	660
	Microstress (s_m MPa)	460	630	460	580
Distorted	a_{t-d} (nm)		0.36648		0.36481

tetragonal phase	c_{t-d} (nm)		0.51864		0.52450
	Cryst. Size (nm)		67		30
	Microstress (s_m MPa)		3600		1700
	Stress vs t-phase		2300		2450
	a_c (nm)	0.51291	0.51507	0.51328	0.51328
Cubic phase	Cryst. Size (nm)	67	39	77	52
	Microstress (s_m MPa)	1200	870	640	750
	tetragonal	76	46	56	35
Weight %	Distorted tetragonal	0	24	0	21.5
	Cubic	24	25	44	42
	Monoclinic	0	5	0	1.5

2.2.3.2 Ageing of 3Y-TZP

Fig. 2-5 shows the variation of the surface monoclinic fraction with applied stress on 3YS samples at different ageing time. A high variability in the monoclinic fraction can be seen (error bars are the standard deviation from measurements taken on at least 2 locations on 2 samples). Larger error bars are seen around 0 stress, the location of 0-stress point on the samples are on both extremities, and thus subjected to more positioning error during XRD measurements. Moreover, the control over residual stresses is far from perfect (since they are obtained indirectly by machining and polishing), and this result in increased scattering of the measurements in 3YSP (and later 4YSP) samples.

A comparison between Fig. 2-5(a) (3YSP) and Fig. 2-5(b) (3YSA) shows that the residual stresses (generated by machining and polishing) obviously accelerated the ageing process at short ageing times. Moreover, the monoclinic fraction on 3YSP (polished) sample surface increased with increasing stress (both tensile and compressive) even for small applied stresses (less than 60 MPa). The same trend was also present, although less significant for 3YSA (annealed) sample, and it required higher applied stresses (more than 100 MPa). Finally, the effect of applied stresses tends to disappear as hydrothermal ageing progresses: flat V_m -stress profiles are observed for 3YSP after 35 h ageing, and for 3YSA after 10h ageing (even before saturation of the transformation).. In addition, the presence of residual or applied stresses doesn't changes the maximum zirconia monoclinic fraction (V_{max}), as can be seen in Fig. 2-6, but only the ageing rate.

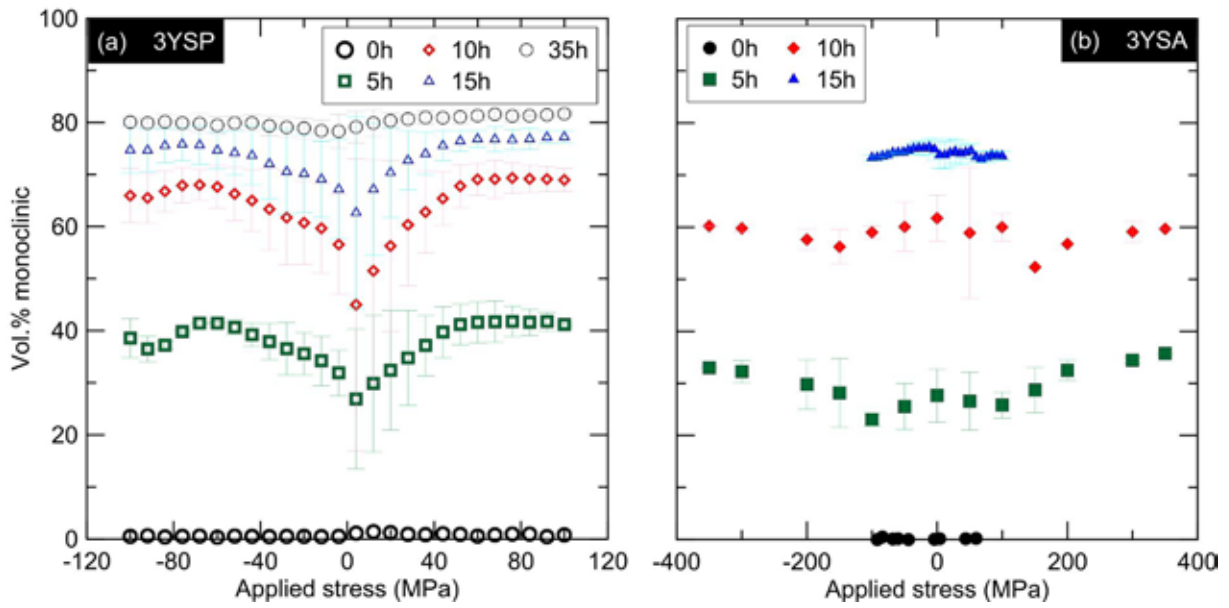


Fig. 2-5 XRD monoclinic fraction measured vs. applied stress on the surface at different ageing time: a.3YSP; b.3YSA. Error bars represent the standard deviation of measurements taken on at least two locations on two samples.

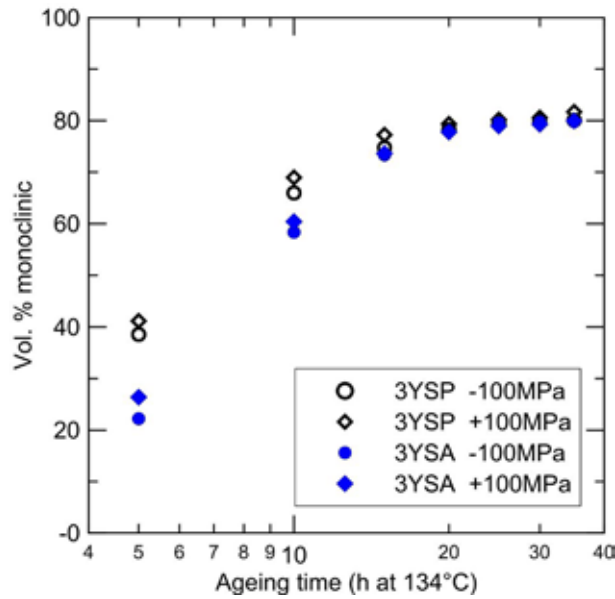


Fig. 2-6. XRD monoclinic fraction measured versus ageing time of 3YS samples

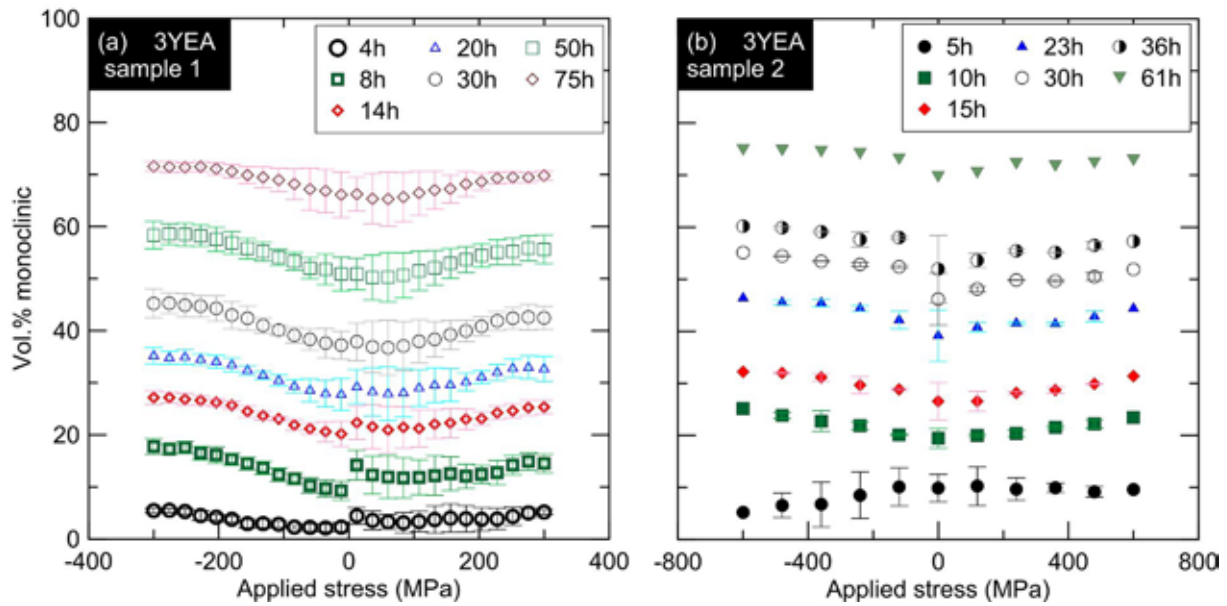


Fig. 2-7. XRD monoclinic fraction measured vs. applied stress on the surface of 3YEA; (a) sample #1; (b) sample #2; when present, error bars represent the standard deviation over 2 measurements on 1 sample.

For 3YEA sample (Fig. 2-7), increasing both compressive and tensile stresses during ageing resulted in increasing slightly the monoclinic fraction. Compared with the 3YS sample, ageing of 3YE is less impacted by applied stress. However, for 3YE samples the effect of applied stresses does not disappear when ageing time increases, at least up to 75 h ageing at 134°C.

Finally, Fig.2-8 (a) and (c) show the evolution of the XRD diagram of 3YSA and 3YSP during ageing. In particular, for both materials cubic phase remains unaffected by ageing, while both tetragonal and distorted tetragonal phases are transformed to monoclinic during the ageing process.

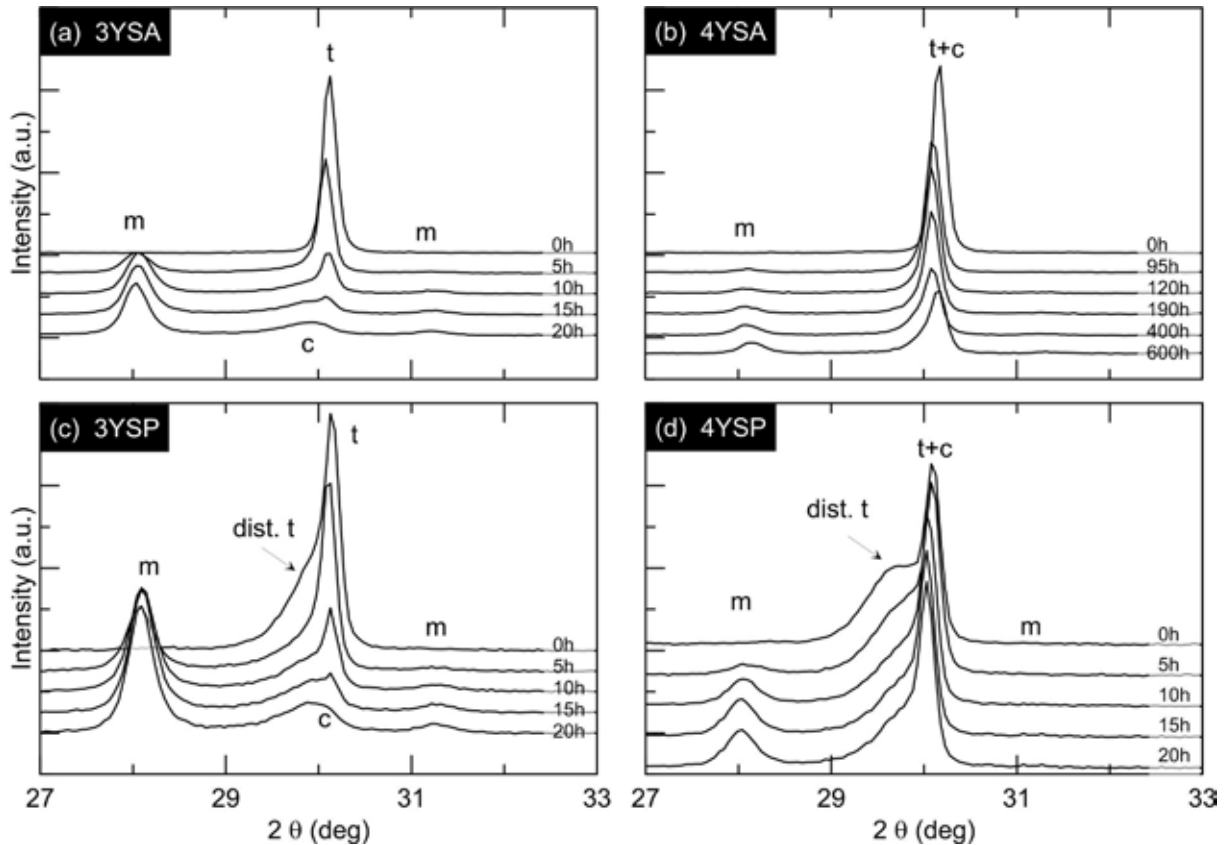


Fig. 2-8 Evolution of XRD diagrams of 3YSA (a), 4YSA (b), 3YSP (c) and 4YSP (d) with ageing time at 134°C.

2.2.3.3 Ageing of 4Y-TZP

Fig.2-9 shows the monoclinic fraction measured vs. applied stress on the surface of 4YS-TZP samples at different ageing time. 4YSP samples present a rather similar behavior than 3YSP ones (although longer ageing times are necessary), with tensile and compressive stresses increasing the monoclinic fraction at the beginning of ageing process. However, the large variability makes these evolutions not very statistically relevant. Ageing of 4YSA samples seemed to be the fastest when no stress is applied. It was slower and slower as tensile stresses increased. With increasing compressive stress the transformation rate first decreased then started to increase again for large compressions stresses (lower than -50 MPa), while always staying lower than the transformation rate of the non-loaded material. As can be seen on Fig. 2-10, residual stresses (generated by machining and polishing) greatly accelerated the ageing process (the process is about 20 times faster in polished samples than in annealed samples) of 4Y-TZP.

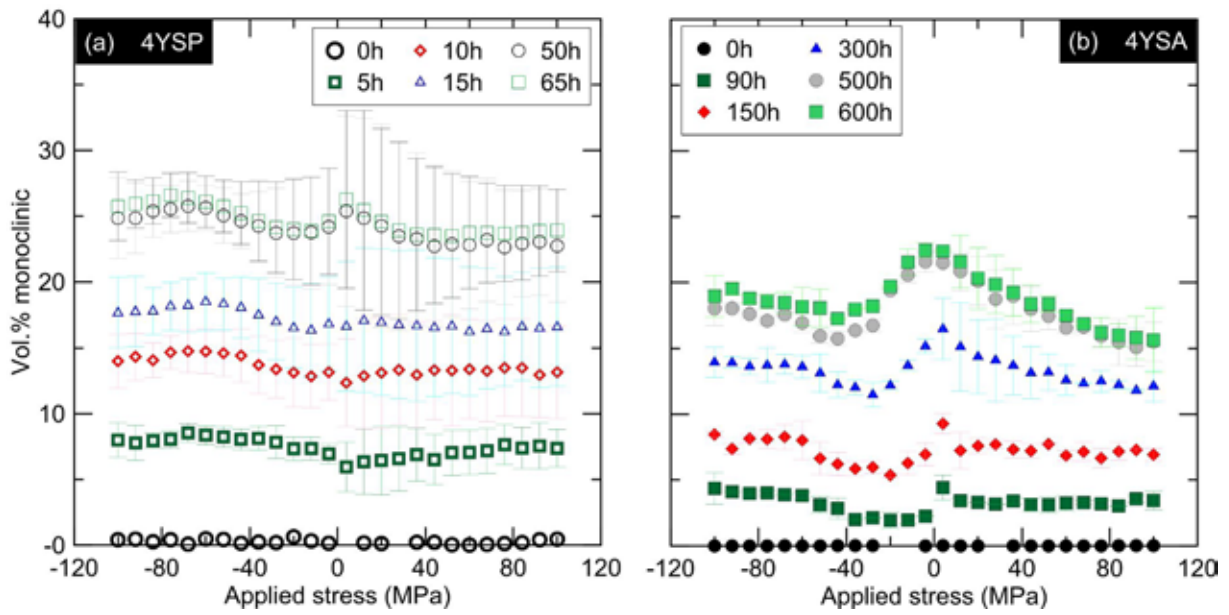


Fig. 2-9 XRD monoclinic fraction measured vs. applied stress on the surface of 4YS-TZP samples. a. 4YSP samples (aged for up to 65h), b. 4YSA (aged for up to 600 h).

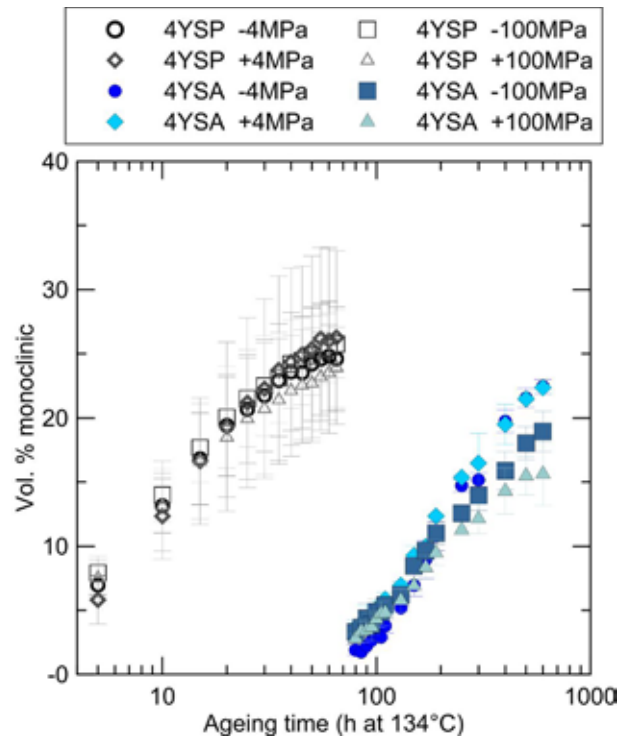


Fig. 2-10 XRD monoclinic fraction measured versus ageing time of 4YS samples

Fig.2-8 (b) and (d) show that in 4YSP, the distorted tetragonal phase is the first to transform, while the tetragonal phase slowly decreases.

2.2.4 Discussions

Microstructural evolutions with annealing

The microstructural evolutions observed after annealing point to the resorptions of the distorted tetragonal phase and of the monoclinic phase. The small changes in the lattice parameters of tetragonal phases are compatible with small increase of the Y₂O₃ content in tetragonal grains (from 2.4% to 2.5% in 3YS, from 2.5% to 2.7% in 4YS). This is coherent with ZrO₂/Y₂O₃ phase diagram that shows more yttria in the tetragonal phase at 1250°C (annealing temperature) than at 1430°C (sintering temperature). However, this should be considered carefully, since machining and polishing induce large stresses that may affect the lattice parameters of all phases. Thus the lattice parameter of the stress-free phases of the polished samples is not known, thus the determination of yttria content in the tetragonal phase of polished samples is not precise at all. On plasma-sprayed zirconia, Lipkin *et al.* [17] saw no significant microstructural changes upon annealing with Hollomon–Jaffe parameter [18] lower than or equal to 45 000. In our case, because of the very short annealing time (0.5 h) HJP is around 40 000. As a consequence we chose to consider that annealing does not change the yttria content, thus that the differences between annealed and polished samples mainly come from the presence of residual stresses.

Macroscopic effect of stresses at long ageing times

At long ageing time, the effect of stresses on ageing seems to disappear. This might be due to two different phenomena. The first one is a measurement artifact related to saturation of the monoclinic fraction: on the one hand, the monoclinic fraction cannot get higher than the initial tetragonal content (if one considers the presence of non-transformable cubic phase); on the other hand, once the volume accessible by XRD is completely transformed, no more evolution of the transformation can be detected by XRD. Thus once saturation is reached, it is obvious that the monoclinic fraction will be independent of applied stress, since it will be at its maximum. The second phenomenon is related to the interplay of residual, applied and t-m transformation-generated stresses[19]: since t-m transformation is accompanied by large volume increase, it gives rise to large stresses that will be superimposed to the existing stress field. Zhang *et al.* [19] found large shifts of the Raman peaks, compatible with tensile stresses, in the tetragonal zone just below the transformed zone. Taking into account the piezospectroscopic coefficients available in the literature [20], these shifts correspond to tensile stresses around 700 MPa, higher than the applied stresses. Thus t-m transformation-generated stresses also influence further ageing, and may become preponderant when the transformed layer is thick enough (Zhang’s article deals with transformed depth about 25 µm, whereas we are limited here to 5 µm or less since we hardly reach saturation).

Effect of stresses on ageing kinetics

In order to understand the influence of applied stress on ageing kinetics of zirconia, all ageing kinetics were fitted using the Mehl–Avrami–Johnson (MAJ) laws (Eq. 2-4).

$$\frac{V_m - V_0}{V_{max} - V_0} = 1 - \exp(-(bt)^n), \quad b = b_0 \exp\left(-\frac{Q}{RT}\right) \quad (2 - 4)$$

where V_m is the monoclinic phase content measured after an exposure of t hours to steam at absolute temperature T, V₀ and V_{max} are the initial and saturation levels of monoclinic phase content, n is an exponent that depends on both nucleation and growth kinetics of the monoclinic phase [10]. b is thermally activated (with Q the activation energy, R the gas constant, and T the absolute temperature). The use of MAJ law derives from the fact that ageing follows a nucleation and growth process. According to previous works, in the MAJ formulation for zirconia ageing the parameter b is proportional to (N_R.a_D³)^{1/4}, where a_D is the growth rate of monoclinic spots diameter and N_R is the nucleation rate (if one assumes that the growth rates of monoclinic spot are proportional in diameter and in height, which is the case due to the crystallography of the t-m transformation). The exponent n depends on the ratio between monoclinic phase created during the growth phase and monoclinic phase created during the nucleation phase. If n remains in the [0.5; 2.5] range, it can be approximated as

$$n \gg 1 + \frac{3}{4} \log \frac{\alpha a_D \dot{\sigma}}{C N_R D^2 \dot{\sigma}} \quad (\text{extrapolated from [11]}) \quad (D \text{ is the size of the monoclinic nuclei and can be assimilated})$$

to the grain size). Thus for a constant grain size (constant D , as it is the case for a same material submitted to different stress levels) one can deduce schematic evolutions of n and b from those of a_D and N_R :

- 1- If a_D and N_R vary in the same proportions, n remains constant while b varies (b increases if a_D and N_R increase).
- 2- If N_R remains constant and a_D increases, both n and b increase.
- 3- If N_R remains constant and a_D decreases, both n and b decrease.
- 4- If N_R increases and a_D remains constant, b increases and n decreases
- 5- If N_R decreases and a_D remains constant, b decreases and n increases.

Reciprocally, one can deduce the evolutions of a_D and N_R from those of n and b by Eq. (2-5):

$$a_D = C_a \cdot b \cdot 10^{\frac{n-1}{3}} \quad \text{and} \quad N_R = C_N \cdot b \cdot 10^{1-n} \quad (2-5)$$

Here C_a and C_N are constants, and only depend on the material via the grain size. They can be calculated as:

$$C_a = \frac{\sqrt{D}}{K} \quad \text{and} \quad C_N = \frac{1}{KD^{3/2}}, \quad \text{with} \quad K = \sqrt[4]{\frac{\rho}{48kl}}, \quad K \text{ being the linear expansion due to the t-m phase}$$

transformation (~1.3%) and l being the depth on which the monoclinic fraction is averaged (~5 μm , if the monoclinic fraction is measured by X-ray diffraction)

Fig. 2-11 shows the evolutions of n and b with applied stress for all materials studied here.

Comparing the polished to annealed samples, both without applied stress, one can infer that residual stress (generated by machining and polishing) can reduce n and increase b , especially for 4YS, which results in accelerated ageing. This is compatible with a higher nucleation rate and a constant growth rate, as in case 4 above. Thus the presence of residual stresses would increase the nucleation rate.

In the annealed samples, applied tensile stress has no significant effect on the value of n , but increases the value of b . This indicates a constant nucleation / growth ratio, but an overall faster transformation rate: similarly to case 1 above, tensile stresses seem to increase the nucleation and growth rates by the same ratio. Still in the annealed samples, applied compressive stress can increase the value of n relative to the tensile stress, while b remains in all cases approximately constant. However, for different materials, the value of n and b show different variation as the compressive stress increases. For 4YSA, n decreases with the increase of compressive stress, while b remains constant around 0.004. For 3YSA, n first increases and then decreases with the increase of compressive stress, and b is fluctuating between 0.115 ± 0.003 with varying compressive stress. For 3YEA, n is fluctuating around 1.0 ± 0.1 with varying applied stress (at ~-50MPa (compressive stress) n is slightly higher than for other applied stresses), while b increases with increasing applied stress.

Fig.2-12 shows the evolutions of a_D and N_R with applied stress for all materials studied. For 4YS samples, residual stresses (generated by machining and polishing) greatly increase the nucleation rate and growth rate, and their nucleation rate increases with the increase of loading stress, while their growth rates have been fluctuating respectively at 0.057 ± 0.003 (polished sample) and 0.0048 ± 0.0004 (annealed sample) being mostly independent on applied stresses. For 3YS samples, residual stresses greatly increase the nucleation rate, but reduce the growth rate. In 3YSA sample, tensile stress (≤ 100 MPa) increases the nucleation rate more than the compressive stress, but compressive stress increases the growth rate more than tensile stress. For 3YE samples, tensile stress increases the nucleation rate more than the compressive stress, and the growth rate is fluctuating around 0.018 ± 0.0015 with varying applied stress.

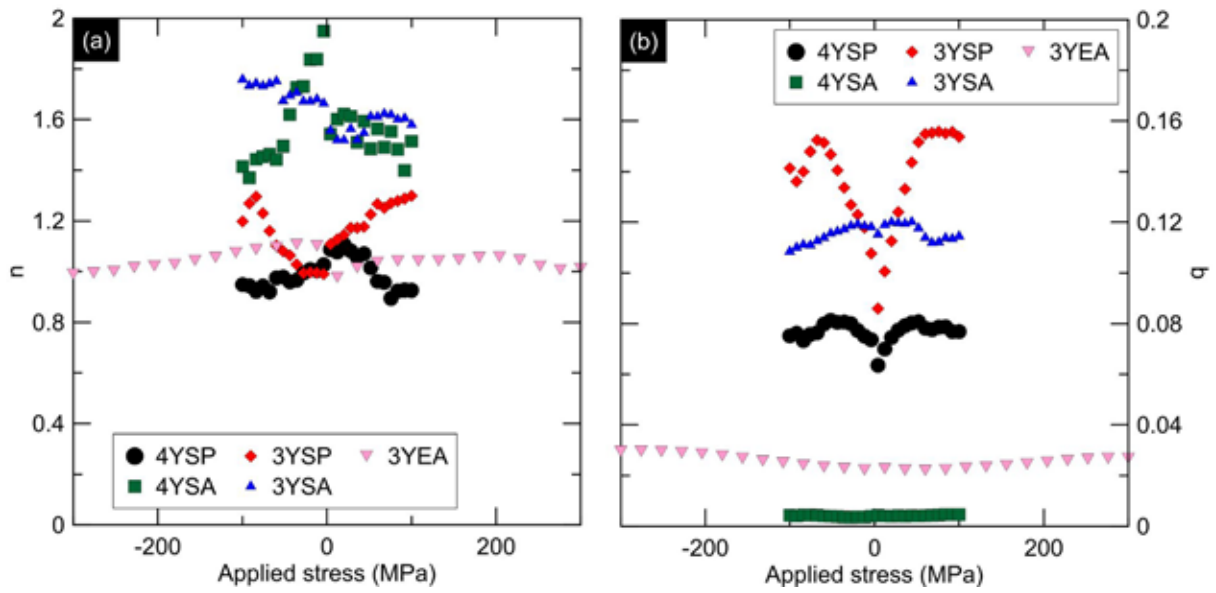


Fig.2-11 n , b in the MAJ equation for Y-TZP samples vs. applied stress. (a) shows the parameter n , (b) shows the parameter b .

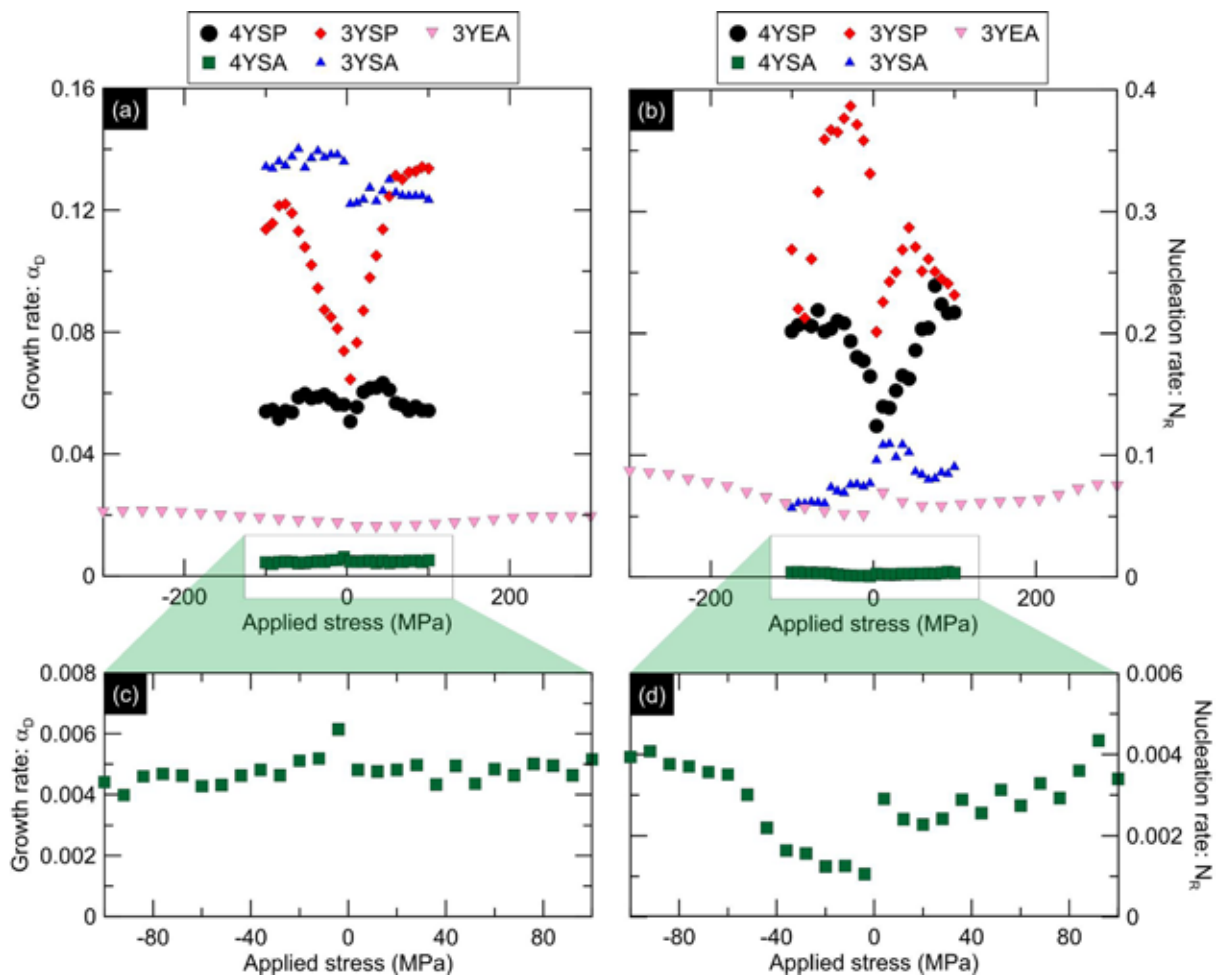


Fig.2-12 α_D and N_R for Y-TZP samples vs. applied stress.

Finally, one could explain the effect of applied stresses by the mechanism schematized in Fig.2-13. In our samples, there is no deformation when no external stress is applied. This means that residual stresses are in fact second-order stresses and should be perceived as the result of a distribution of microstrain (at the grain-size scale). High residual stresses (such as the ones obtained in polished samples, where tensile stresses higher than a GPa and large microstress were measured, see table 2-2) correspond to a wide distribution, while low residual stresses correspond to a narrower distribution. t-m phase transformation is sometimes described as being triggered when the local stress is higher than a critical stress σ_c^m [21]. With a large stress distribution, the probability that the residual stress locally exceeds σ_c^m is high. It is even higher if an applied stress is superimposed to the stress distribution. Figure 2-13(a) shows this effect: the continuous curve represents the residual stresses, that exceeds twice σ_c^m (full disks) while the dashed line represents the same residual stresses with a superimposed, constant stress, and exceeds 10 times σ_c^m . On the other hand, when the residual stress distribution is narrow, it may never exceed σ_c^m even in the presence of the same superimposed applied stresses (Fig.2-13 (b)). This explains why increasing stress can lead to increased nucleation and growth rates in polished samples but not in annealed samples (or at a lower degree).

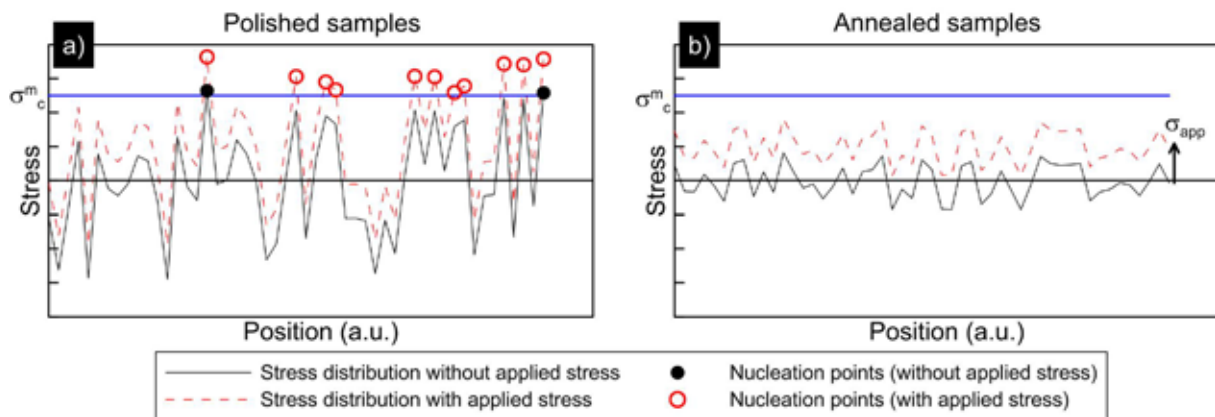


Fig. 2-13: Schematic effect of stresses on nucleation of monoclinic phase

Because the thermal activation energy of the combination of aluminum and vacancy (Al/Y/Zr-V_δ) is higher than Y/Zr-V_δ [22, 23], 3YE samples have a higher resistance to applied stress due to the doping of alumina than other samples during ageing process. 4YS samples, that contain more stabilizing ions (Y) than 3YS samples, have a greater number of the oxygen vacancies structures with low thermal activation energy (Y/Zr-V_δ), which in turn leads to a higher sensitivity to stress, or rather to mechanical energy brought by stress, than other samples.

2.2.5 Conclusion

The effect of stresses on hydrothermal ageing kinetics of zirconia should be examined considering three types of stresses: residual stresses (here tensile stresses due to machining and polishing, reaching the GPa as an order of magnitude, and microstresses), applied stresses (here between -600 and +600MPa, applied by a three points bending test apparatus), and t-m transformation-generated stresses. In general, transformation-generated stresses and residual stresses are larger than applied stresses. However, the effect of applied stresses was quite measurable: an acceleration of ageing with applied stress (both tensile and compressive) was observed. The effect of residual stresses was also obvious in 4YS samples: annealing these samples resulted in strongly decreasing residual stresses and strongly slowing the ageing process.

2.3 The influence of internal stresses on ZTA hydrothermal ageing

Etude des contraintes internes et du vieillissement dans des composites alumine-zircone

Abstract

Zirconia based bioceramics are often used in orthopaedic and dental implants. The low temperature degradation behaviour of zirconia under water environments is an important factor affecting the lifetime of zirconia-based biomaterials. ZTA (Zirconia-toughened alumina) composite is a representative of these materials. In this paper, the ZTA composites with zirconia inclusion particles with different sizes were obtained by different milling procedures, and the internal stress state and ageing behaviour of zirconia inclusions in the composites were studied by Raman analysis and XRD analysis. The results show that the zirconia particles are tensile in the composite, and that the tensile stress increases almost linearly with the local alumina amount around the inclusions. The polishing causes a slight transformation towards the monoclinic phase, reduces on average the residual stresses but causes a widening of their distribution, making it more likely the presence of zones under strong stresses.

Moreover, the maximum fraction of monoclinic phase after ageing seems to decrease when the internal stress increases. Finally, the incidence of cracking increases with the size of the zirconia inclusions.

Résumé

Les céramiques biocompatibles à base de zircone, telles les composites alumine-zircone (ZTA / *Zirconia Toughened Alumina*) sont très utilisées dans les implants orthopédiques et en implantologie dentaire. Leur vieillissement hydrothermal est le principal phénomène limitant leur utilisation.

Nous examinons ici le vieillissement de différents composites, de composition et microstructures contrôlées. En effet, sur ces matériaux obtenus par coulage en barbotine, en changeant la procédure de dispersion des poudres dans la barbotine nous avons obtenus plusieurs composites présentant des inclusions de zircone de tailles différentes. Sur ces composites, les contraintes résiduelles et le vieillissement hydrothermal ont été étudiés (par diffraction des rayons X et spectroscopie Raman).

Les résultats montrent que les particules de zircone sont en traction dans le composite, et que la contrainte de traction augmente presque linéairement avec le taux local d'alumine autour des inclusions. Le polissage provoque une légère transformation vers la phase monoclinique, diminue en moyenne les contraintes résiduelle mais provoque un élargissement de leur distribution, rendant plus probable la présence de zones sous fortes contraintes.

De plus, la fraction maximale de phase monoclinique après vieillissement semble décroître quand la contrainte interne augmente.

Enfin, l'incidence de fissuration augmente avec la taille des inclusions de zircone.

2.3.1 Introduction

More and more Zirconia-Toughened-Alumina (ZTA) composites are used for the fabrication of medical implants, mainly in the orthopaedic and dental field. Their main physico-chemical degradation mechanism, called hydrothermal ageing (also called LTD for Low Temperature Degradation) of zirconia-based biomaterials under water environments has been a hot topic in recent years. It consists in a tetragonal-to-monoclinic (t-m) phase transformation in the presence of water, potentially leading to roughness increase and microcracking. The ageing process is affected by many factors, such as stabilizer nature and content, density, surface finish, grain size, cubic phase content, stress and etc.[1]. This work focuses on the stress state of the zirconia inclusion particles in the composites and the corresponding ageing behaviour, which will contribute to the development of zirconia-based bio-ceramics as other works [24].

Although many researches on zirconia ageing are conducted using X-ray diffraction (XRD), Raman spectroscopy is also a powerful tool for this study, and gives access to complementary information. In particular, micro-Raman spectroscopy has spatial resolution around the micrometer (around 10^3 smaller than XRD), and Raman spectra also reflect the stress state of the examined material. For example, Ma and Clarke found that the stress states of single crystals and polycrystalline ceramics can be measured by using their fluorescence spectral shifts[25]. Afterwards, Raman spectra analysis was used to study the stress states of zirconia ceramics respectively by other researchers. Pezzotti and Porporati pointed out that the band located at 144.68 cm^{-1} is highly reliable and sensitive to stress among tetragonal phase bands in the stress state study of tetragonal zirconia[20]. And V. Sergo et al. found that the tensile stress in the tetragonal zirconia phase is enhanced although the overall residual stress in the deformation bands is compressive stress by studying the residual stresses within a deformation band in a ceria-stabilized tetragonal zirconia and alumina composite[26]. In addition, DePortu et al. found that the stress field had a direct relationship with the layer thickness, and the stress distribution of the TZP layer exhibits a parabolic profile, moreover substantial stress intensification occurs near the junctions between neighboring layers by studying the residual stress distributions of multilayered composites consisting of $\text{Al}_2\text{O}_3/3\text{Y-TZP}$ (3 mol% Y_2O_3 -stabilized ZrO_2) layers by Raman and fluorescence piezo-spectroscopy[27].

This part mainly aims at studying the effect of stresses on the hydrothermal ageing of zirconia particles (present as inclusions in an alumina matrix). To apply different levels of stresses on these particles, it was decided to fabricate composites with different amounts of zirconia (thus different Young modulus of the matrix) and with different particle sizes. Ageing is then examined globally using XRD, and locally using micro-Raman spectroscopy.

2.3.2. Materials and methods

2.3.2.1. Material preparation

The powders were 3 mol% Y_2O_3 co-precipitated zirconia powder (TZ-3Y, Tosoh, Japan) and high purity alumina powder (AKP50, Sumitomo, Ltd.), with mixing ratios of either 10 vol.% or 25 vol.% zirconia (respectively referred to as ZTA10- and ZTA25- materials). The powders were dispersed in water by ball-milling with zirconia balls, using Darvan 821A (Vanderbilt Minerals, LLC) as a dispersing agent. In order to prepare several materials containing zirconia with different aggregates sizes, different mixing schedules were used:

- Co-milling zirconia and alumina powders during 7 days (referred to as “ZTA25-7d-” materials), or
- Co-milling zirconia and alumina powders for 1 day (referred to as “ZTA25-1d-” materials), or
- Milling alumina powder alone for one day firstly, and then adding zirconia powder and milling again for 8 minutes (referred to as “ZTA10-1d8m-” and ZTA25-1d8m-”)

The mixed slurries were then cast in porous plaster moulds and dried until composite green bodies were obtained. Then the cast green bodies were debinded and sintered in a programmable furnace (first dwell of 5h at 550°C ($1^\circ\text{C}/\text{min}$ heating ramp), then heating at $5^\circ\text{C}/\text{min}$ to a second dwell at 1430°C for 3 h, and finally cooling down to room temperature at $5^\circ\text{C}/\text{min}$). The samples were then polished. Some of them were annealed to remove residual stresses by machining and polishing (1250°C for 0.5h at $5^\circ\text{C}/\text{min}$ [28]). The samples studied here are summarized in Table 2-3.

Table 2-3 Samples prepared for the study of internal stress

	Milling procedure		
	Co-milling 7 days	Co-milling 1 days	firstly milling Al ₂ O ₃ 1 days then co-milling 8 min
Zirconia amount	ZTA25-7d-A	ZTA25-1d-A	ZTA25-1d8m-A
25vol.%	ZTA25-7d-P	ZTA25-1d-P	ZTA25-1d8m-P
			ZTA10-1d8m-A
10vol.%			ZTA10-1d8m-P

2.3.2.2. X-ray diffraction

The amount of monoclinic phase was measured by X-ray diffraction using a D8 advance Diffractometer (Bruker, Germany) with K α radiations, in Bragg-Brentano configuration. XRD patterns were recorded in the 27-33° (2 θ) range with a scan speed of 0.2 min⁻¹ and a step size of 0.05°. The monoclinic ZrO₂ phase content (V_m) was expressed the equation 2-3 and 2-4.

2.3.2.3 Raman spectroscopy

Raman spectroscopy is a spectroscopic technique used to study the crystal material properties. The principle of the measurement is to send a beam of monochromatic light (laser) on the sample, and to analyse the scattered radiation, which will depend in particular on the atomic bonds and the crystal structure of the material. In general, a Raman spectrum is represented in terms of the intensity of the signal as a function of the frequency shift, called Raman shift, in cm⁻¹. The position of characteristic bands makes it possible to pair a type of bond (or a crystal structure) and its intensity is representative of the quantity. Meanwhile the offset of the characteristics band position can reflect the stress state of the crystal structure. The amount of tetragonal to monoclinic phase transformation was measured by Raman spectroscopy (Horiba Jobin-Yvon LabRAM HR800 imageur). The Raman spectra were recorded from 90 to 600 cm⁻¹, using a laser at 532 nm. The monoclinic phase content (V_m) was calculated according to the formula[29]:

$$V_m = \frac{I_m^{179} + I_m^{190}}{(I_m^{179} + I_m^{190}) + 0.32(I_t^{146} + I_t^{256})} \quad (2 - 6)$$

Where I_p^D is the area of the peak related to the Raman shift of the characteristic bands of phase p (m for monoclinic and t for tetragonal). Typical Raman spectra are shown on fig 2-14.

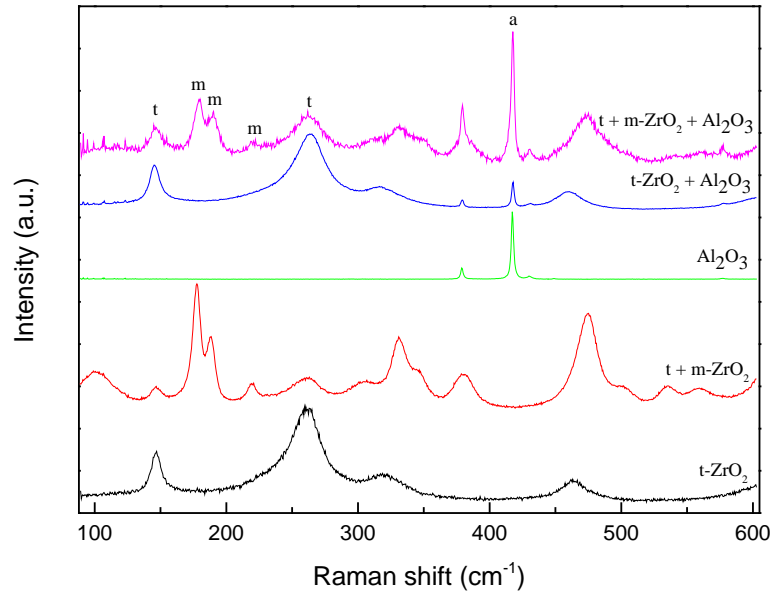


Fig.2-14 Typical Raman spectra of tetragonal zirconia (t), a mixed tetragonal and monoclinic zirconia phase (t+m), Al₂O₃ phase, t+Al₂O₃ phase, and t+m+Al₂O₃ phase from 90 to 600 cm⁻¹. Here the peaks labeled by t, m and a are only related to tetragonal zirconia, monoclinic zirconia, and Al₂O₃ phase respectively.

The microscopic stress distribution was measured by collecting Raman spectra over linear or two-dimensional arrays on the sample surface. The automatically collected arrays of spectra in relatively large two-dimensional maps were typically 5 μm-spaced and the laser spot size was about 1 μm. In previous reports [20, 25, 30], it was found that the stress tensor of the crystal phase has an approximately linear relationship with its associated spectral shift ($\Delta\nu$), as:

$$\Delta\nu = 3\Pi_u\sigma_p \quad (2-7)$$

Where σ_p is the stress tensor (mean normal stress) of p phase, Π_u is uniaxial piezo-spectroscopic coefficient corresponding to the characteristic band, $\Delta\nu$ is the spectral shift. Since Π_u of each characteristic band is constant, a quantitative analysis of stresses can be conducted by measuring the spectral offset $\Delta\nu$.

In this work, the spectral offset of the 146 cm⁻¹ band was used for stress assessment in tetragonal zirconia (as the highest reliability band for this purpose), the position of the same band measured on TZ-3Y powder being taken as the corresponding stress-free position. The value of -0.6 cm⁻¹/GPa for Π_u which is found from Pezzotti's results[20] will be used for this work.

2.3.2.4 Assessment of ageing kinetics

Ageing kinetics were evaluated by performing accelerated ageing tests on all samples in water steam at 134 °C, under 2 bars pressure. It has been reported that 1 h at 134 °C would roughly correspond to 2–3 years of hydrothermal ageing in vivo. The hydrothermal ageing kinetics are rationalized by fitting the t-m transformation curves with the Mehl–Avrami–Johnson equation 2-4.

2.3.2.5 Microstructural observations

Microstructures were observed using scanning electron microscopy (SEM, ZEISS Supra55-VP, Germany) without conductive coating, in high vacuum at low accelerating voltage (2 kV). The average size of zirconia and alumina in the annealed samples was calculated respectively from the average size of at least 500 grains selected randomly. The average size of zirconia agglomerates was calculated respectively from about 200 agglomerates selected randomly.

2.3.3 Results and discussions

2.3.3.1. Microstructure

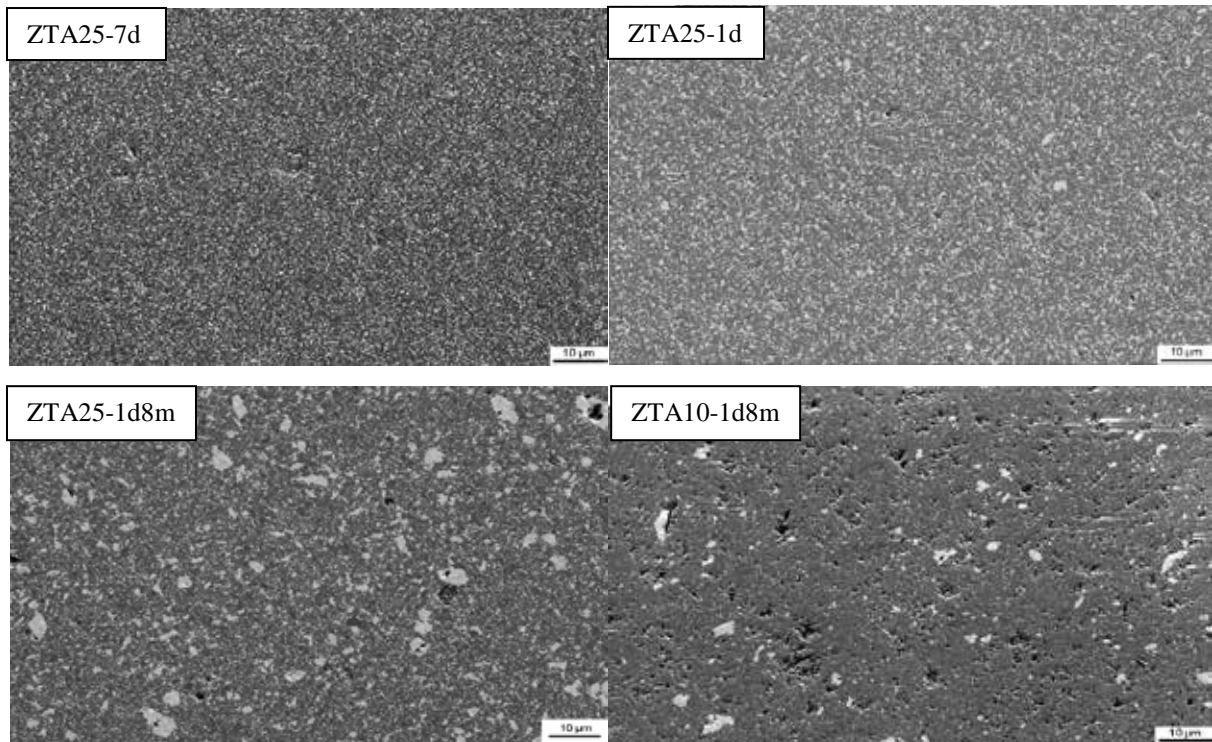


Fig.2-15 SEM images of ZTA specimens under different milling procedure.

Fig.2-15 shows micrographs of all ZTA specimens. The microstructures of these specimens are reported in table 2-4. The average grain sizes of zirconia and alumina in ZTA25-7d sample are smallest, a bit bigger in ZTA25-1d. In both 1d8m the dispersion of zirconia agglomerates was not complete, and big zirconia agglomerates remain together with well dispersed small zirconia grains. Interestingly, the mean size of zirconia grains in the agglomerate is larger than the size of dispersed grains.

Table 2-4 microstructures of ZTA materials

Material	ZTA25-7d	ZTA25-1d	ZTA25-1d8m	ZTA10-1d8m
Alumina grain size (nm)	576	670	663	781
Size of isolated zirconia grains (nm)	217	287	292	323
Size of zirconia grains in agglomerates (nm)		398	430	435
Size of zirconia agglomerates (nm)		2124	4586	3493
% zirconia in agglomerates (estimation)		0.8	14	35

2.3.3.2. Quantitative analysis of Al₂O₃ Phase in ZTA by Raman Spectroscopy

This work mainly studies the stress distribution of zirconia inclusion in alumina and their ageing behavior. It seems that the content of alumina phase plays an important role in the analysis of results. Therefore, it is necessary to quantitatively analyze the local content of Al₂O₃ phase around non-uniformly distributed zirconia inclusions. The local alumina volume fraction (V_a) is determined from the proportion of relevant peaks areas as shown in the following equation:

$$V_a = \frac{k \times I_a^{417}}{k \times I_a^{417} + (I_m^{179} + I_m^{190}) + 0.32(I_t^{146} + I_t^{256})} \quad (2-8)$$

Where I_p^{shift} is the area of the peak related to the Raman shift of the characteristic bands of phase p (m for monoclinic, t for tetragonal and a for alumina phase) and k is a constant.

Since the zirconia distribution in ZTA25-7d samples is very homogeneous, and the volume fraction of the alumina phase is known (75%), these samples can be used to determine k: a value of 29.31 was calculated from 722 Raman spectra of ZTA25-7d samples.

2.3.3.3. Analysis of internal stress before ageing

The analysis results of XRD show that the surface of all samples before ageing test is mainly composed of alumina phase and zirconia tetragonal phase.

Stress state of zirconia particles uniformly distributed in alumina

Due to the uniform distribution of zirconia in ZTA25-7d and ZTA25-1d samples, the Raman scattering spectra on the surface of these samples are collected by selecting some linear maps across the zirconia particles: ZTA25-7d-A (53 points); ZTA25-7d-P (620 points); ZTA25-1d-A (339 points); ZTA25-1d-P (289 points). The results are shown in table 2-5. Fig.2-16 shows that the internal stress in t phase of ZTA25-7d and ZTA-1d samples. It was also found that the zirconia particles mixed in the alumina are mainly subjected to a certain tensile stress, and polishing process can weaken this internal tensile stress. In addition, a small amount of monoclinic zirconia ranging between 0 and 20% was found from the Raman spectra of some position points of these polished samples (ZTA25-7d-P and ZTA25-1d-P).

Table 2-5 The spectral shift and mean stress in ZTA25-7d and ZTA25-1d samples

sample name	N°of of measuring points	spectral shift $\Delta\nu(\text{cm}^{-1})$	
		standard deviation	stress(MPa)
ZTA25-7d-A	53	-1.5±0.092	833±51
ZTA25-7d-P	620	-1.17±0.274	650±152
ZTA25-1d-A	339	-1.34±0.085	744±47
ZTA25-1d-P	289	-1.21±0.165	672±92

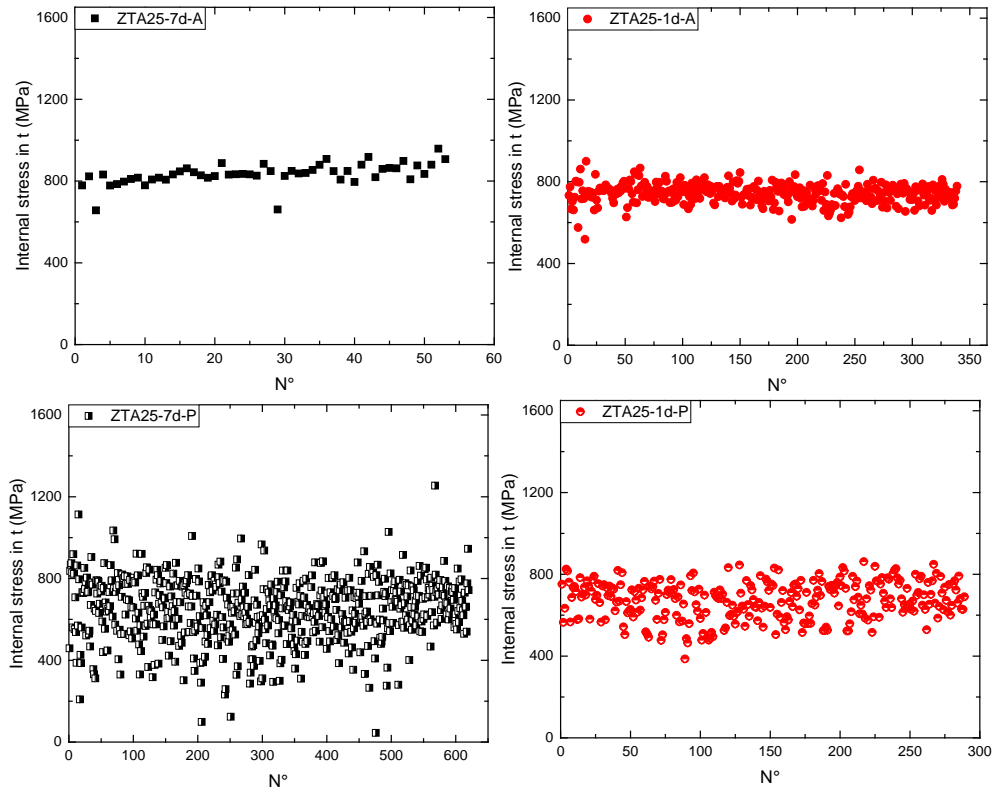
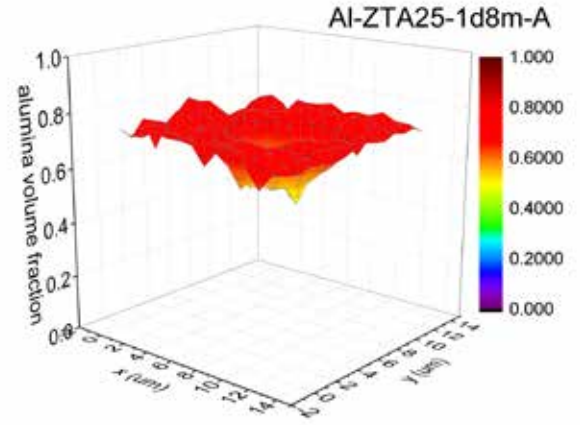
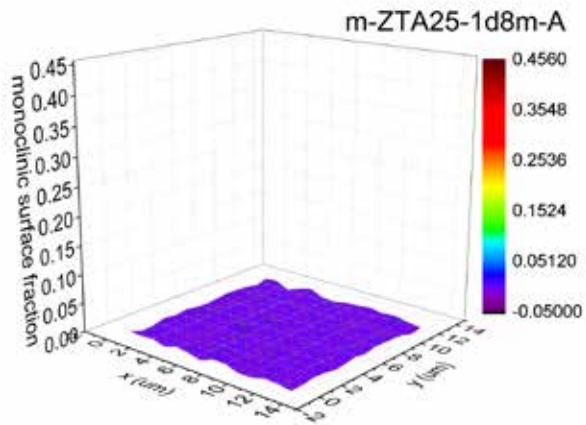
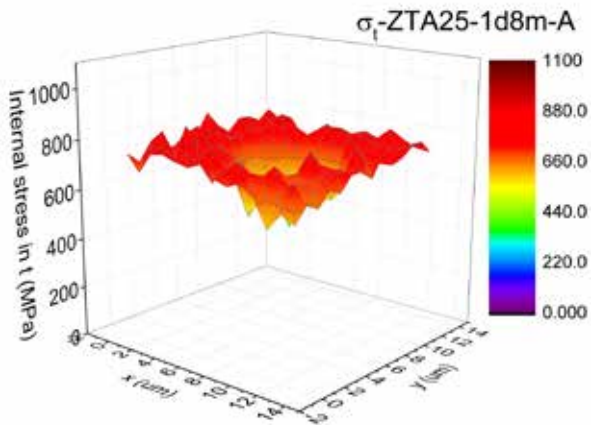
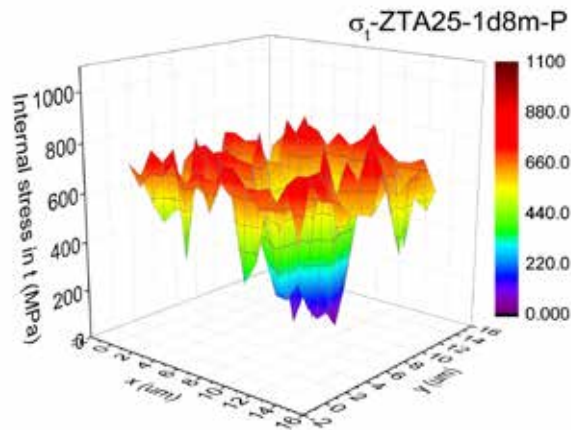
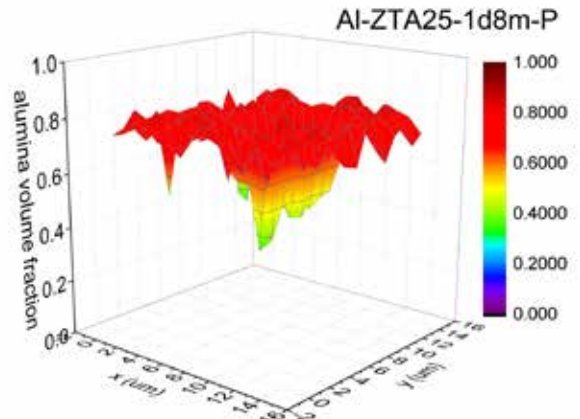
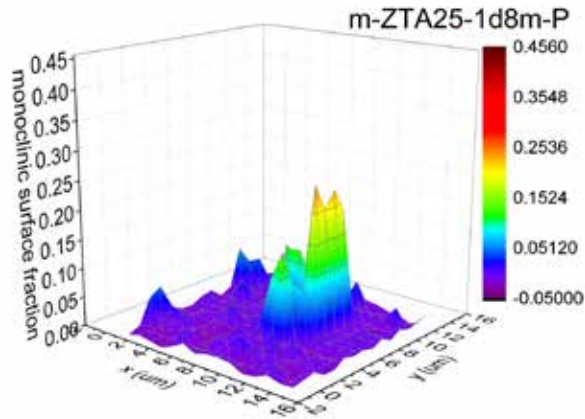


Fig.2-16 Internal stress in t phase distribution at each point on the surface of the samples (ZTA25-7d and ZTA25-1d)

Stress analysis of large zirconia agglomerates ($>2 \times 2 \mu\text{m}$)

In the four materials ZTA10-1d8m-A, ZTA10-1d8m-P, ZTA25-1d8m-A and ZTA25-1d8m-P, zirconia inclusions were large enough so that Raman maps could be performed around them.

Fig.2-17 shows examples of monoclinic fraction, stress and alumina fraction around large zirconia agglomerates. In all 4 materials (ZTA10-1d8m-A, ZTA10-1d8m-P, ZTA25-1d8m-A, ZTA25-1d8m-P) monoclinic phase appears at the center of the zirconia agglomerates where tensile stresses are lowest. Comparing the polished samples to the annealed ones, it can be inferred that the polishing process seems to favour the presence of monoclinic phase. Moreover, a small amount of monoclinic zirconia appeared in ZTA10-1d8m-A samples (but not in ZTA25-1d8m-A samples), hinting to an effect of the composition on the presence of monoclinic phase. This should be induced by a greater internal stress caused by changes in the alumina volume fraction in alumina matrix. In order to explain it more intuitively, ZTA10-1d8m-A samples and ZTA25-1d8m-A samples were compared, and it is found that the reference to the spectral shift of ZTA10-1d8m-A samples is greater than the other due to the different of zirconia volume fraction in the alumina matrix, which means that the tensile stress of zirconia in ZTA10-1d8m-A samples is generally greater than that of the other. Meanwhile in order to better study the effect of alumina volume fraction on the stress of tetragonal zirconia particles, we chose to analyse the Raman spectra of the two annealed ZTA25-1d8m-A and ZTA10-1d8m-A samples (except for spectrum containing monoclinic zirconia). The results are shown in fig.2-18. It is found that as the alumina volume fraction increases, the zirconia grains are subjected to greater tensile stress and there is a near-linear relationship between them.



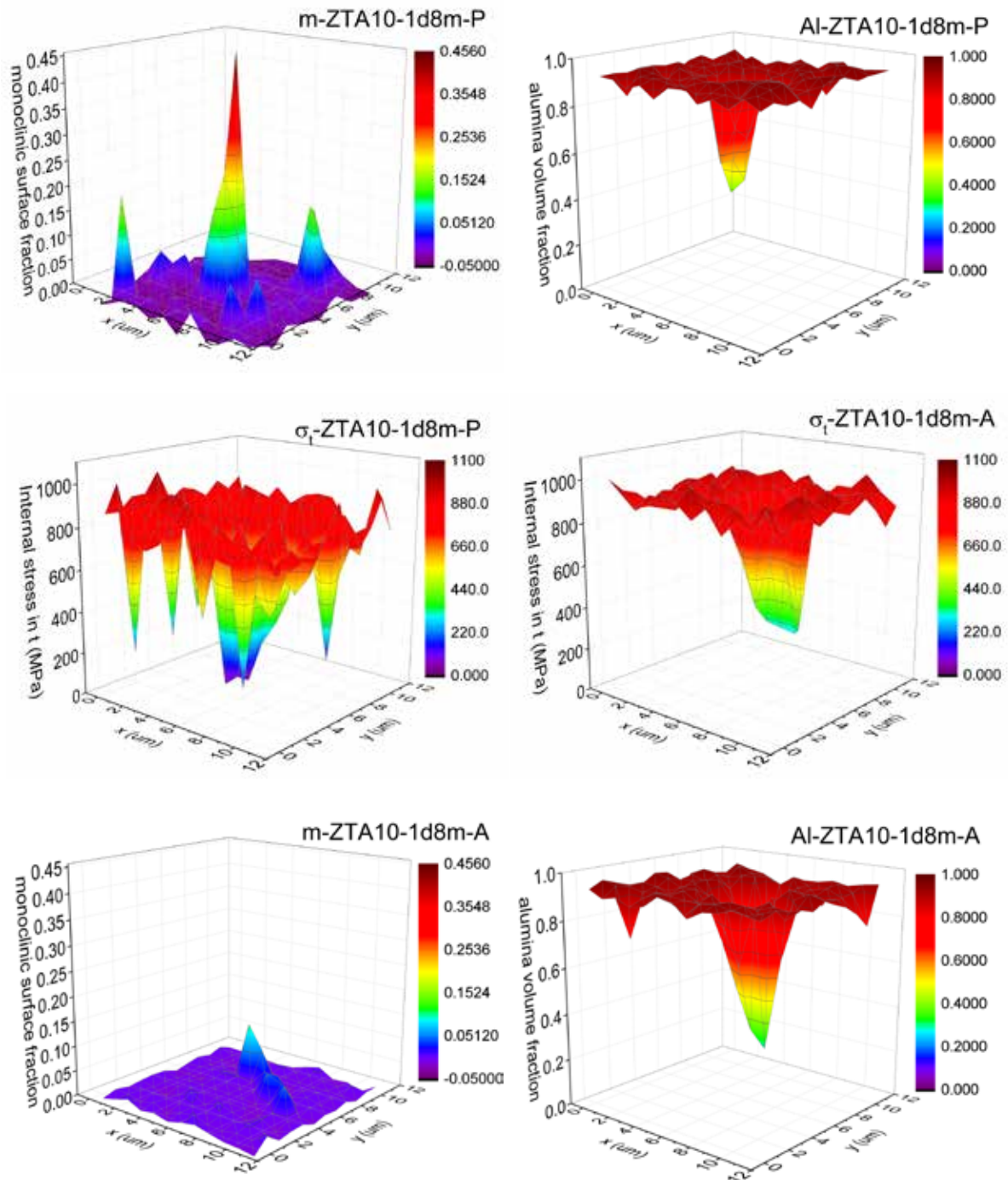


Fig.2-17 monoclinic zirconia, alumina volume fraction and internal stress in tetragonal phase distribution on the surface of large zirconia agglomerates and their surroundings in the samples (ZTA25-1d8m and ZTA10-1d8m) before ageing.

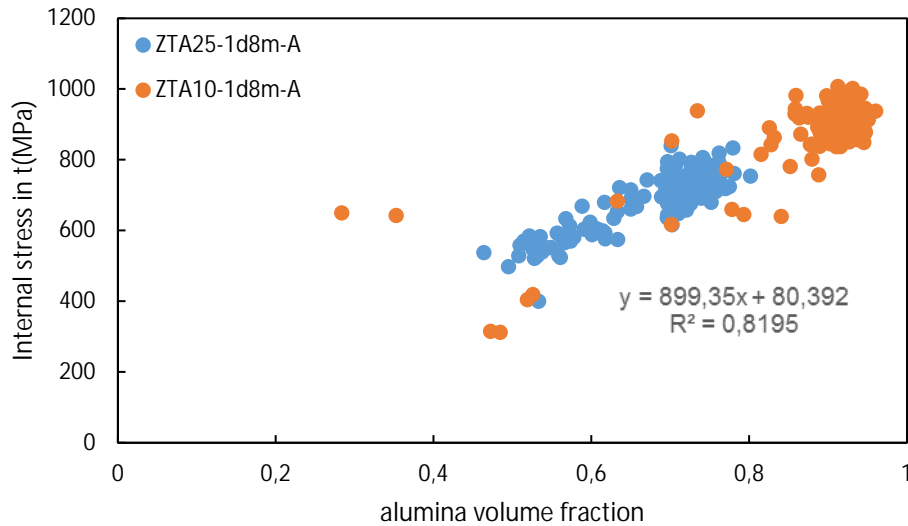


Fig.2-18 Residual internal stress in tetragonal phase versus alumina volume fraction in the samples (ZTA25-1d8m-A and ZTA10-1d8m-A samples)

2.3.3.4 Ageing process

After ageing at 134 °C for 1200 hours, ZTA25-7d-A, ZTA25-7d-P and ZTA25-1d-A samples do not suffer from ageing according to XRD data. The ageing kinetics of other samples are shown in Fig.2-19. It was found that the ageing rates of each sample are not very different, but the maximum monoclinic content after ageing vary between 5% and 20%, thus are significantly different for each sample. Moreover, as shown in Fig. 2-20, the maximum monoclinic fraction has a linear relationship with the average spectral shift at 146 cm^{-1} of t-ZrO₂ (mean internal stress), and it decreases with increasing tensile stress in ZTA25 and ZTA10 samples.

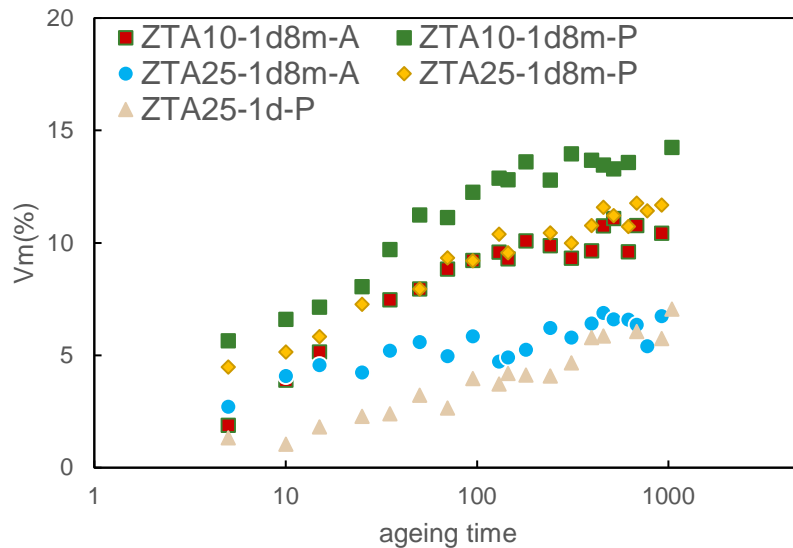


Fig.2-19 XRD monoclinic fraction measured versus ageing time

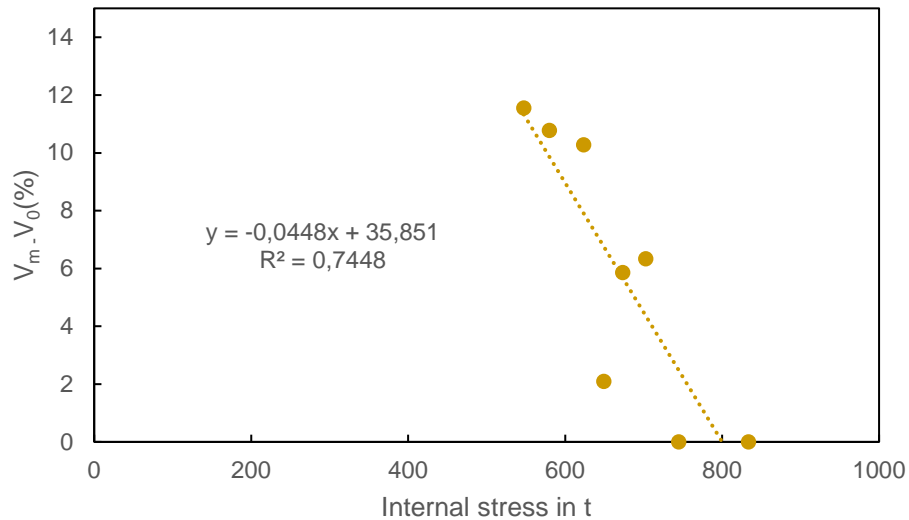
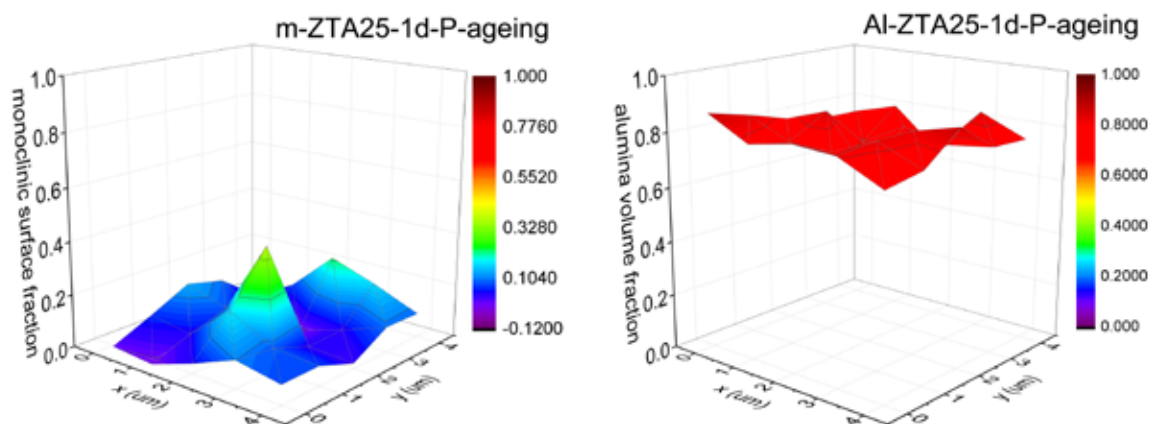
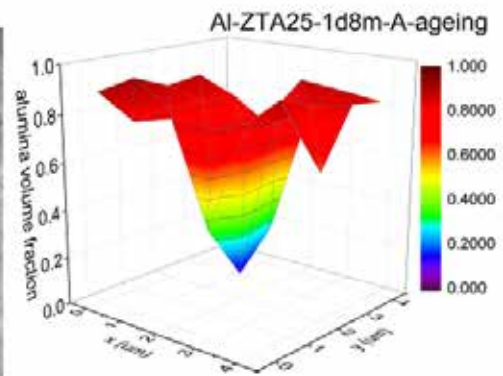
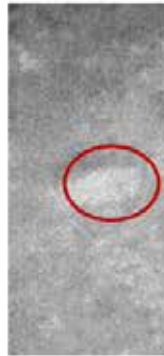
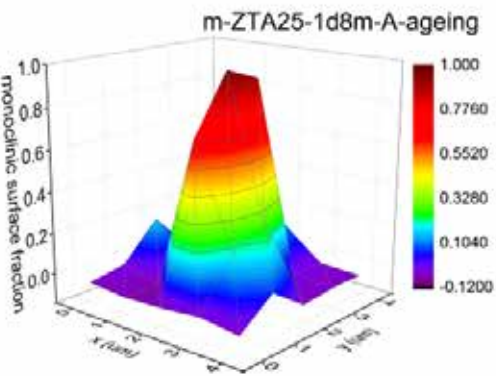
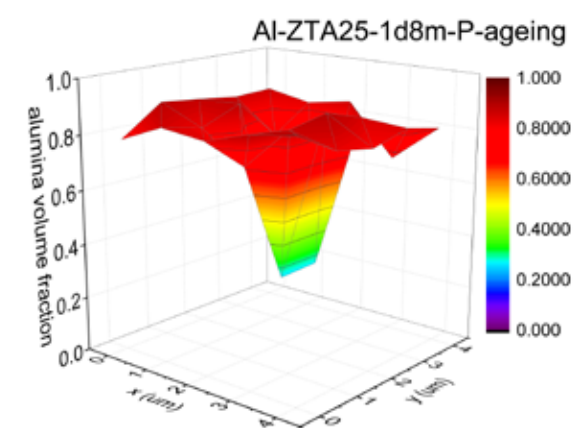
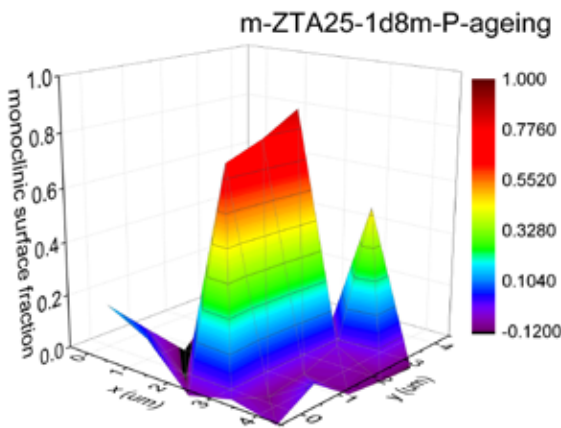
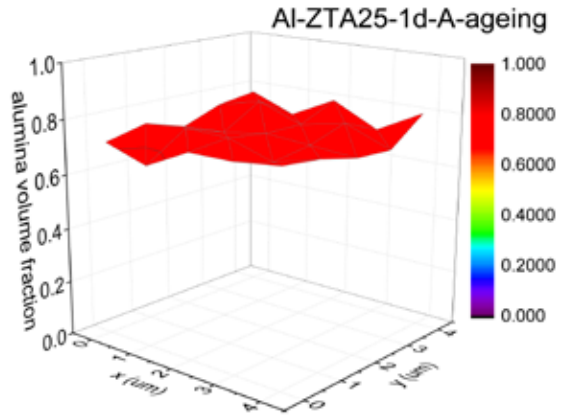
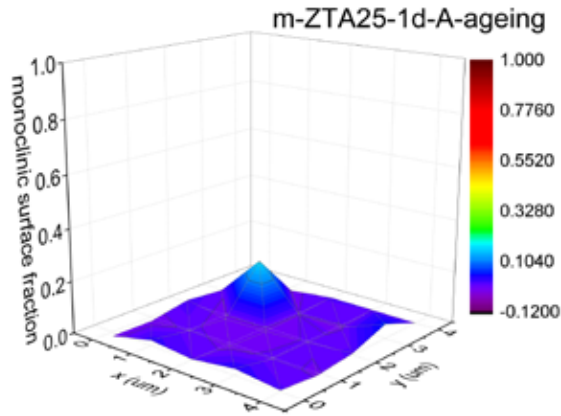


Fig.2-20 XRD maximum monoclinic fraction measured versus the mean internal stress in t-ZrO₂ for each sample after 1200 h ageing

2.3.3.5. Phase analysis of large zirconia agglomerates after ageing

Fig. 2-21 shows that the maximum monoclinic zirconia surface fraction has a strong dependence on the alumina content and decreases with the increase of alumina content. Comparing the zirconia particles 1-1 and 1-2 in the ZTA10-1d8m-P sample, it is shown that the big particle size in the composite results in a larger range of alumina volume fraction distribution, which in turn leads to the transformation of more tetragonal zirconia into monoclinic phase. In the section 2.3.3.4, it is known that the maximum monoclinic fraction has a certain dependence on the mean internal stress in the composite. The mean internal stress in ZTA10 samples and ZTA25 samples is different, and here they are studied separately (Fig.2-22). In ZTA10 samples, the maximum monoclinic fraction exhibits a non-linear decrease with increasing alumina content, meanwhile the tetragonal phase is fully transformed to the monoclinic phase in large zirconia agglomerates. And in ZTA25 samples, the monoclinic fraction decreases with increasing alumina content after ageing at 134°C for 1200h, here it is speculated that if aging for a long enough time, the tetragonal phase will all be transformed into a monoclinic phase in large zirconia agglomerates as same as ZTA10 samples.





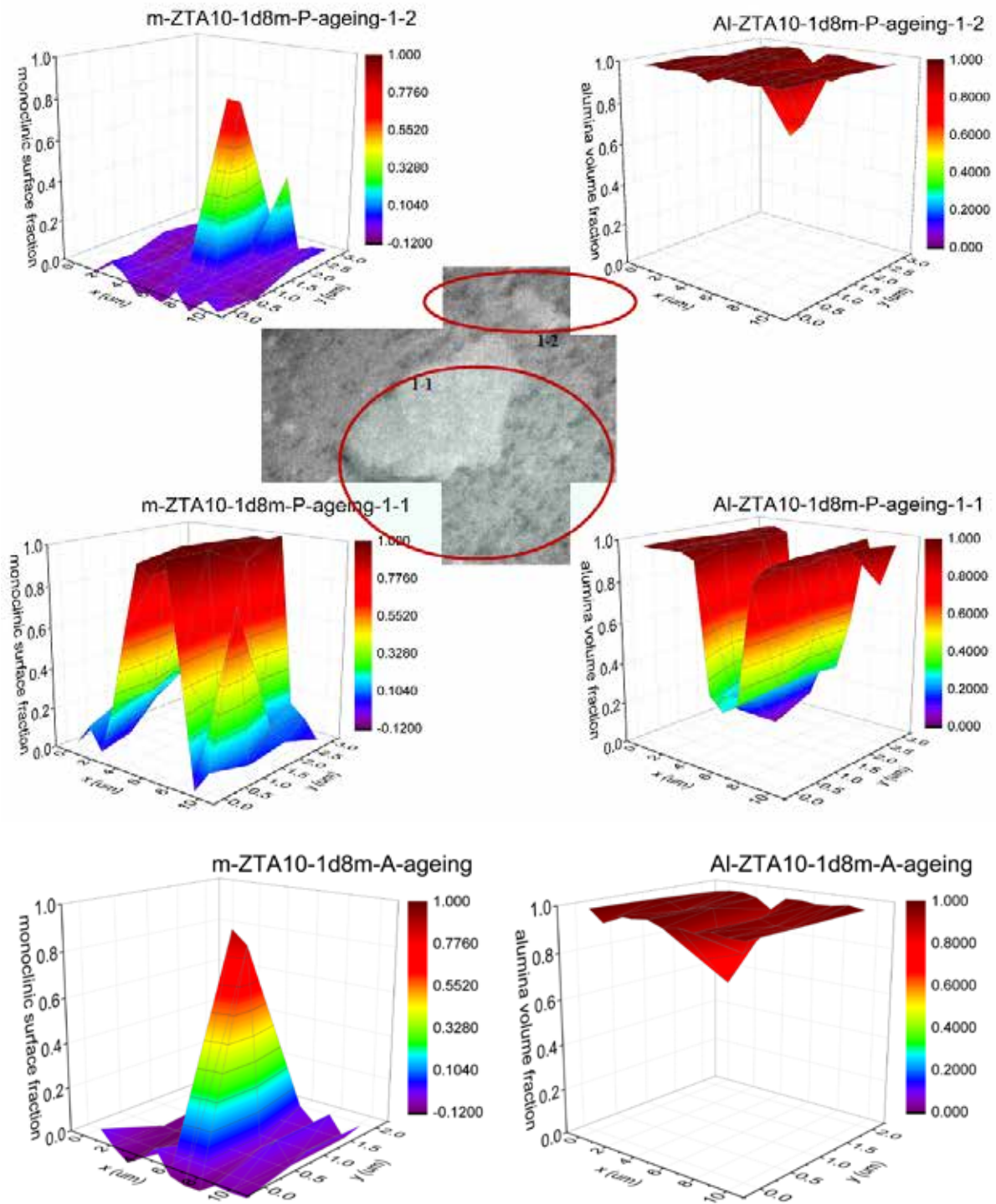


Fig.2-21 Monoclinic zirconia surface fraction and alumina volume fraction distribution on the surface of zirconia agglomerates and their surrounding in ZTA25 and ZTA10-1d8m samples after ageing at 134°C for 1200h.

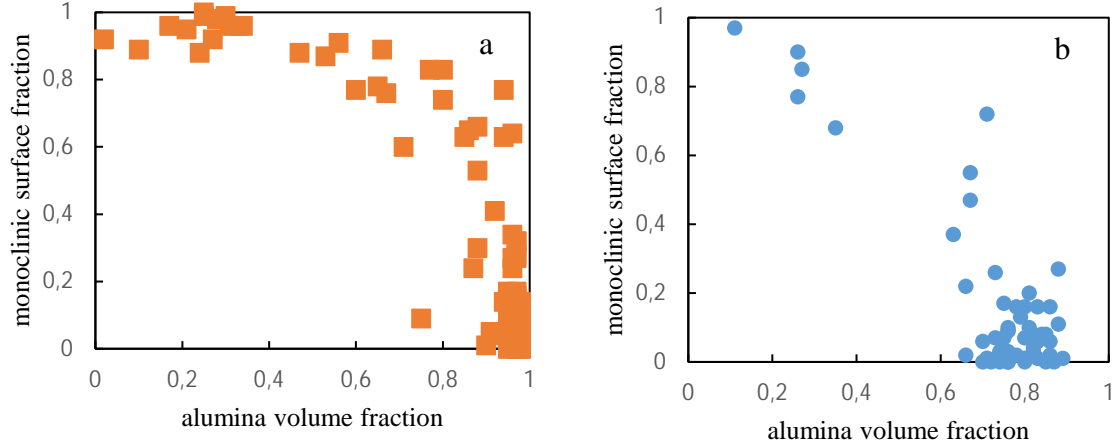


Fig.2-22 Monoclinic zirconia surface fraction versus alumina volume fraction for the samples after ageing at 134°C for 1200h: a. ZTA10-1d8m and b. ZTA25 samples

2.3.3.6. Discussions

Effect of alumina content

The influence on internal stress before ageing

Our results show that the internal stress of zirconia in tetragonal zirconia and alumina two-phase composite increases with increasing alumina content, which is consistent with their results [27, 31]. Sergo and Pompe [26, 32, 33] pointed out that the residual stress of zirconia in tetragonal zirconia and alumina two-phase composite after cooling down from sintering temperature can be written as:

$$\sigma_t = \frac{3K_t(\alpha_A - \alpha_t)\Delta T V_A(1+n)}{V_A(1+n) + V_t(1+n\frac{K_t}{K_A})}, \quad n = \frac{2(1-2\nu_t)}{(1+\nu_t)} \quad (2-9)$$

Where σ_t is the internal stress of zirconia in ZTA composites, caused mainly by the thermal expansion mismatch of the alumina phase and the zirconia phase. K_t, K_A are the bulk modulus of zirconia and alumina phase respectively. α_A, α_t are the thermal expansion coefficient of zirconia and alumina phase respectively. ΔT is the difference between room temperature and the temperature on cooling down at which stress can no longer be relaxed. ν_t is the Poisson ratio of zirconia phase. V_t, V_A are the volume fraction of zirconia and alumina phase in the composites respectively, and their sum is 1.

Then it is given by,

$$\frac{1}{\sigma_t} = \frac{k_s}{V_A} + b_s \quad (2-10)$$

And k_s, b_s are calculated by Equation (2-11):

$$k_s = \frac{1+n\frac{K_t}{K_A}}{3K_t(\alpha_A - \alpha_t)\Delta T(1+n)}, \quad b_s = \frac{n(1-\frac{K_t}{K_A})}{3K_t(\alpha_A - \alpha_t)\Delta T(1+n)} \quad (2-11)$$

From equation (2-11), one can calculate the theoretical spectral shift of the 146 cm^{-1} zirconia band versus the alumina volume fraction. The theoretical curves are reported in Fig.2-23, both for the bulk (where equation (2-7) applies) and for the surface, where equation (2-7) should be replaced by equation (2-12) since $\sigma_{33} = 0$.

$$\Delta\nu = 2\Pi_u\sigma_p \quad (2-12)$$

Of course, this approach does not take into account the fact that the internal stress of the inclusions is related to the shape and size of the inclusions [34-37].

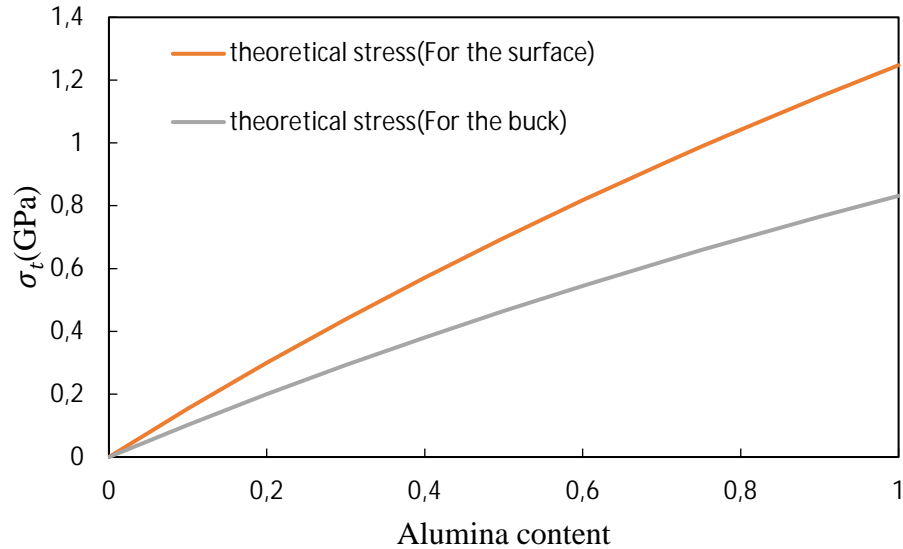


Fig. 2-23 the theoretical curves of the internal stress of zirconia in ZTA composites vs. alumina content

The influence on ageing process

It can be found from this work that the maximum monoclinic fraction after ageing decreases with the increase of alumina content, which is consistent with Deville's results [38]. There are three main reasons for explaining these results: 1. the alumina content is increasing, the alumina grains block the growth of micro-cracks caused by volume expansion during zirconia phase transformation (T→M), and reduce the diffusion channel of the water molecules between the zirconia grains, thus preventing the occurrence of ageing; 2. With more alumina added, the combination number of the bond Al/Zr-VÖ [23] which is more stable than Y/Zr-VÖ becomes more, increase thermal activation energy, thus delaying the ageing phenomenon.

Effect of zirconia agglomerates size

In ZTA25 samples, the different milling procedures lead to a significant difference in the size of zirconia inclusions in the composites. From SEM images, it is found that the order of the average size of zirconia agglomerates is: ZTA25-7d < ZTA25-1d < ZTA25-1d8m. The average spectral shifts of zirconia 146 cm⁻¹ peak in the corresponding annealed samples respectively are -1.5 cm⁻¹, -1.34 cm⁻¹ and -1.26 cm⁻¹. These results indicate that the average tensile stress of the zirconia inclusions decreases as the inclusions size increases. The zirconia inclusions size has a very important effect on ageing behaviour of ZTA composites. The results (maps on Fig.2-18) show that ageing often occurs first in the central region of large size zirconia agglomerates where the tensile stress is minimal. Larger zirconia particles in the ageing process will lead to more transformation from tetragonal zirconia into monoclinic phase.

Analysis of cracks behavior in ZTA composite after ageing

It can be seen from the Fig.2-24 that macro-cracks in the ZTA composites after ageing process are more likely to be found in large-sized zirconia particles in ZTA10-1d8m samples. The presence of large-sized agglomerates reduces the effect of alumina, resulting in a large number of phase transformation occurring. These phase transformations are accompanied by volume expansion, which in turn leads to large internal stresses and promotes the generation of cracks. At the same time, transformed, large-sized zirconia agglomerates also provide a favourable environment for the growth of cracks. The zirconia particles in the ZTA composites with high content alumina itself suffer from greater internal stresses. When large-sized zirconia-entrapped particles appear in such composites, it will make the cracks easier to generate and grow. This is also the reason why the ZTA10-1d8m samples are more likely to exhibit cracks like Fig.2-25.

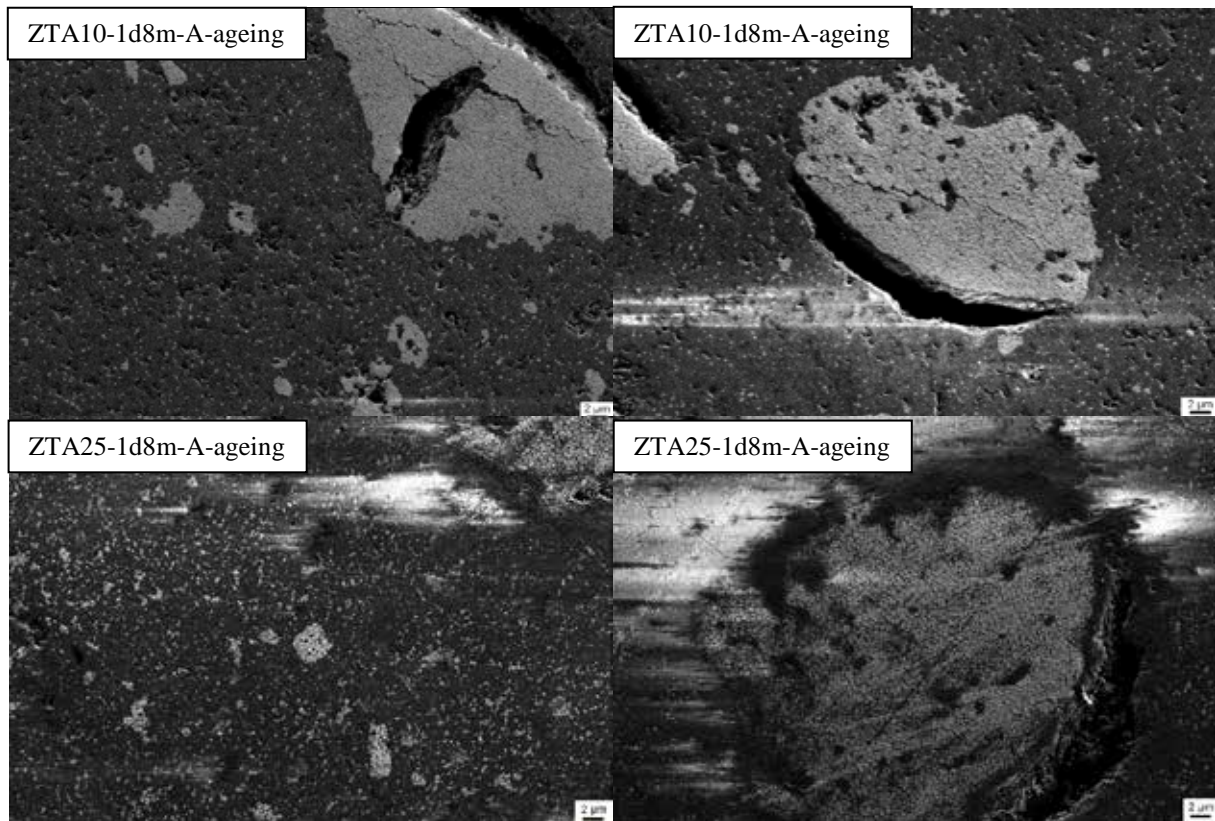


Fig.2-24 SEM photos after ageing process

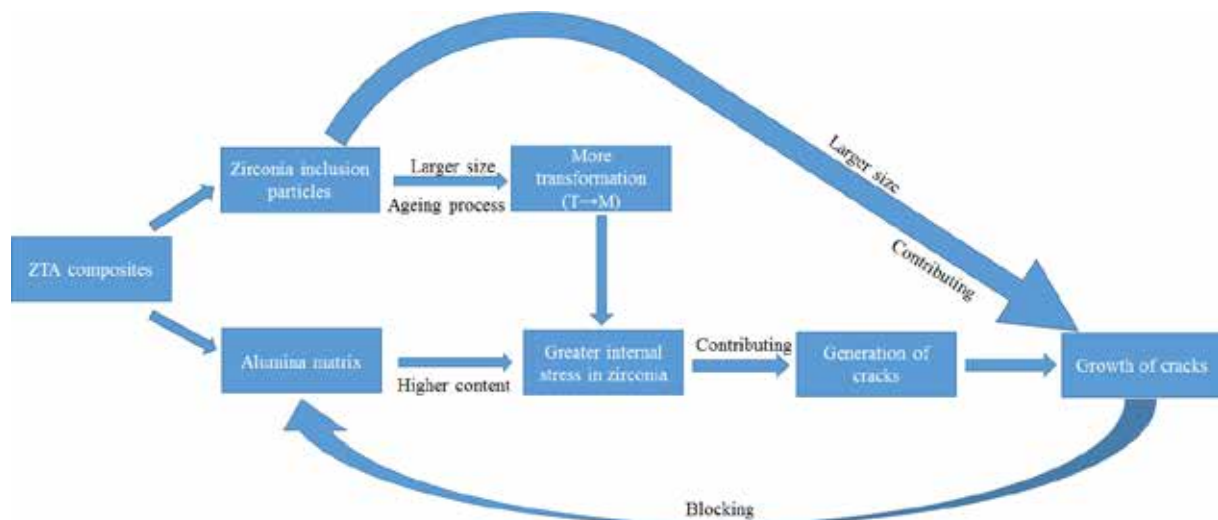


Fig.2-25 Analysis of cracks behavior in ZTA composite after ageing

2.3.4. Conclusion

1. The zirconia particles in ZTA composites are mainly subjected to a certain tensile stress, and the stress increases with increasing alumina content with a near- linear relation. At the same time, the polishing process triggering a small amount of phase transformation (t→m) can increase their distribution, making more probable the presence of highly stressed zones.
2. The monoclinic fraction reached after ageing at 134°C for 1200h of these ZTA composites has a close relation with its own overall stress and alumina content.
3. Macro-cracks are prone to happen in large-size zirconia inclusion particles in the ZTA composites with high content alumina.

2.4 Common conclusion

In this chapter, the influences of stress on hydrothermal ageing of zirconia ceramic are described. However, for different zirconia ceramics, the influence of stress on ageing process can be is very different.

Residual stresses caused by machining and polishing, reaching the GPa as an order of magnitude, trigger lattice distortion to form a small amount of distorted tetragonal phase easily converted into monoclinic phase, which in turn accelerates the aging process of 3YS and 4YS samples, especially 4YS samples. The effect of applied stresses (both tensile and compressive) due to less than transformation-generated stresses slightly accelerates the aging process: 3YE samples is less sensitive to applied stress than other samples.

In ZTA composites, the tensile internal stress of zirconia particles increases linearly with the increase of the content of alumina. Larger tensile stresses may cause tetragonal zirconia to nucleate more quickly into transform monoclinic phase. However, the monoclinic phase content after ageing decreases linearly with the increase of the average tensile internal stress.

References

- [1] J. Chevalier, What future for zirconia as a biomaterial?, *Biomaterials* 27(4) (2006) 535-543.
- [2] S. Schmauder, H. Schubert, Significance of Internal Stresses for the Martensitic Transformation in Yttria-Stabilized Tetragonal Zirconia Polycrystals During Degradation, *Journal of the American Ceramic Society* 69(7) (1986) 534-540.
- [3] H. Schubert, F. Frey, Stability of Y-TZP during hydrothermal treatment: neutron experiments and stability considerations, *Journal of the European Ceramic Society* 25(9) (2005) 1597-1602.
- [4] A.G. Gebresilassie, Atomic scale simulations in zirconia: Effect of yttria doping and environment on stability of phases, (2016).
- [5] J. Li, L. Zhang, Q. Shen, T. Hashida, Degradation of yttria stabilized zirconia at 370 K under a low applied stress, *Materials Science and Engineering: A* 297(1) (2001) 26-30.
- [6] V. Lughì, V. Sergo, Low temperature degradation-ageing-of zirconia: A critical review of the relevant aspects in dentistry, *Dental Materials* 26(8) (2010) 807-820.
- [7] S. Deville, J. Chevalier, L. Gremillard, Influence of surface finish and residual stresses on the ageing sensitivity of biomedical grade zirconia, *Biomaterials* 27(10) (2006) 2186-2192.
- [8] S. Deville, G. Guénin, J. Chevalier, Martensitic transformation in zirconia, *Acta Materialia* 52(19) (2004) 5697-5707.
- [9] S. Deville, G. Guénin, J. Chevalier, Martensitic transformation in zirconia: part II. Martensite growth, *Acta Materialia* 52(19) (2004) 5709-5721.
- [10] J. Chevalier, B. Cales, J.M. Drouin, Low-temperature ageing of Y-TZP ceramics, *Journal of the American Ceramic Society* 82(8) (1999) 2150-2154.
- [11] L. Gremillard, J. Chevalier, T. Epicier, S. Deville, G. Fantozzi, Modeling the ageing kinetics of zirconia ceramics, *Journal of the European Ceramic Society* 24(13) (2004) 3483-3489.
- [12] J. Chevalier, C. Olagnon, G. Fantozzi, Study of the residual stress field around Vickers indentations in a 3Y-TZP, *Journal of Materials Science* 31(10) (1996) 2711-2717.
- [13] J. Roa, M. Turon-Vinas, M. Anglada, Surface grain size and texture after annealing ground zirconia, *Journal of the European Ceramic Society* 36(6) (2016) 1519-1525.
- [14] H.G. Scott, Phase relationships in the zirconia-yttria system, *Journal of Materials Science* 10(9) (1975) 1527-1535.
- [15] H. Toraya, M. Yoshimura, S. Somiya, Calibration Curve for Quantitative Analysis of the Monoclinic-Tetragonal ZrO₂ System by X-Ray Diffraction, *Journal of the American Ceramic Society* 67(6) (1984).
- [16] R.C. Garvie, P.S. Nicholson, Phase Analysis in Zirconia Systems, *Journal of the American Ceramic Society* 55(6) (1972) 303-305.
- [17] D.M. Lipkin, J.A. Krogstad, Y. Gao, C.A. Johnson, W.A. Nelson, C.G. Levi, Phase Evolution upon Ageing of Air-Plasma Sprayed t'-Zirconia Coatings: I—Synchrotron X-Ray Diffraction, *Journal of the American Ceramic Society* 96(1) (2013) 290-298.
- [18] J. H. Hollomon, L. D. Jaffe, Time-Temperature Relations in Tempering Steel, *Trans. AIME, Iron Steel Div.* 162 (1945) 223-49.
- [19] F. Zhang, M. Inokoshi, K. Vanmeensel, B. Van Meerbeek, I. Naert, J. Vleugels, Lifetime estimation of zirconia ceramics by linear ageing kinetics, *Acta Materialia* 92 (2015) 290-298.
- [20] G. Pezzotti, A.A. Porporati, Raman spectroscopic analysis of phase-transformation and stress patterns in zirconia hip joints, *BIOMEDO* 9(2) (2004) 372-384.

- [21] R. McMeeking, A. Evans, Mechanics of Transformation-Toughening in Brittle Materials, *Journal of the American Ceramic Society* 65(5) (1982) 242-246.
- [22] X. Guo, R. Waser, Electrical properties of the grain boundaries of oxygen ion conductors: acceptor-doped zirconia and ceria, *Progress in Materials Science* 51(2) (2006) 151-210.
- [23] A. Samodurova, A. Kocjan, M.V. Swain, T. Kosmač, The combined effect of alumina and silica co-doping on the ageing resistance of 3Y-TZP bioceramics, *Acta Biomaterialia* 11 (2015) 477-487.
- [24] J. Chevalier, L. Gremillard, Ceramics for medical applications: A picture for the next 20 years, *Journal of the European Ceramic Society* 29(7) (2009) 1245-1255.
- [25] Q. Ma, D.R. Clarke, Stress Measurement in Single-Crystal and Polycrystalline Ceramics Using Their Optical Fluorescence, *Journal of the American Ceramic Society* 76(6) (1993) 1433-1440.
- [26] V. Sergo, D.R. Clarke, W. Pompe, Deformation Bands in Ceria-Stabilized Tetragonal Zirconia/Alumina: I, Measurement of Internal Stresses, *Journal of the American Ceramic Society* 78(3) (1995) 633-640.
- [27] G.d. Portu, L. Micele, Y. Sekiguchi, G. Pezzotti, Measurement of residual stress distributions in Al₂O₃/3Y-TZP multilayered composites by fluorescence and Raman microprobe piezo-spectroscopy, *Acta Materialia* 53(5) (2005) 1511-1520.
- [28] J. Chevalier, C. Olagnon, G. Fantozzi, Study of the residual stress field around Vickers indentations in a 3Y-TZP, *J. Mater. Sci.* 31 (1996) 2711-2717.
- [29] J.A. Muñoz Tabares, M.J. Anglada, Quantitative Analysis of Monoclinic Phase in 3Y-TZP by Raman Spectroscopy, *Journal of the American Ceramic Society* 93(6) (2010) 1790-1795.
- [30] V. Sergo, D.M. Lipkin, G.D. Portu, D.R. Clarke, Edge Stresses in Alumina/Zirconia Laminates, *Journal of the American Ceramic Society* 80(7) (1997) 1633-1638.
- [31] K. Fan, J. Ruiz-Hervias, J.Y. Pastor, J. Gurauskis, C. Baudín, Residual stress and diffraction line-broadening analysis of Al₂O₃/Y-TZP ceramic composites by neutron diffraction measurement, *International Journal of Refractory Metals and Hard Materials* 64 (2017) 122-134.
- [32] W. Kreher, Internal Stresses and Relations between Effective Thermoelastic Properties of Stochastic Solids – Some Exact Solutions, *ZAMM - Journal of Applied Mathematics and Mechanics / Zeitschrift für Angewandte Mathematik und Mechanik* 68(3) (1988) 147-154.
- [33] W. Kreher, W. Pompe, *Internal Stresses in Heterogeneous Solids*, Akademie Verlag ed., John Wiley & Sons Incorporated, Berlin, 1989.
- [34] C.W. Lim, Z.R. Li, L.H. He, Size dependent, non-uniform elastic field inside a nano-scale spherical inclusion due to interface stress, *International Journal of Solids and Structures* 43(17) (2006) 5055-5065.
- [35] C.Q. Ru, Analytic Solution for Eshelby's Problem of an Inclusion of Arbitrary Shape in a Plane or Half-Plane, *Journal of Applied Mechanics* 66(2) (1999) 315-523.
- [36] I. Schmidt, D. Gross, The equilibrium shape of an elastically inhomogeneous inclusion, *Journal of the Mechanics and Physics of Solids* 45(9) (1997) 1521-1549.
- [37] P. Sharma, S. Ganti, Size-Dependent Eshelby's Tensor for Embedded Nano-Inclusions Incorporating Surface/Interface Energies, *Journal of Applied Mechanics* 71(5) (2004) 663-671.
- [38] S. Deville, J. Chevalier, G. Fantozzi, J.F. Bartolomé, J.n. Requena, J.S. Moya, R. Torrecillas, L.A. Díaz, Low-temperature ageing of zirconia-toughened alumina ceramics and its implication in biomedical implants, *Journal of the European Ceramic Society* 23(15) (2003) 2975-2982.

Chapter 3:

**Influence of
structural
parameters on
zirconia
hydrothermal ageing**

Chapter 3. Influence of structural parameters on zirconia hydrothermal ageing

Vers une prédiction du vieillissement hydrothermal de la zircone 3Y-TZP à partir des paramètres d'élaboration

This work was published in Acta Materialia:

C. Wei, L. Gremillard, *Towards the prediction of hydrothermal ageing of 3Y-TZP bioceramics from processing parameters*, Acta Materialia, 2018, 144, pp. 245-56, <https://doi.org/10.1016/j.actamat.2017.10.061>

Abstract

Hydrothermal ageing of yttria-stabilized tetragonal zirconia ceramics can have a strong influence on the lifetime of zirconia devices. Ageing kinetics are often described by the Mehl–Avrami–Johnson equation, most often used as a phenomenological description of the kinetics. This work seeks to relate the parameters of MAJ equations (V_{\max} , n , b_0 and Q) to physical characteristics of the zirconia material: grain sizes, Y_2O_3 partitioning, and monoclinic, tetragonal and cubic phases ratio. Samples with identical nominal composition of 3Y-TZP were prepared with grain sizes ranging from 190nm to 773nm. The microstructural parameters (content of Y_2O_3 in tetragonal phase, proportion of cubic phase, grain size) were measured. From these results, a relationship between microstructural parameters and sintering cycles was first proposed, followed by a relationship between ageing parameters (b_0 , Q , n , V_{\max}) and microstructural parameters. These results provide a convenient framework to better develop the sintering cycle of zirconia biomaterial in order to maximize their resistance to hydrothermal ageing.

Resumé

Le vieillissement hydrothermal peut avoir une influence importante sur la durée de vie des pièces en zircone stabilisée à l'yttrium. Les cinétiques de vieillissement sont souvent décrites par une équation de Mehl-Avrami-Johnson (MAJ), la plupart du temps utilisée comme une description empirique. Dans ce chapitre, nous cherchons mieux comprendre l'équation de MAJ et reliant ses paramètres (V_{\max} , n , b_0 et Q) aux caractéristiques microstructurales des zircons (taille de grain, distribution de l'yttrium, quantité de phases cubique et quadratique...).

Nous avons donc préparé des échantillons de composition nominale identique (à partir de la même poudre de 3Y-TZP) mais de microstructures différentes (par exemple, avec des temps et températures de frittage différents, nous avons obtenu des taille de grains variant de 190 à 770 nm). Nous avons ensuite proposé une relation semi-empirique entre les paramètres microstructuraux et les paramètres d'élaboration.

Finalement nous proposons une autre relation liant empiriquement, mais assez précisément, les paramètres de vieillissement à la microstructure. Dans cette étude, tous les matériaux présentent une valeur de n proche de 1 (0.92). Mais V_{\max} dépend linéairement de la quantité de phase cubique et de la taille de grains, alors que b_0 dépend fortement de la quantité d'yttrium dans la phase quadratique et de la taille de grains.

En conclusion, pour un même cycle de frottage, des poudres différentes peuvent mener à des microstructures différentes. Comme d'autre part une relation forte entre les paramètres de frittage et la microstructure a été mise en évidence, il n'est pas toujours possible de prédire le vieillissement de la zircone directement à partir des paramètres d'élaboration. En revanche, il est possible de le prédire à partir de la microstructure, indépendamment de la poudre utilisée (en restant naturellement dans des compositions proches de celles utilisées ici).

3.1 Introduction

Zirconia-based materials, especially yttria-stabilized tetragonal zirconia polycrystals (Y-TZP), exhibit the best mechanical properties of oxide ceramics: this is the consequence of phase transformation toughening, which increases its crack propagation resistance [1-3]. Furthermore, they are high-temperature resistant and offer low thermal conductivity, good ionic conductivity, good biocompatibility and superior aesthetic appearance[2]. Therefore Y-TZP ceramics are very attractive for a wide range of biomaterial applications such as fixed-partial denture in restorative dentistry, femoral heads in orthopedics [4, 5]. For zirconia-based biomaterials, many works not only focused on mechanical properties in orthopedics, but also studied their sensitivity to low temperature degradation (LTD). Low-Temperature Degradation of zirconia (also called hydrothermal ageing) can be summarized as follows: the presence of water in the environment of zirconia pieces triggers the tetragonal to monoclinic (t-m) transformation of some grains on the surface, which potentially leads to roughening and micro-cracking because of the high volume increase (~5%) associated to the t-m transformation. Hydrothermal ageing is driven by the annihilation of oxygen vacancies by water-derived species [6, 7]. This process both destabilizes the tetragonal phase and overstabilizes the monoclinic one [8]. Ageing kinetics are usually described by the Mehl–Avrami–Johnson equation [9] (eq. 3-1).

$$\frac{V_m - V_0}{V_{max} - V_0} = 1 - \exp(-(b \cdot t)^n) \quad (3-1)$$

In this equation, the parameter b is thermally activated: $b = b_0 \exp\left(\frac{-Q}{RT}\right)$.

V_m is the monoclinic phase content after ageing during a duration t at absolute temperature T , V_0 and V_{max} are the initial and saturation levels of monoclinic phase content, and R is the ideal gas constant. Q is the activation energy, typically around 100 kJ/mol. The value of the parameter n is typically between 0.3 and 3.5[10].

Many factors such as different grain size, residual or applied stresses, density, content of Y_2O_3 in tetragonal phase, proportion of cubic phase, doping with more than one oxide, all contribute towards the ageing process [11-17]. Jansen *et al.* reported that doping with ceria or decreasing the grain size strongly improved the ageing resistance of Y-TZP [18]. For example, 3Y-TZP ceramics with grain size lower than 100nm exhibit almost no ageing, whereas submicrometric 3Y-TZP ceramics may undergo severe degradation under the same conditions [19]. A critical value of grain size around 300nm, below which ageing processes do not occur, was sometimes proposed [15], but later researches showed that this critical value has no physical basis [20] and may be dependent on other materials parameters [21]. Chevalier *et al.* reported that cubic grains are enriched by yttrium, which in turn leads to a decrease of the yttrium content in the neighboring tetragonal grains, making these Y-poor tetragonal grains more susceptible to transformation into monoclinic phase and thus affecting the ageing behavior of zirconia [11].

However, all the parameters mentioned above are interdependent, in particular through processing parameters: for instance, increasing the sintering time may increase both the grain size and the proportion of cubic phase [22], and the amount of cubic phase may also influence internal stresses. It is thus quite difficult to understand what parameters directly influence ageing [23]. Therefore, by carefully analyzing the microstructure and ageing behavior of several zirconia ceramics fabricated from the same powder. This chapter seeks to isolate and quantify the influence of grain sizes, content of Y_2O_3 in tetragonal phase and amount of cubic phase on ageing kinetics parameters (V_{max} , n , b_0 , Q) of 3Y-TZP.

3.2 Materials and methods

3.2.1. Material preparation

The samples were fabricated starting from ultra-pure Y-TZP powders (TZ3YE) produced by Tosoh. TZ3YE contain 3mol%(5.2wt%) yttria plus controlled alumina and silica doping. The zirconia green bodies used in the present study were prepared by slip casting. Firstly, the slurry were prepared by dispersing 150g of TZ3YE powder in 37.5g H_2O , using 2.25g Darvan 821A as dispersant. Complete dispersion was achieved by ball milling with 150 g Y-TZP milling balls during 48 hours. The resulting slurries were then cast in porous plaster molds and dried in air at 25°C for 7days. Finally the green bodies were sintered in a programmable electrical furnace,

under different sintering conditions so as to obtain different microstructures: two materials were obtained by conventional sintering (samples 1430-2h and 1430-5h); two other materials were obtained by two step sintering (conditions chosen to obtain fully dense materials with small grain size [24]: TSS1 and TSS2 materials); finally some series of samples obtained using the TSS2 sintering conditions were submitted to different post-sintering thermal treatment in order to modify their microstructure (materials PS1150-100h, PS1150-200h, PS1430-20h, PS1500-2h, PS1550-20h). The exact sintering cycles used for all materials are summarized in table 3-1. All samples were shaped as 10x10 mm plates, polished, and annealed after polishing to remove any extra residual stress induced by machining and polishing. The density of all samples was then measured by using Arthur's method, based on Archimede's principle.

Table 3-1 List of samples: processing hydrothermal ageing conditions; TSS stands for "Two Steps Sintering", PS for "Post Sintering" (post sintering heat treatment applied to TSS2 materials).

Sample	sintering condition	annealing conditions	ageing temperature/°C	density
TSS1	T1 1300°C T2 1150°C-15h	1150°C-1h	85, 110, 134, 140	6.04
TSS2	T1 1280°C T2 1150°C-25h	1150°C-1h	85, 110, 134, 140	6.07
1430-2h	1430°C-2h	1250°C-0.5h	85, 110, 134, 140	6.05
1430-5h	1430°C-5h	1250°C-0.5h	85, 110, 134, 140	6.04
PS1150-100h	TSS2+post sintering 1150°C-100h		134+stepwise procedure	6.07
PS1150-200h	TSS2+post sintering 1150°C-200h		134+stepwise procedure	6.07
PS1430-20h	TSS2+post sintering 1430°C-20h		134+stepwise procedure	6.07
PS1500-2h	TSS2+post sintering 1500°C-2h		134+stepwise procedure	6.07
PS1550-2h	TSS2+post sintering 1550°C-2h		134+stepwise procedure	6.07

In addition, a stepwise ageing procedure [25] was designed as indicated in Table3-2 in order to determine the values of Q_b for sample PS1150-200h, PS1430-20h, PS 1500-2h, PS1550-2h. The stepwise procedure is based on ageing measurements at different temperature on a single sample, and can largely reduce the time necessary for correct extrapolations. Following this procedure, PS1150-200h sample was aged between 150°C and 80°C, and PS1430-20h, PS 1500-2h, PS1550-2h samples were aged between 134°C and 80°C respectively.

Table3- 2 Stepwise ageing procedure for PS1150-200h, PS1430-20h, PS 1500-2h, PS1550-2h

PS1150-200h		PS1430-20h,PS 1500-2h, PS1550-2h	
T _i (°C)	D _t (h)	T _i (°C)	D _t (h)
150	26	134	2
141	20	141	2
110	100	110	30
121	50	121	18
134	25	100	75
100	145	90	178
90	267	80	265
80	259		

3.2.2 Microstructural analyses: grain size, proportion of cubic phase, yttria content

SEM observations were conducted using a Zeiss Supra55 VP microscope. For each group of samples, grain size was obtained from micrographs taken on both side of 4 samples using the linear intercept method, and multiplying by 1.56 the average linear intercept length of at least 500 grains [26].

The average Y₂O₃ content in tetragonal phase was obtained from XRD data. To summarize, first a calibration curve of the amount of Y₂O₃ in the cubic and tetragonal phases *versus* the lattice parameters was established, from PDF files and previous work by Scott [27-29] (Fig.3-1). Then XRD patterns were recorded over a large angular range (15-120 deg. 2 θ) and analyzed using an iterative procedure based on Rietveld refinement. Rietveld refinement was conducted with Topas 4.0 software (Bruker), using a fundamental parameters approach; only scale factors, lattice parameters, crystallite size and systematic diffractometer-related angular errors were set free during the refinements. The outcomes of the first iteration of Rietveld refinement were mainly the approximate proportions of the different phases (cubic and tetragonal) and the lattice parameters of the tetragonal phase (in most materials cubic peaks were lost in the background or convoluted with some tetragonal peaks). The amount of yttria in the tetragonal phase was then calculated from the calibration curve. Since the total amount of Y₂O₃ is known (3mol.%) from the composition of the powder, it was thus possible to determine the amount of yttria in the cubic phase (considering the approximate proportion of cubic phase) and thus its lattice parameter. The following iterations were conducted while setting the cubic phase lattice parameter as a constant, which allowed evaluating more and more precise phases proportions and tetragonal phase lattice parameter, thus recalculating a more and more precise cubic phase lattice parameter. The iterations were continued until convergence (2 to 4 iterations).

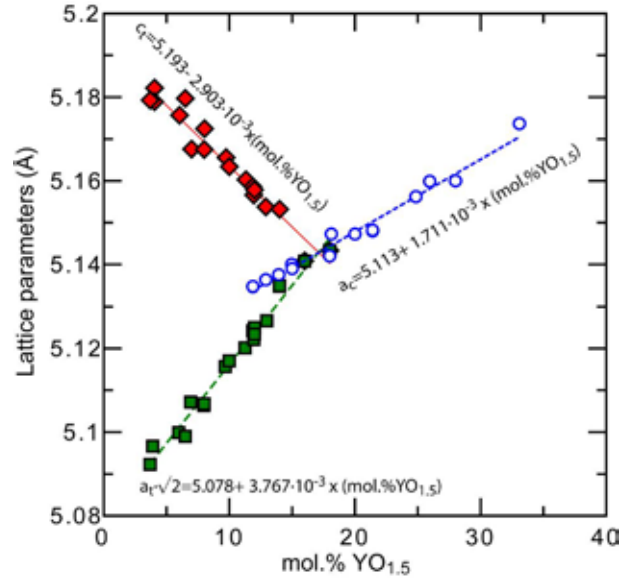


Fig. 3-1 Calibration curve giving the lattice parameters of tetragonal and cubic zirconia vs yttrium amount.

3.2.3 Assessment of ageing kinetics parameters.

Ageing kinetics were evaluated by performing accelerated ageing tests on all samples in water vapour in an autoclave (Wolf Sanoclav), at temperatures ranging from 80 to 150°C.

The amount of tetragonal to monoclinic phase transformation was measured at different time points by X-ray diffraction (XRD). XRD patterns were recorded in the 27-33° (2 θ) range with a scan speed of 0.2 deg·min⁻¹ and a step size of 0.05°, using a Bruker D8-advance diffractometer. The monoclinic ZrO₂ phase content (V_m) [30] was calculated as:

$$V_m = \frac{1.311X_m}{1+0.311X_m} \quad (3-2-a)$$

In which the value of X_m [31] was determined directly from the diffraction diagrams using Garvie and Nicholson's equation:

$$X_m = \frac{I_m^{-111} + I_m^{111}}{I_m^{-111} + I_m^{111} + I_t^{101}} \quad (3-2-b)$$

Where I_p^{hkl} is the area of the diffraction peak related to the (hkl) plane of phase p (m for monoclinic and t for tetragonal).

The hydrothermal ageing kinetics are rationalized by fitting the transformation curves with the Mehl–Avrami–Johnson laws [9] as explained in the introduction. For each material, the fitting procedure consists in minimizing the total quadratic error by optimizing an identical set of parameters (V_0 , V_m , b_0 , Q , n) for the kinetics measured at all temperatures.

For the stepwise ageing procedure, equation (3-3) is used for initial assessment of the Q value, before an optimization procedure takes place to determine V_0 , V_m , b_0 , Q and n (for detailed process, see reference [25]):

$$\ln \left[\frac{1}{\Delta t_i} \ln \left(\frac{V_{max} - V_{i-1}}{V_{max} - V_i} \right) \right] \approx \ln(nb_0) - \frac{Q}{RT_i} \quad (3-3)$$

3.3 Results

3.3.1 Microstructural analyses

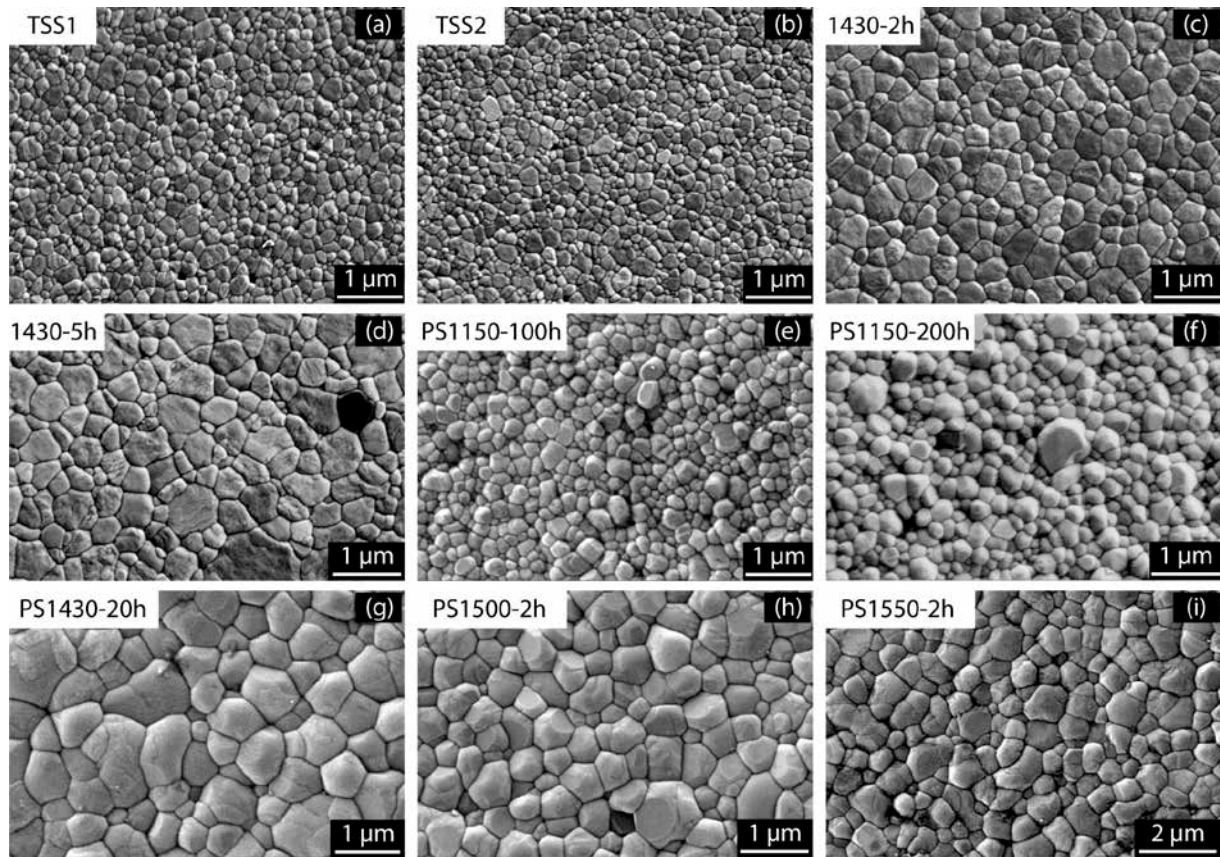


Fig.3-2 SEM micrographs of all specimens after annealing

Density higher than 99% of the theoretical density (6.08) was achieved for all samples (density values are summarized in table 3-1). Fig.3-2 shows SEM micrographs of all the specimens. Even though they were manufactured using the same powder, due to the different sintering thermal treatments the samples exhibit grain sizes ranging from 190 to 779 nm. Very fine-grained zirconia ceramics were obtained by two step sintering, while materials with larger grains were obtained by conventional sintering. The phase content and phase partitioning were analyzed by X-ray diffraction coupled to Rietveld analysis. The results of these microstructural analyses are shown in Table 3-3.

Table 3-3 Microstructural features of zirconia samples before ageing

Sample	wt.% cubic	mol%Y ₂ O ₃ in tetragonal	Grain size (nm)	mol%Y ₂ O ₃ in cubic
TSS1	0.107	2.90	210	3.84
TSS2	0.117	2.87	190	3.97
PS1150-100h	0.151	2.58	290	5.33
PS1150-200h	0.175	2.34	320	6.16
PS1430-20h	0.304	2.13	750	4.75
1430-2h	0.176	2.55	410	4.81
1430-5h	0.205	2.41	520	5.30
PS1500-2h	0.263	2.37	600	4.75
PS1550-2h	0.268	2.34	770	4.80

A few trends can be distinguished from these data. In particular, for a given sintering temperature (here, 1430°C or 1150°C), the content of Y₂O₃ in tetragonal phase decreases linearly and the content of cubic phase increase linearly with increasing holding time (Fig.3-3); the variation are faster with increasing sintering temperature. Moreover, the grain size increases with increasing holding time, following a square root law.

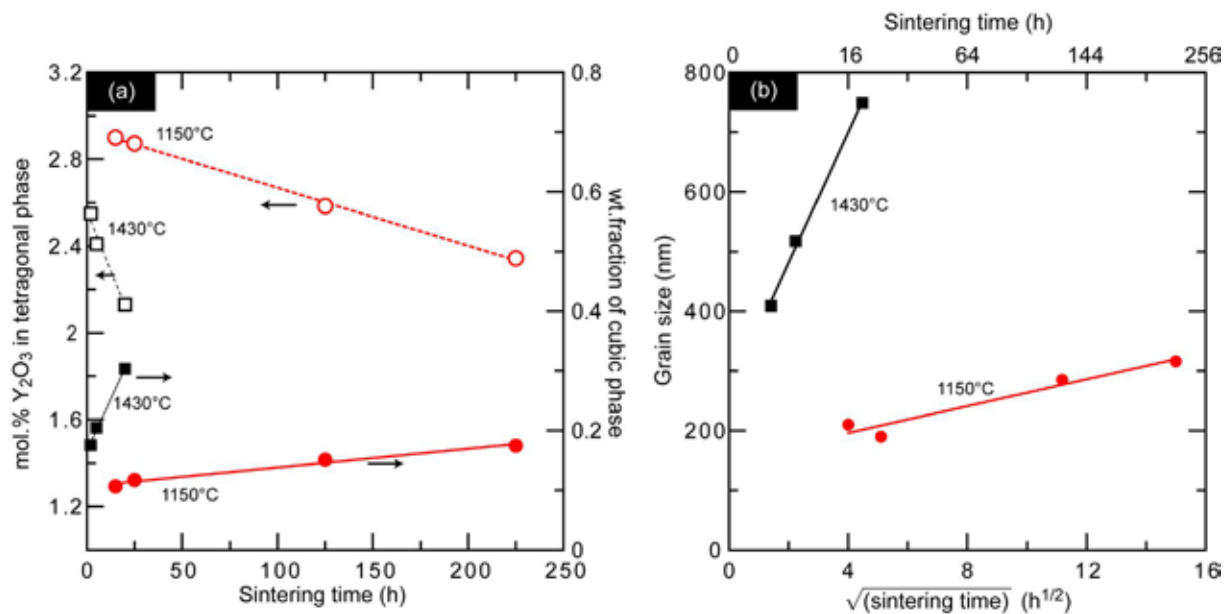


Fig. 3-3 (a) Y₂O₃ content in tetragonal phase, proportion of cubic phase and (b) grain size versus holding time for sintering cycles at 1430°C or 1150°C.

For identical holding times during sintering, the Y₂O₃ content in tetragonal phase decreases and the content of cubic phase increases with increasing sintering temperature (Fig.3-4 (a)). In the same conditions, the grain size increases linearly with increasing sintering temperature (Fig.3-4 (b)). Thus both higher sintering temperatures and longer dwell times can increase the ZrO₂ grain size. Fig.3-3 shows that the grain size is much more sensitive to sintering temperature than to sintering time.

Fig.3-5 shows that the grain size increases linearly with the proportion of cubic phase, while the Y_2O_3 content in tetragonal phase decreases linearly with increasing proportion of cubic phase. As a result, the Y_2O_3 content in tetragonal phase decreases when the grain size increases.

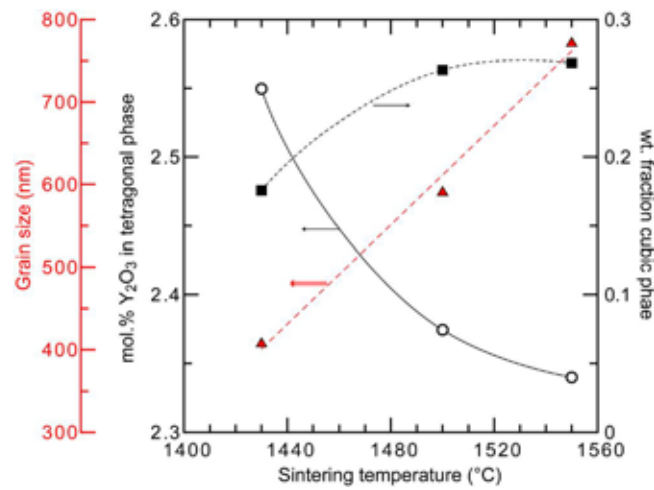


Fig.3-4 Y_2O_3 content in tetragonal phase (open circles), proportion of cubic phase (squares) and grain size (triangles) versus sintering temperature for a 2h holding time during sintering.

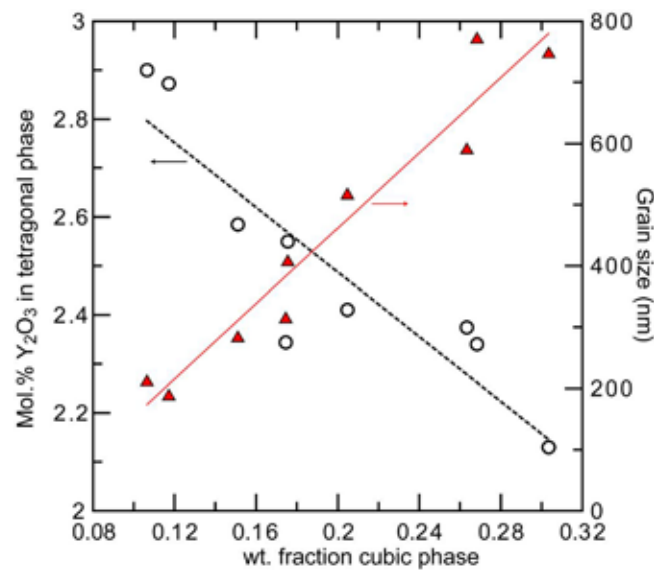


Fig.3-5 Y_2O_3 content in tetragonal phase and grain size versus the content of cubic phase.

3.3.2 Ageing kinetics

TSS1 and TSS2 samples do not suffer from ageing, even after more than 2700 hours autoclave at 134°C, 1500 hours at 140°C and 3000 hours at 90°C.

The surface phase transformation curves for the other samples as a function of the hydrothermal ageing time are shown in Fig.3-6. The ageing kinetics measured at 134 °C are shown in Fig.3-7. PS1430-20h, PS1500-2h, PS1550-2h, 1430-2h and 1430-5h materials exhibit a similar ageing behavior, while PS1150-200h and PS1150-100h age much more slowly. These results are apparently coherent with the existence of a grain-size threshold (~300 nm) under which hydrothermal ageing is not measurable using XRD [15].

The parameters of MAJ equation of the different samples were obtained using the procedure described in section 3.2.3, and reported in table 3-3. Unfortunately, these parameters could not be evaluated on PS1150-100h (this material ages too slowly: less than 10% monoclinic phase after 5000h ageing). For all materials considered here, the value of Vmax increases approximately linearly with increasing grain size and content of cubic phase and decreasing the content of Y₂O₃ in tetragonal phase. The value of n decreases slightly with increasing grain size and content of cubic phase. When considering the values of b₀ and Q, two groups of samples can be distinguished: a group with b₀ around 10¹³ and Q around 115 kJ/mol, while b₀=8·10² and Q=41 kJ/mol for PS1150-200h. As a result, PS1150-200h ages very slowly at 134°C, but faster than all other samples at 37°C (Fig. 3-7); this is obvious from the values of b at 134 and 37°C in table 3-3. 1h in an autoclave at 134 °C represents around 5 years of hydrothermal ageing *in vivo* at 37°C for 1430-2h, 1430-5h, PS1430-20h, PS1500-2h and PS1550-2h samples, but 44h at 37°C for PS1150-200h samples. From Table 3-4 it can be speculated that the 1430-5h sample has the best ageing resistance (lowest value of b) at 37°C.

Table 3-4 Parameters of MAJ equation of the samples

samples	Vmax	n	b(134°C) (h ⁻¹)	b (37°C) (h ⁻¹)	b ₀	Q (kJ/mol)
1430-2h	0.82	1.00	5.66·10 ⁻²	1.19·10 ⁻⁶	5.01·10 ¹³	116.4
1430-5h	0.8	0.88	4.61·10 ⁻²	1.07·10 ⁻⁶	2.98·10 ¹³	115.3
PS1150-200h	0.85	0.99	4.38·10 ⁻³	1.00·10 ⁻⁴	7.67·10 ²	40.8
PS1430-20h	0.77	0.83	6.94·10 ⁻²	1.42·10 ⁻⁶	6.73·10 ¹³	116.7
PS1500-2h	0.79	0.92	5.04·10 ⁻²	1.13·10 ⁻⁶	3.65·10 ¹³	115.7
PS1550-2h	0.78	0.89	7.32·10 ⁻²	2.18·10 ⁻⁶	2.13·10 ¹³	112.6

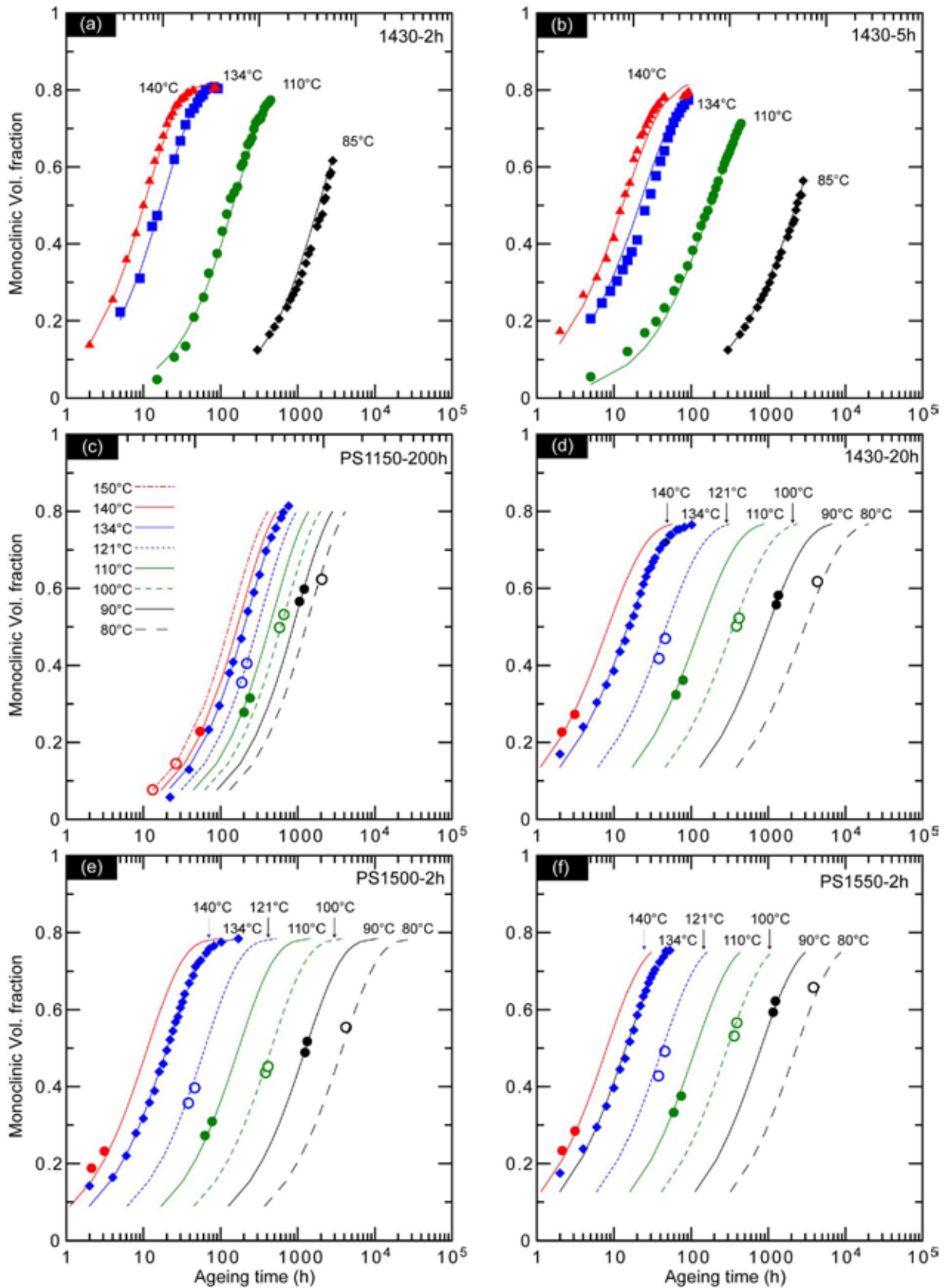


Fig.3-6 Hydrothermal ageing kinetics between 80 and 140°C for samples 1430-2h (a), 1430-5h(b), PS1150-200h(c), PS1430-20h (d), PS1500-2h (e), PS1550-2h (f).

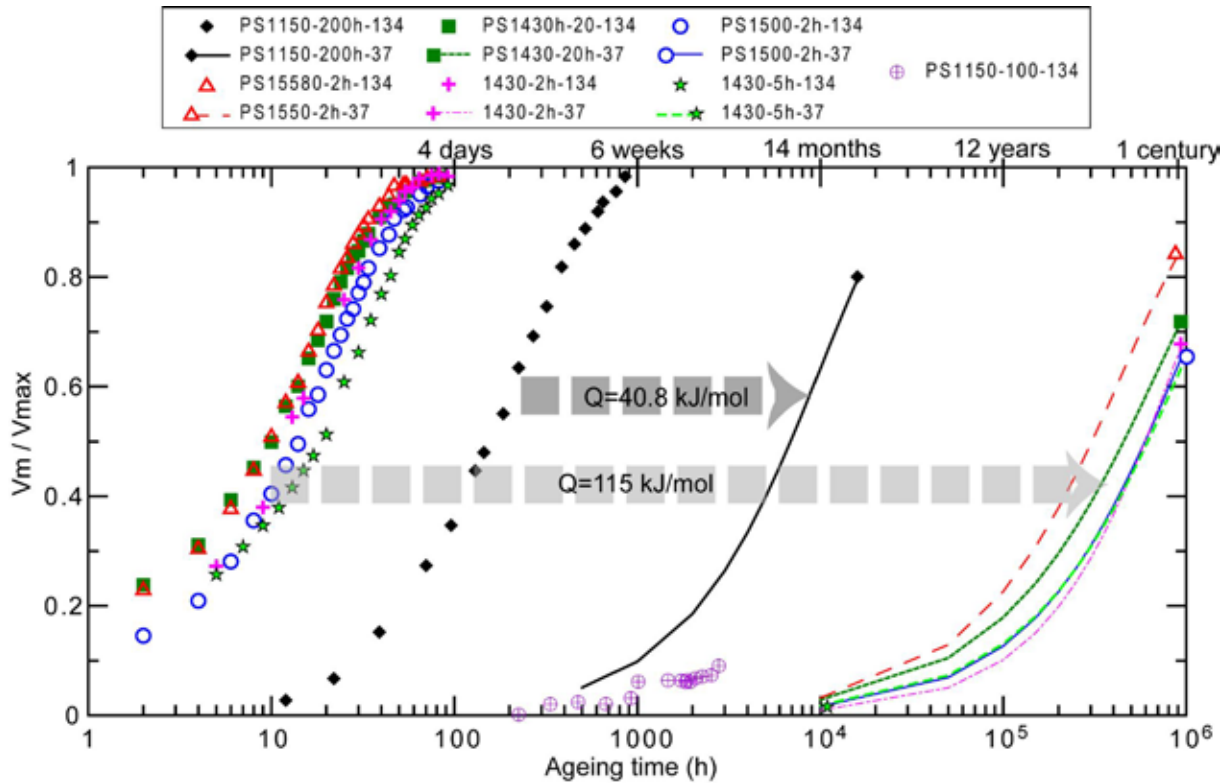


Fig.3-7 Ageing kinetics of all samples at 134°C (symbols) and 37°C (dotted lines).

3.4 Discussion

3.4.1 Correlation analysis of structural parameters and sintering cycle

In order to be able to better develop the sintering cycle, the results of this work can be combined to determine a relationship between structural parameters and sintering cycle. A few hypotheses can guide the choice of simple mathematical, phenomenological models for these relationships.

At constant temperature, the formation of cubic phase from tetragonal grains follows a nucleation and growth mechanism (nucleation being driven by Y diffusion [32]), thus can be described by a MAJ law (Eq. 3-4).

$$f(T, t) = f_0 + (f_{max} - f_0)(1 - \exp(-(c \cdot t)^{n_c})) \quad (3-4)$$

In this equation, the parameter c is thermally activated: $c = c_0 \exp\left(\frac{-Q_c}{RT}\right)$; f is the cubic phase content obtained after the sintering process during a duration t at absolute temperature T , f_0 and f_{max} are the initial and saturation levels of cubic phase content, and R is the gas constant. Q_c is an apparent activation energy for the formation of cubic phase. Theoretically, f_{max} could be calculated from the yttria-zirconia phase diagram (f_{max} is determined by the temperature and the content of yttria). However, on the one hand this work involves rather complicated thermal treatments (two-step sintering and post-sintering annealing), and on the other hand after most thermal treatments the equilibrium phase partitioning may not be reached (thus the equilibrium phase diagram is not useful); thus it is easier and more correct to consider f_{max} as an adjustable parameter.

Assuming a homogeneous initial distribution of Yttrium, the Yttrium concentration in the tetragonal phase is directly controlled by the diffusion of Y from the tetragonal phase to the grain boundaries and to the cubic phase[32]. Thus again a decreasing exponential law can be applied (eq. 3-5).

$$y(T, t) = y_0 - y_{dmax} \cdot (1 - \exp(-(s \cdot t)^{n_y})) \quad (3-5)$$

In this equation, the parameter s is thermally activated: $s = s_0 \exp\left(\frac{-Q_s}{RT}\right)$; y is the content of Y_2O_3 in tetragonal phase during sintering process during a duration t at absolute temperature T , y_0 is the initial content of Y_2O_3 in tetragonal phase, y_{dmax} are the maximum content of Y_2O_3 diffusing into the cubic phase, and R is the gas constant. Q_s is the apparent activation energy for yttrium diffusion.

Finally, since TZ3YE powder contains small amounts of alumina and silica that are mainly located at the grain boundaries as solute species, an equation of grain growth taking solute drag into account [33] can be used (eq. 3-6).

$$D^3(T, t) = D_0^3 + d \cdot t \quad (3-6)$$

In this equation, the parameter d is thermally activated: $d = d_0 \exp\left(\frac{-Q_d}{RT}\right)$; D is the grain size during sintering process during a duration t at absolute temperature T , D_0 is the initial grain size, and R is the gas constant. Q_d is the apparent activation energy for grain growth.

Then a numerical solver (“GRG Nonlinear solver” implemented in Microsoft Excel, based on the Generalized Reduced Gradients method) is used to determine these parameters (f_{max} , f_0 , n_c , c_0 , Q_c , y_0 , y_{dmax} , n_y , s_0 , Q_s , D_0 , d_0 , Q_d), taking into account all steps of the sintering treatment; their optimized values are shown in table 3-5. These calculations result in a good agreement between the calculated values of grain size, proportion of cubic phase and yttrium concentration in the tetragonal phase (obtained from the parameters in table 3-5) and their experimental values, as shown in Fig.3-8.

Table 3-5 Summary of the parameter of the microstructural models.

Cubic content	f_{max}	n_c	Q_c (kJ/mol)	c_0	f_0
	0.45	0.48	350.5	$2.46 \cdot 10^9$	0.078
mol% Y_2O_3 in tetragonal	y_{dmax}	n_y	Q_s (kJ/mol)	s_0	y_0
	1	0.68	278.1	$9.86 \cdot 10^7$	3.1
Grain size	D_0 (nm)	d_0 (m ² /s)	Q_d (kJ/mol)		
	221.2	$2.0 \cdot 10^{42}$	895.6		

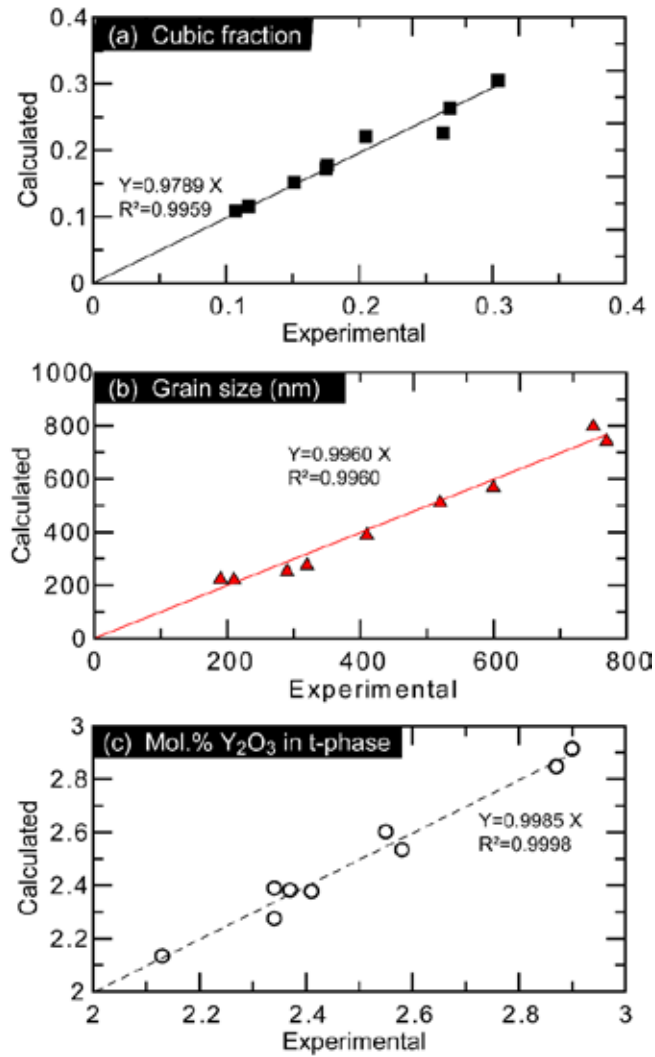


Fig.3-8 Comparison of the calculated and experimental values of f , y , D . Both the slopes of the trend lines and the R^2 values, close to 1, show a good agreement between measured and calculate values.

3.4.2 Prediction of ageing kinetics parameters from micro structural parameters

Activation energies for ageing (Q) between 41 and 117 kJ/mol were found (table 3-3). Due to scattering of the measured monoclinic fraction data, it was decided that differences of less than 2 kJ/mol were not significant, thus the average activation energy (115.3 ± 1.6 kJ/mol) of samples 1430-2h, 1430-5h, PS1430-20h, PS1500-2h and PS1550-2h was attributed to all these samples. The same argument applies for n , thus the average value of n (0.92) was chosen for all samples. Finally the parameters V_{max} and b_0 were recalculated according to these new values of n and Q (Table 3-6).

Finally a multiple regression analysis (equation (3-7) and (3-8)) was applied to calculate the evolutions of $\frac{b_0 - \langle b_0 \rangle}{\sigma_{b_0}}$ and $\frac{V_{max} - \langle V_{max} \rangle}{\sigma_{V_{max}}}$ versus $(\frac{f - \langle f \rangle}{\sigma_f}, \frac{y - \langle y \rangle}{\sigma_y}$ and $\frac{D - \langle D \rangle}{\sigma_D})$. (Here, $\langle x \rangle$ is average value of x and σ_x is its standard deviation). This approach was attempted using measured values of f , y and D summarized in Table 3-6. The values of a_f , a_y , a_D obtained are summarized in Table 3-7, and the absolute value of these coefficients can reflect the degree of correlation of the corresponding parameters. The calculated evolutions of V_{max} and b_0 are summarized in Fig.3-9.

$$\frac{b_0 - \langle b_0 \rangle}{\sigma_{b_0}} = a_f^b \cdot \frac{f - \langle f \rangle}{\sigma_f} + a_y^b \cdot \frac{y - \langle y \rangle}{\sigma_y} + a_D^b \cdot \frac{D - \langle D \rangle}{\sigma_D} \quad (3-7)$$

$$\frac{V_{max} - \langle V_{max} \rangle}{\sigma_{V_{max}}} = a_f^V \cdot \frac{f - \langle f \rangle}{\sigma_f} + a_y^V \cdot \frac{y - \langle y \rangle}{\sigma_y} + a_D^V \cdot \frac{D - \langle D \rangle}{\sigma_D} \quad (3-8)$$

Table 3-6 Summary of parameters of all samples sensitive to ageing (when necessary, b_0 and V_{\max} were recalculated with $n=0.92$ and $Q=115.3$ kJ/mol)

Samples				f :	y :	D :	
	V_{\max}	b_0	Q (kJ/mol)	wt. % cubic	mol% Y_2O_3 in t	Grain (nm)	size
1430-2h	0.82	$3.64 \cdot 10^{13}$	115.3	17.6	2.55	410	
1430-5h	0.8	$3.01 \cdot 10^{13}$	115.3	20.5	2.41	520	
PS1150-200h	0.85	$7.64 \cdot 10^2$	40.8	17.5	2.34	320	
PS1430-20h	0.77	$4.43 \cdot 10^{13}$	115.3	30.4	2.13	750	
PS1500-2h	0.79	$3.28 \cdot 10^{13}$	115.3	26.3	2.37	600	
PS1550-2h	0.78	$4.75 \cdot 10^{13}$	115.3	26.8	2.34	770	

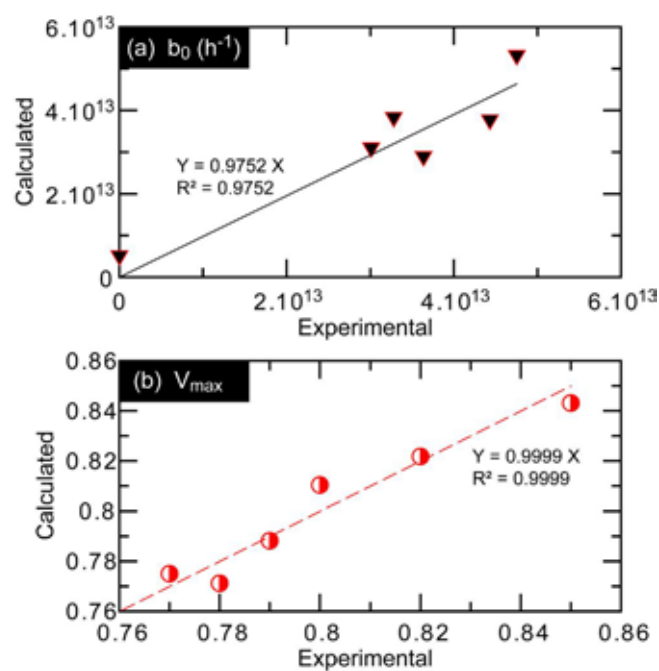


Fig. 3-9 Comparison between experimental values of b_0 , V_{\max} and values of b_0 and V_{\max} recalculated from the multiple regression analysis.

Table 3-7 Values of a_f , a_y , a_D

	a_f	a_y	a_D	$\langle b_0 \rangle$ $\langle V_{\max} \rangle$	or S_{b_0} $S_{V_{\max}}$	or
$\frac{b_0 - \langle b_0 \rangle}{\sigma_{b_0}}$	0.12	0.57	1.05	$3.18 \cdot 10^{13}$	$1.70 \cdot 10^{13}$	
$\frac{V_{\max} - \langle V_{\max} \rangle}{\sigma_{V_{\max}}}$	-0.52	-0.26	-0.63	80.17	2.93	

In such a linear regression (that uses only standardized data) the highest coefficients indicate which variable are the ones with prominent importance. Accordingly, considering the results summarized in Table 3-7. b_0 mainly depends on the grain size and a bit less on the Y concentration inside the tetragonal grains, whereas V_{max} mainly depends on the grain size and the amount of cubic phase.

3.4.3 Predictive ability of the phenomenological models

The models presented here (equations (3-4) to (3-8)) were established on a limited set of 9 materials obtained from a single powder. The question of their predictive power can thus be raised. To answer this, it can be interesting to compare their predictions to the microstructure and ageing kinetics of materials published by other authors [34-37].

Table 3-8 Summary of 3YTZP ceramics studied by other authors. Grain sizes, wt.% cubic and mol/ Y_2O_3 in t. of materials from [35] and [37] were recalculated with the methods exposed in the present article, using the micrographs shown in [35] and [37] and the original XRD data kindly provided by Dr. Inokoshi and Dr. Zhang. These data are thus different from the published ones.

	Sintering conditions		Data from other researchers			Calculated values using our parameters values		
	T	t	Grain size (nm)	wt.% cubic	mol% Y_2O_3 in t	Grain size (nm)	wt.% cubic	mol% Y_2O_3 in t
Inokoshi's results[35] (In-Ceram YZ)	1450	1	388	6	3	362	16.2	2.71
	1450	2	448	23.4	2.76	438	19.0	2.55
	1450	4	537	27.6	2.57	540	22.4	2.38
	1550	1	642	24.1	2.72	599	22.1	2.46
	1550	2	806	29.7	2.52	748	26.1	2.29
	1550	4	925	32.5	2.41	938	30.4	2.17
	1650	1	1209	29.53	2.54	985	29.3	2.23
	1650	2	1537	32.4	2.41	1239	33.8	2.14
	1650	4	2522	30.1	2.39	1560	38.0	2.11
Gremillard's results (other powders) [34]	1300	5	273			272		
	1350	5	330			335		
	1400	5	415			436		
	1450	5	500	25.1	2.41	579	23.6	2.32
	1500	5	793			768		
	1600	5	837			1310		
Zhang's Results[37] (TZ-3YE)	1450	2	438	20.8	2.61	438	19.0	2.55
	1500	2	536	21.9	2.57	573	22.3	2.41
	1550	2	722	24	2.49	748	26.1	2.29

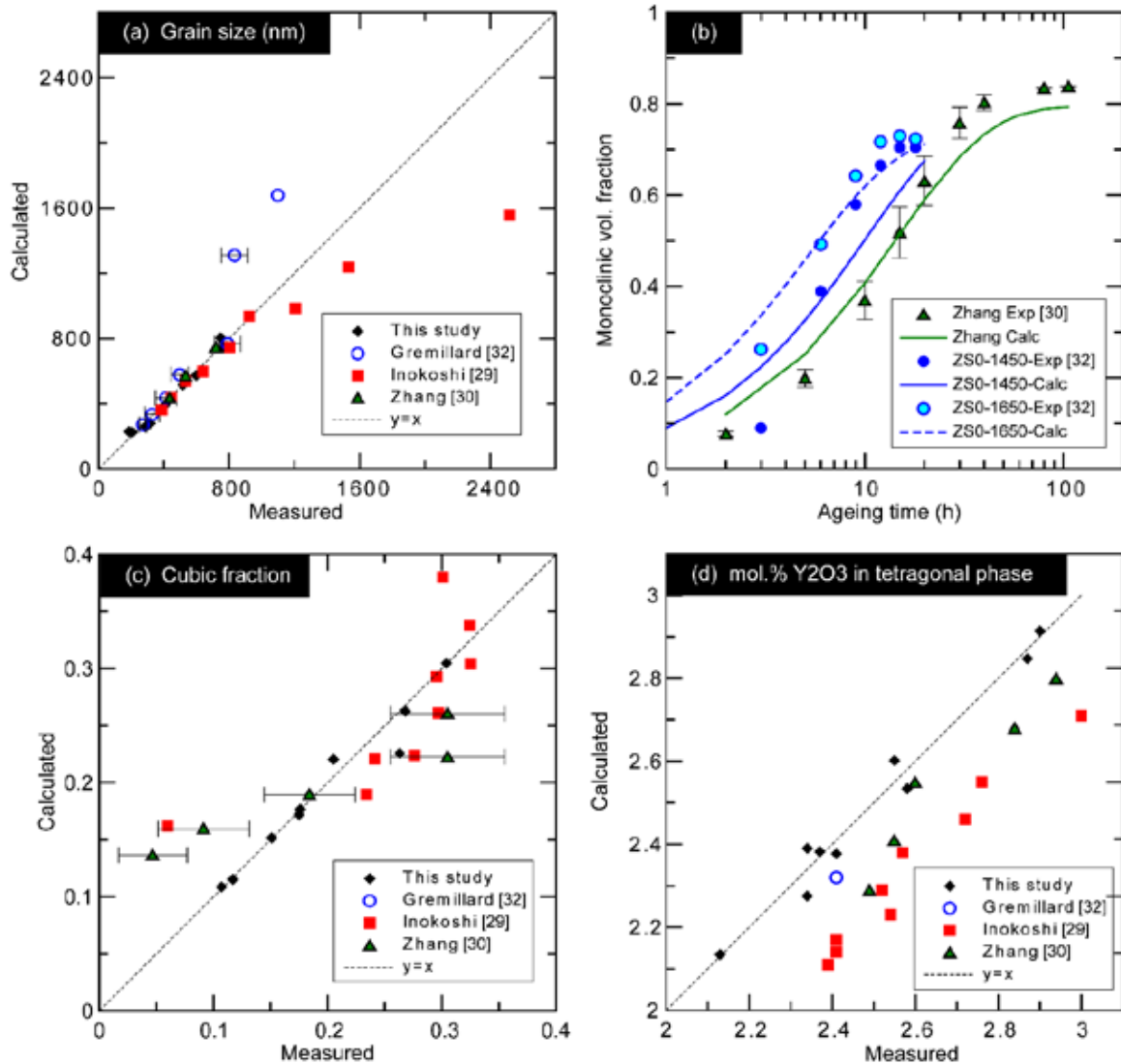


Fig.3-10 Comparison of the calculated and experimental values of several 3Y-TZP materials. (a) grain size, Inoshoki and Gremillard use other zirconia powders; (b) Predicted surface phase transformation curves, compared with the experimental results of Zhang's TZ3YE sample [36] and Gremillard's TZ3YS samples. Although the matches are not perfect, the orders of magnitude are correct and the ranking of samples is the same for the calculated ageing kinetics and the measured ones. (c) and (d): comparison of calculated and measured cubic fraction and mol.% yttria in the tetragonal phase on materials from the same authors.

An overall good agreement is found between the microstructural parameters measured by the different authors and the ones calculated by eq. (3-4) to (3-8) (see table 3-8 and fig.3-10(a)). This is particularly true for grain size. However, discrepancies arise above 1600°C for Gremillard's materials: these materials (fabricated with a different powder: TZ3Y-S) exhibit a lower grain size than what is predicted by eq. (3-6). This could be attributed to the presence of a very small amount of amorphous phase at high temperature in TZ3YE, that can accelerate diffusion and grain growth as compared to amorphous-phase-free zirconia (such as TZ3YS). Between 1300 and 1600°C, both powders behave similarly and excellent predictions can be reached by eq. (3-6).

Even if the correlation is less good than for grain size, the proportion of cubic phase can be reasonably well predicted for all samples. However predictions for content of Y_2O_3 in tetragonal phase are not very good for Inokoshi's materials, which may be due in particular to the fact that the total amount of yttria inside these samples (based on Vita Inceram YZ) is not precisely known (the producer of Vita InCeram YZ guarantees a

weight fraction of Y_2O_3 between 4 and 6%, corresponding to a molar fraction between 2.2 and 3.6, thus this material may not be precisely a 3Y-TZP).

Fig.3-10 (b) shows ageing kinetics measured on three different materials at 134°C, together with the ones calculated with a MAJ equation using b_0 and V_{max} extrapolated from the microstructural parameters by eq. (3-7) and (3-8) (and considering $Q=115$ kJ/mol and $n=0.92$). Here we need to point out that the Q value of these samples is reported to be about 106 kJ/mol [9], while the predicted one is 115 kJ/mol. Being unable to calculate also Q and n from the microstructural parameters is clearly a limitation of our work. Even with this limitation in mind, the correlation between measured and calculated ageing kinetics is very good for Zhang's samples. It is less good for Gremillard's samples. Indeed for these samples the experimental kinetics exhibit a n value of 3.5 and 1 respectively for ZS0-1450 and ZS0-1600, much higher than the 0.92 used here. However the orders of magnitude are correct as well as the ranking among the materials.

Although these comparisons may be biased by factors that are not considered (internal stresses, nature of the powder...), in all cases tested here the models give rather good approximations of the real microstructure and ageing behavior of 3Y-TZP materials.

3.4.4 Influence of the microstructure on ageing kinetics of zirconia

In general, decreasing grain size helps to enhance zirconia ageing resistance. Here this rule applies only at 134 °C, but is not systematically valid anymore at body temperature (see the example of PS1150-200 material). This is explained by a balance between b_0 and Q . Many articles only focus on the study of Q [9] but ignore the changes in b_0 , even though both reducing b_0 and increasing Q can delay the ageing process at a given ageing temperature [4]. Here we show that each sample presents a unique combination of b_0 and Q . TSS1 and TSS2 samples do not suffer from ageing (thus b_0 and Q cannot be determined), PS1150-200h sample has the smallest b_0 and Q among all samples, and samples 1430-2h, 1430-5h, PS1430-20h, PS1500-2h, PS1550-2h have Q around 115 ± 2 kJ/mol. The differences between the last 5 samples seem to be related mostly to the grain size ($a^b_p \sim 1.1$ is the highest coefficient in eq. 3-7) and (a little bit less) to the content of yttrium in the tetragonal phase ($a^b_y \sim 0.57$ is the second highest coefficient in eq.3-7), that directly influence its stability. Indeed, lower Y content in the tetragonal grains directly means less stable tetragonal phase. The effect of grain size is less easy to explain. At least two explanations are possible. The first one is that larger grain size leads to larger internal stresses and easier transformation. The second calls on the defect structure of grain boundaries. Indeed, considering Paul's experimental results [19], when the grain size becomes smaller, the specific surface area of grain boundaries becomes higher, as well as the number of oxygen vacancies ($Y/Zr - V_O$) exposed to grain boundaries, and when their number increases to a certain extent, this leads to a dramatic change of b_0 and Q . This would also explain the difference between this group of 5 samples and PS1150-200h samples, that present the smallest grain size but similar percentage of yttrium in the t phase.

Finally, this work lacks data on Q and n . Indeed, activation energies for ageing found in the literature cover a 40 to 120 kJ/mol, however here only two groups (40 and 115) could be distinguished. As for n , in the literature values between 0.5 and 4 were found, whereas here all values of n are close to 1. Thus one can deduce that grain size, amount of yttrium in the tetragonal phase and proportion of cubic phase do not influence n . Changes in n (and Q) might then be related to other factors, such as perhaps the presence of internal and applied stresses or change in the chemistry of the zirconia powder.

3.5 Conclusions

In this chapter, we provide a predictive, phenomenological model of the influence of sintering conditions on the microstructure (amount of cubic phase, yttria content in the different phases, average grain size) of 3Y-TZP ceramics, based on results obtained on nine 3Y-TZP materials fabricated from the same powder but with different sintering cycles and validated on materials fabricated by other authors.

Moreover, we propose another phenomenological model that can approximate rather precisely the ageing behavior of 3Y-TZP materials (via the parameters n , Q , V_{max} , V_0 and b_0 of the MAJ law describing ageing kinetics), based on their microstructure. All materials in the present study presented a n value of 0.92. From the

model, it was deduced that V_{\max} has a strong linear relationship with both the content of cubic phase and the grain size. b_0 is closely linked with yttria content in the tetragonal phase and grain size.

Finally, it can be concluded that different powders can give different microstructures for a same sintering cycle. Since a strong relation was evidenced between ageing parameters and microstructural features, hydrothermal ageing of zirconia ceramics cannot always be predicted directly from processing parameters. However, it can be predicted from the microstructural features, independently of the powder used.

References

- [1] R. Garvie, R. Hannink, R. Pascoe, Ceramic steel?, *Nature* 258(5537) (1975) 703-704.
- [2] J. Chevalier, What future for zirconia as a biomaterial?, *Biomaterials* 27(4) (2006) 535-543.
- [3] C. Piconi, G. Maccauro, Zirconia as a ceramic biomaterial, *Biomaterials* 20(1) (1999) 1-25.
- [4] J. Chevalier, L. Gremillard, A.V. Virkar, D.R. Clarke, The tetragonal monoclinic transformation in zirconia: lessons learned and future trends, *Journal of the American Ceramic Society* 92(9) (2009) 1901-1920.
- [5] N. Eliaz, *Degradation of implant materials*, Springer Science & Business Media 2012.
- [6] X. Guo, Hydrothermal degradation mechanism of tetragonal zirconia, *Journal of materials science* 36(15) (2001) 3737-3744.
- [7] H. Schubert, F. Frey, Stability of Y-TZP during hydrothermal treatment: neutron experiments and stability considerations, *Journal of the European Ceramic Society* 25(9) (2005) 1597-1602.
- [8] A.G. Gebresilassie, Atomic scale simulations in zirconia: Effect of yttria doping and environment on stability of phases, (2016).
- [9] J. Chevalier, B. Cales, J.M. Drouin, Low-Temperature Aging of Y-TZP Ceramics, *Journal of the American Ceramic Society* 82(8) (1999) 2150-2154.
- [10] L. Gremillard, J. Chevalier, T. Epicier, S. Deville, G. Fantozzi, Modeling the aging kinetics of zirconia ceramics, *Journal of the European Ceramic Society* 24(13) (2004) 3483-3489.
- [11] J. Chevalier, S. Deville, E. Münch, R. Jullian, F. Lair, Critical effect of cubic phase on aging in 3mol% yttria-stabilized zirconia ceramics for hip replacement prosthesis, *Biomaterials* 25(24) (2004) 5539-5545.
- [12] S. Deville, Etude des mécanismes de renforcement et de dégradation des céramiques biomédicales à base de zircone: du macroscopique au nanoscopique: contribution de la microscopie à force atomique, Villeurbanne, INSA, 2004.
- [13] S. Deville, J. Chevalier, L. Gremillard, Influence of surface finish and residual stresses on the ageing sensitivity of biomedical grade zirconia, *Biomaterials* 27(10) (2006) 2186-2192.
- [14] L. Gremillard, L. Martin, L. Zych, E. Crosnier, J. Chevalier, A. Charbouillot, P. Sainsot, J. Espinouse, J.-L. Aurelle, Combining ageing and wear to assess the durability of zirconia-based ceramic heads for total hip arthroplasty, *Acta biomaterialia* 9(7) (2013) 7545-7555.
- [15] L. Hallmann, A. Mehl, P. Ulmer, E. Reusser, J. Stadler, R. Zenobi, B. Stawarczyk, M. Özcan, C.H. Hämmerle, The influence of grain size on low temperature degradation of dental zirconia, *Journal of Biomedical Materials Research Part B: Applied Biomaterials* 100(2) (2012) 447-456.
- [16] J. Muñoz-Saldaña, H. Balmori-Ramírez, D. Jaramillo-Vigueras, T. Iga, G. Schneider, Mechanical properties and low-temperature aging of tetragonal zirconia polycrystals processed by hot isostatic pressing, *Journal of materials research* 18(10) (2003) 2415-2426.
- [17] S. Schmauder, H. Schubert, Significance of internal stresses for the martensitic transformation in Yttria stabilized tetragonal zirconia polycrystals during degradation, *Journal of the American Ceramic Society* 69(7) (1986) 534-540.
- [18] S. Jansen, A.J. Winnubst, Y. He, H. Verweij, P.T. Van der Varst, G. De With, Effects of grain size and ceria addition on ageing behaviour and tribological properties of Y-TZP ceramics, *Journal of the European Ceramic Society* 18(5) (1998) 557-563.
- [19] A. Paul, B. Vaidyanathan, J.G. Binner, Hydrothermal Aging Behavior of Nanocrystalline Y TZP Ceramics, *Journal of the American Ceramic Society* 94(7) (2011) 2146-2152.
- [20] S. Deville, G. Guénin, J. Chevalier, Martensitic transformation in zirconia, *Acta Materialia* 52(19) (2004) 5697-5707.
- [21] J. Eichler, J. Rödel, U. Eisele, M. Hoffman, Effect of Grain Size on Mechanical Properties of Submicrometer 3Y TZP: Fracture Strength and Hydrothermal Degradation, *Journal of the American Ceramic Society* 90(9) (2007) 2830-2836.
- [22] L. Ruiz, M.J. Readey, Effect of Heat Treatment on Grain Size, Phase Assemblage, and Mechanical Properties of 3 mol% Y-TZP, *Journal of the American Ceramic Society* 79(9) (1996) 2331-2340.

- [23] D. Bučevac, T. Kosmač, A. Kocjan, The influence of yttrium-segregation-dependent phase partitioning and residual stresses on the aging and fracture behaviour of 3Y-TZP ceramics, *Acta Biomaterialia* 62(Supplement C) (2017) 306-316.
- [24] I.-W. Chen, X. Wang, Sintering dense nanocrystalline ceramics without final-stage grain growth, *Nature* 404(6774) (2000) 168.
- [25] L. Gremillard, C. Wei, J. Chevalier, K. Hans, T. Oberbach, A fast, stepwise procedure to assess time-temperature equivalence for hydrothermal ageing of zirconia-based materials, *Journal of the European Ceramic Society* 38(1) (2018) 181-186.
- [26] M.I. Mendelson, Average Grain Size in Polycrystalline Ceramics, *Journal of the American Ceramic Society* 52(8) (1969) 443-446.
- [27] F. Lange, D. Marshall, J. Porter, Controlling Microstructures Through Phase Partitioning from Metastable Precursors The ZrO₂-Y₂O₃ System, *Ultrastructure processing of advanced ceramics* (1988) 519-532.
- [28] H. Scott, Phase relationships in the zirconia-yttria system, *Journal of Materials Science* 10(9) (1975) 1527-1535.
- [29] T. Stoto, M. Nauer, C. Carry, Influence of Residual Impurities on Phase Partitioning and Grain Growth Processes of Y-TZP Materials, *Journal of the American Ceramic Society* 74(10) (1991) 2615-2621.
- [30] H. Toraya, M. Yoshimura, S. Somiya, Calibration Curve for Quantitative Analysis of the Monoclinic Tetragonal ZrO₂ System by X-Ray Diffraction, *Journal of the American Ceramic Society* 67(6) (1984).
- [31] R.C. Garvie, P.S. Nicholson, Phase analysis in zirconia systems, *Journal of the American Ceramic Society* 55(6) (1972) 303-305.
- [32] K. Matsui, H. Horikoshi, N. Ohmichi, M. Ohgai, H. Yoshida, Y. Ikuhara, Cubic-Formation and Grain-Growth Mechanisms in Tetragonal Zirconia Polycrystal, *Journal of the American Ceramic Society* 86(8) (2003) 1401-1408.
- [33] K. Matsui, H. Yoshida, Y. Ikuhara, Isothermal Sintering Effects on Phase Separation and Grain Growth in Yttria-Stabilized Tetragonal Zirconia Polycrystal, *Journal of the American Ceramic Society* 92(2) (2009) 467-475.
- [34] L. Gremillard, Relations microstructure-durabilité dans une zircone biomédicale, thèse en sciences des matériaux, Lyon: INSA de Lyon, 2002.
- [35] M. Inokoshi, F. Zhang, J. De Munck, S. Minakuchi, I. Naert, J. Vleugels, B. Van Meerbeek, K. Vanmeensel, Influence of sintering conditions on low-temperature degradation of dental zirconia, *Dental Materials* 30(6) (2014) 669-678.
- [36] F. Zhang, K. Vanmeensel, M. Batuk, J. Hadermann, M. Inokoshi, B. Van Meerbeek, I. Naert, J. Vleugels, Highly-translucent, strong and aging-resistant 3Y-TZP ceramics for dental restoration by grain boundary segregation, *Acta biomaterialia* 16 (2015) 215-222.
- [37] F. Zhang, K. Vanmeensel, M. Inokoshi, M. Batuk, J. Hadermann, B. Van Meerbeek, I. Naert, J. Vleugels, 3Y-TZP ceramics with improved hydrothermal degradation resistance and fracture toughness, *Journal of the European Ceramic Society* 34(10) (2014) 2453-2463.

Chapter 4:

Surface treatment methods for hydrothermal ageing mitigation

Chapter 4. Surface treatment methods for hydrothermal ageing mitigation

Abstract

Hydrothermal ageing is highly sensitive to the surface characteristics. For example, several studies highlighted the interest of chemical modifications of the surfaces over a few microns, using nitridation, carburation or infiltration with cerium.

In this chapter, the efficiency of different surface treatments to prevent or slow down hydrothermal ageing of 3Y-TZP is tested. These treatments consist of post-sintering thermal treatments on powder beds of different compositions (TZ3YE, TZ4YS, 12Ce-TZP, Al₂O₃, CeO₂). The microstructure, ageing kinetics and mechanical properties of the treated samples are then evaluated.

Treatments with alumina and ceria lead to inhomogeneous surfaces and were then considered no further. Treatments with 12Ce-TZP proved to be the most efficient to limit ageing at 134°C while keeping good mechanical properties. However, this was accompanied by a decrease of the activation energy for ageing, thus an acceleration of ageing at lower temperature (37°C or room temperature for example).

Résumé

Le vieillissement hydrothermal est particulièrement sensible aux caractéristiques de la surface. Par exemple, plusieurs études ont montré l'intérêt de modifier chimiquement la surface de la zircone sur quelques micromètres (par exemple en la nitrurant, en la carburant ou en l'infiltrant avec du cérium).

Dans ce chapitre, nous examinons donc l'efficacité de différents traitements de surface de zircone 3YTZP, consistant en des traitements thermiques post-frittage sur des lits de poudres de composition différentes (TZ3YE, TZ4YS, 12Ce-TZP, Al₂O₃, CeO₂). Les cinétiques de vieillissement des échantillons ainsi traités sont ensuite mesurées, ainsi que leurs propriétés mécaniques (dureté, seuil de propagation).

Les traitements à l'alumine et à la cérium ont mené à des surfaces inhomogènes, et ont donc été abandonnés. Les traitements à la 12Ce-TZP se sont avérés les plus efficaces pour limiter le vieillissement à 134°C tout en conservant de bonnes propriétés mécaniques. Mais ceci s'accompagne d'une diminution de l'énergie d'activation du vieillissement, qui accélère le vieillissement aux températures plus basses (37°C, ambiante...).

4.1 Introduction

In the presence of water vapor, hydrothermal ageing (LTD) of zirconia takes place first on the surface. Therefore hydrothermal ageing is particularly sensitive to surface characteristics. Thus how to get a superior anti-ageing surface without sacrificing the excellent mechanical properties of zirconia becomes a hot topic for improving zirconia lifetime. Numerous studies have been conducted along these axes, with various success. For example, Chevalier et al. studied zirconia dental implants coated with a porous zirconia layer (aimed at better osseointegration), but showed that the porous coating accelerated hydrothermal ageing [1]. Oblak et al. found that the initial strength and survival rate of a dental Y-TZP ceramic material to fatigue testing was highly dependent upon surface preparation: in particular ground samples and sandblasted samples (especially sandblasted ones) have better resistance to LTD than as-sintered samples [2]. Deville et al. studied the effects of surface finish on ageing kinetics of biomedical grade zirconia and pointed out that rough polishing was beneficial for ageing resistance [3]. Inokoshi et al. found that surface treatments (rough polishing, sandblasting with Al₂O₃, tribochemical silica sandblasting) improved the ageing resistance of Y-TZP zirconia, decreased the ageing resistance of Y-TZP/Al₂O₃ composite, and did not affect the LTD behavior of Ce-TZP/Al₂O₃ composites. Pozzobon et al. pointed out that the tribochemical treatment (sandblasting treatment) and silica nano-film deposition did not reduce mechanical properties of Y-TZP ceramic [4]. Camosilvan et al. proposed a cerium-containing anti-ageing surface, formed during sintering after impregnating porous pre-sintered zirconia samples with a cerium-containing solution [5].

In this chapter, we examine the efficiency of different surface treatments of zirconia, consisting in a post-sintering heat treatment of fully dense materials on powder beds of different compositions. This chapter mainly consists of two parts. The first part describes preliminary experiments aimed at finding appropriate compositions for the powder bed. Laboratory-made Zirconia (3Y-TZP) samples placed on different powders (TZ3YE, TZ4YS, 12Ce-TZP, Al₂O₃, CeO₂) were subjected to post-sintering treatment, and their ageing kinetics at 134 °C were measured. The second part deals with post-sintering surface treatments of commercial samples placed on different powders (TZ3YE, TZ8YS, 12Ce-TZP); their ageing behavior and some mechanical properties are tested.

4.2 Experimental materials and methods

4.2.1 Experimental samples

TSS1 polished samples (see chapter 3 for details) were prepared for the preliminary experimentations, and shaped as about 10x10 mm plates. The powders used for the powder beds during post-sintering treatment were ultra-pure Y-TZP powders (TZ3YE, TZ4YS, TZ8YS) produced by Tosoh, 12Ce-TZP (CeZ12, Daiichi) and high purity alumina powder (AKP50, Sumitomo, Japan), and ceria powder. Commercial samples are 3Y-TZP polished disc (Doceram, Germany), with 20 mm diameter and 1 mm height. During post-sintering treatment, TSS1 samples were placed on different powder beds (TZ3YE, TZ4YS, 12Ce-TZP, Al₂O₃, and CeO₂), heated to 1430°C for 3 h at 5°C/min, and cooled down to room temperature at 5°C/min. The post-sintering processes of commercial samples were slightly different: commercial samples were placed on different powder beds (TZ3YE, TZ8YS, 12Ce-TZP); then two thermal treatments were tested: the first one consisted in heating to 1490°C for 0.3 h at 5°C/min, cooling down to 1350°C for 1 h at 200°C/min, and finally cooling down to room temperature at 5°C/min; the second thermal treatment was applied only to the treatments with 12Ce-TZP, and consisted in heating to 1550°C for 0.5 h at 5°C/min, and cooling down to room temperature at 5°C/min. The samples prepared during this study are summarized in Table 4-1. They will be named : (TSS/CS)-(Powder)-(Post Sintering temperature): for example, the sample TSS-3Y-1430 refers to the TSS1 sample treated at 1430°C on a TZ3YE powder bed (CS stands for Commercial Sample).

Table 4-1 Sample preparation summary. *X is powder name (3Y, 8Y, 12Ce...)*

Sample name	original sample	post sintering condition	powder	ageing temperature/°C	number
TSS-X-1430	TSS1	1430°C-3h	TZ3YE, TZ4YS, 12Ce-TZP, Al ₂ O ₃ , CeO ₂	134	2 per every powder
Control	Commercial samples	Control : no treatment		90, 100, 111, 121, 134	7
CS-X-1490	Commercial samples	T1 1490°C-0.3h, T2 1350°C-1h	TZ3YE, TZ8YS, 12Ce-TZP	90, 100, 111, 121, 134	7 per every powder
CS-12Ce-1550	Commercial samples	1550°C-0.5h	12Ce-TZP	90, 100, 111, 121, 134	7

4.2.2 Microstructural analyses: proportion of cubic phase, yttria content

SEM observations were conducted using a Zeiss Supra55 VP microscope. The average Y₂O₃ content in tetragonal phase was obtained from XRD data. To summarize, first a calibration curve of the amount of Y₂O₃ in the cubic and tetragonal phases *versus* the lattice parameters was established, from PDF files and previous work by Scott [6-8] (Fig.4-1). Then XRD patterns were recorded over a large angular range (15-120 deg. 2 θ) and analyzed using an iterative procedure based on Rietveld refinement (with Topas 4.0 software). The outcomes of the first iteration of Rietveld refinement were mainly the approximate proportions of the different phases (cubic

and tetragonal) and the lattice parameters of the tetragonal phase (in most materials cubic peaks were lost in the background or convoluted with some tetragonal peaks). The amount of yttria in the tetragonal phase was then calculated from the calibration curve. Since the total amount of Y_2O_3 is known (3 mol.%) from the composition of the powder, it was thus possible to determine the amount of yttria in the cubic phase (considering the approximate proportion of cubic phase) and thus its lattice parameter. The following iterations were conducted while setting the cubic phase lattice parameter as a constant, which allowed evaluating more and more precise phases proportions and tetragonal phase lattice parameter, thus recalculating a more and more precise cubic phase lattice parameter. The iterations were continued until convergence (generally reached after 2 to 4 iterations).

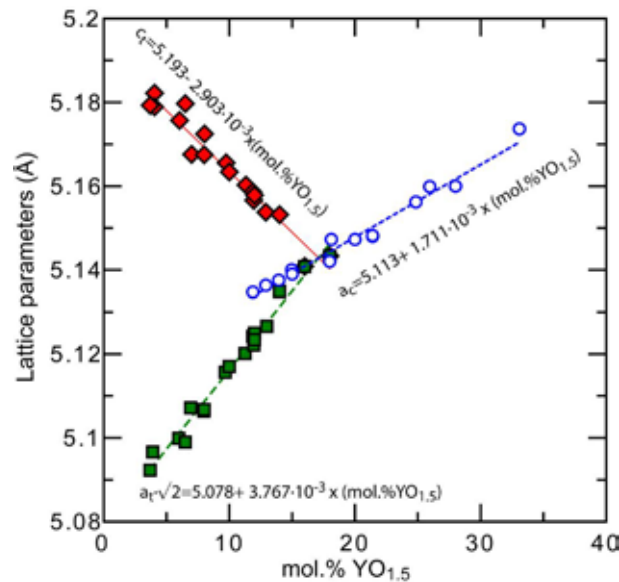


Fig. 4-1: Calibration curve giving the lattice parameters of tetragonal and cubic zirconia vs yttrium amount.

4.2.3 Hardness analysis and crack propagation threshold

The hardness was measured by using a Vickers hardness tester with a load of 20 kg and a dwell time of 10 s. The threshold for crack propagation (K_{I0}) was evaluated from the radial crack pattern accompanying the Vickers indentations (measured at least 72 hours after indentation so that the radial cracks reached a stable shape) and calculated according to Anstis' equation [9]. The reported values are the mean and standard deviation of 20 indentations on 2 samples for every group.

4.2.4 Assessment of ageing kinetics

Ageing kinetics was evaluated by performing accelerated ageing tests on all samples in water steam at 134 °C, under 2 bars pressure. The hydrothermal ageing kinetics are rationalized by fitting the transformation curves with the Mehl–Avrami–Johnson laws[10]:

$$f = \frac{V_m - V_0}{V_{max} - V_0} = 1 - \exp(-bt)^n, \quad b = b_0 \exp\left(-\frac{Q}{RT}\right) \quad 4-1$$

where V_m is the monoclinic phase content, V_{max} and V_0 are respectively the saturation and initial levels of monoclinic phase content, n is an exponent that depends on both nucleation and growth kinetics of the monoclinic phase [11] and b is a thermally activated parameter (with Q the activation energy, R the gas constant, and T the absolute temperature).

The amount of tetragonal to monoclinic phase transformation was measured by X-ray diffraction. XRD patterns were recorded in the 27-33° (2 θ) range with a scan speed of 0.2 min⁻¹ and a step size of 0.05°. The monoclinic ZrO₂ phase content (V_m) [12] was calculated by:

$$V_m = \frac{1.311X_m}{1+0.311X_m} \quad 4-2$$

The value of X_m [13] being calculated as:

$$X_m = \frac{I_m^{-111} + I_m^{111}}{I_m^{-111} + I_m^{111} + I_t^{101}} \quad 4-3$$

Where I_p^{hkl} is the area of the diffraction peak related to the (hkl) plane of phase p (m for monoclinic and t for tetragonal).

4.3 Results of preliminary experiments

4.3.1 Surface topography

Fig.4-1 shows the surface morphologies of TSS1 samples after post sintering treatments with different powders. The surface of the samples treated with alumina and ceria powders were uneven, with protruding particles attached to the surface being alumina and ceria particles, respectively. On the other hand, the samples using other zirconia powders had a more homogeneous surface topography. SEM observations show that the surface of TSS-3Y-1430 samples retained a narrow distribution of the grain size, while TSS-4Y-1430 samples exhibited a bimodal grain size distribution, with a few large grains inside a small-grained matrix; finally, the surface of TSS-12Ce-1430 samples was formed of coarse grains of homogeneous size.

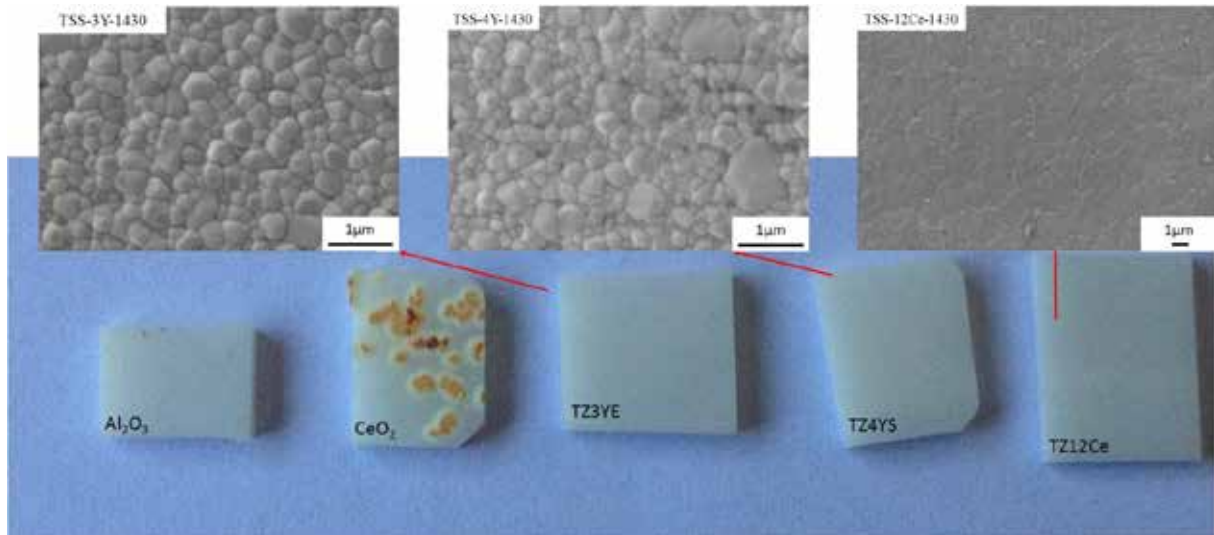


Fig. 4-1 Surface morphology of TSS1 samples after post sintering treatment on different powders

4.3.2 Ageing kinetic

The Fig.4-2 shows XRD monoclinic fraction measured on post-sintered samples with homogeneous surface versus ageing time at 134°C. The ageing process of TSS-12Ce-1430 samples was delayed about 100 times compared to using other powders, possibly due to the formation of a large number of Ce-doped tetragonal zirconia grains.

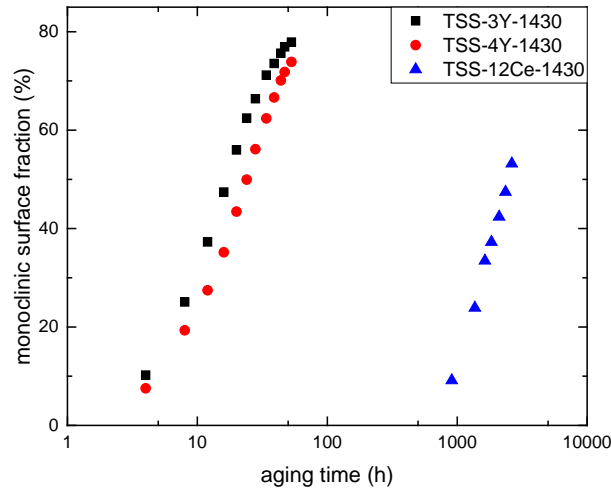


Fig. 4-2 XRD monoclinic fraction measured of TSS1 samples surface after post-sintering versus ageing time at 134 °C.

Thus, the results of the preliminary experiments lead to the choice of only three powders for the post-sintering treatment for the commercial samples: TZ3YE, TZ8YS, and 12Ce-TZP powders. Since TSS-4Y-1430 did not exhibit an improved ageing resistance, TZ8YS was chosen in place of TZ4YS in the hope of further reducing further ageing kinetics by bringing more yttria to the surface. Ceria and alumina powders were discarded due to the formation of non-homogeneous surfaces.

4.4 Results on commercial samples

4.4.1 Microstructural analyses

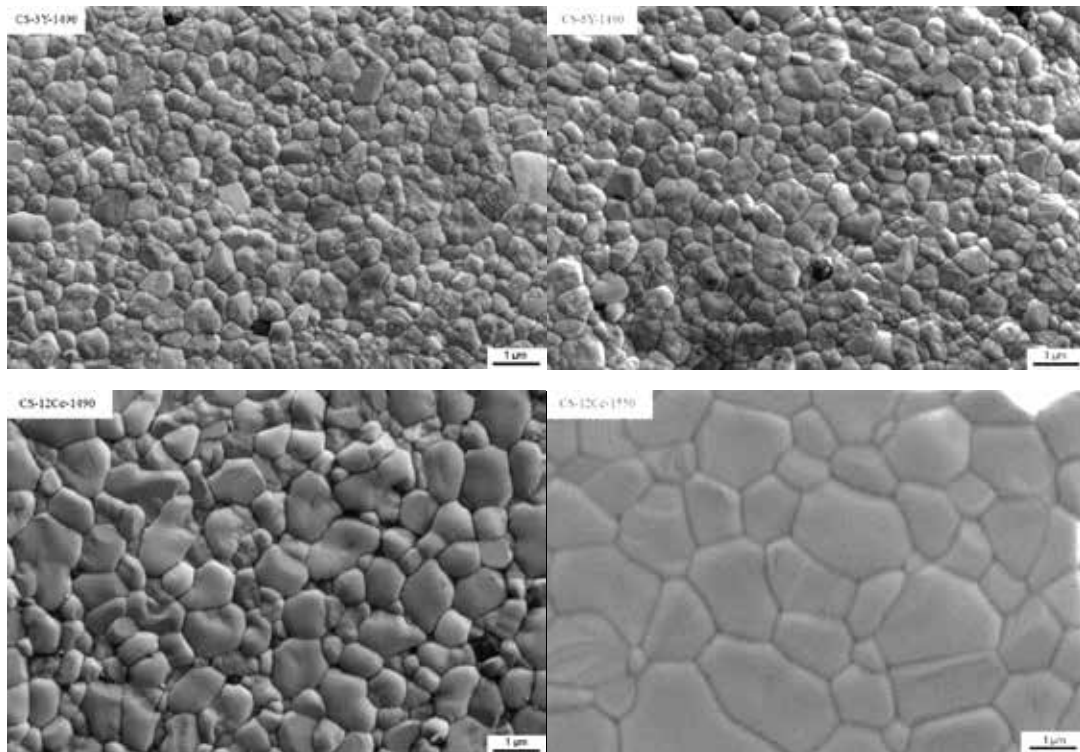


Fig. 4-3 SEM micrographs of commercial samples after post sintering

Fig.4-3 shows that there is no significant difference between the surfaces of the two samples treated using TZ3YE and TZ8YS powders. , and the large-sized grains appear on the surface using the CeZ12 powder under the same post-sintering conditions. CS-12Ce were treated at two different temperatures. The highest post-sintering temperature lead to larger grains on the surface. The phase content and phase partitioning were analyzed by X-ray diffraction coupled to rietveld analysis. The results of these microstructural analyses are shown in Table 4-2. The use of CeZ12 powder in the post sintering process will increase cubic phase content of the sample surface. Unfortunately, no calibration curve could be established to determine the Y and Ce content in Y-Ce-TZP from the lattice parameters. Thus the stabilizers contents in CS-12Ce- samples are not known from XRD measurements. Finally a secondary tetragonal phase was found on CS-12Ce-1550 sample, and attributed to a small amount of Ce-doped tetragonal grains.

Table 4-2 Rietveld compositional analysis of every group samples

sample	wt.% cubic	wt.% tetragonal	wt.% tetragonal	ce- mol% in c	mol% Y ₂ O ₃ in t	mol% Y ₂ O ₃	Grain size(nm)
Control*	25.9	52.3	0		2.32		
CS-3Y-1490	26.4	73.6	0	6.17	2.39		628
CS-8Y-1490	26.2	73.8	0	6.36	2.42		625
CS-12Ce-1490	33.5	66.5	0				1083
CS-12Ce-1550	33.1	65.2	1.7				1997

* in the Control sample, polishing procedure led to the apparition of shoulders on the left of diffraction peaks of the tetragonal phase, attributed to a “distorted tetragonal phase” accounting for 21.7 wt.% of the analyzed material, and that prevented analyzing the Y content in cubic phase.

4.4.2 Mechanical properties

The crack propagation threshold and Vickers hardness of each group of sample are shown in Fig.4-4. Vickers hardness are around 13.0 GPa, with no significant difference between samples. Moreover, crack propagation threshold (K_{I0}) fluctuates between 3.25 and 3.75 MPa.m^{1/2}. Even though the higher crack propagation threshold is obtained for the control sample, these surface treatments allow retaining good mechanical properties.

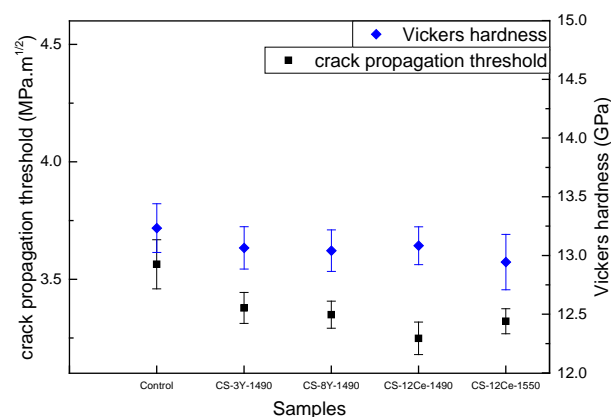


Fig.4-4 Crack propagation threshold and Vickers hardness

4.4.3 Analysis of ageing kinetics

The surface t-m phase transformation curves as a function of the hydrothermal ageing time are shown in Fig.4-5. The related parameters of ageing kinetics are summarized in the table 4-3. The thermal activation energies Q of CS-3Y-1490, CS-8Y-1490 and CS-12Ce-1490 are identical. However, CS-12Ce-1550 shows a strong resistance to ageing at 134°C, but ages faster than all other materials at 90°C, thus exhibits a lower activation energy.

Fig.4-6 shows the hydrothermal ageing kinetics at 90°C, 134°C for CS-3Y-1490 and CS-12Ce-1550 samples. And the resistance to ageing of CS-12Ce-1550 samples weakened at 90 °C compared to 134°C.

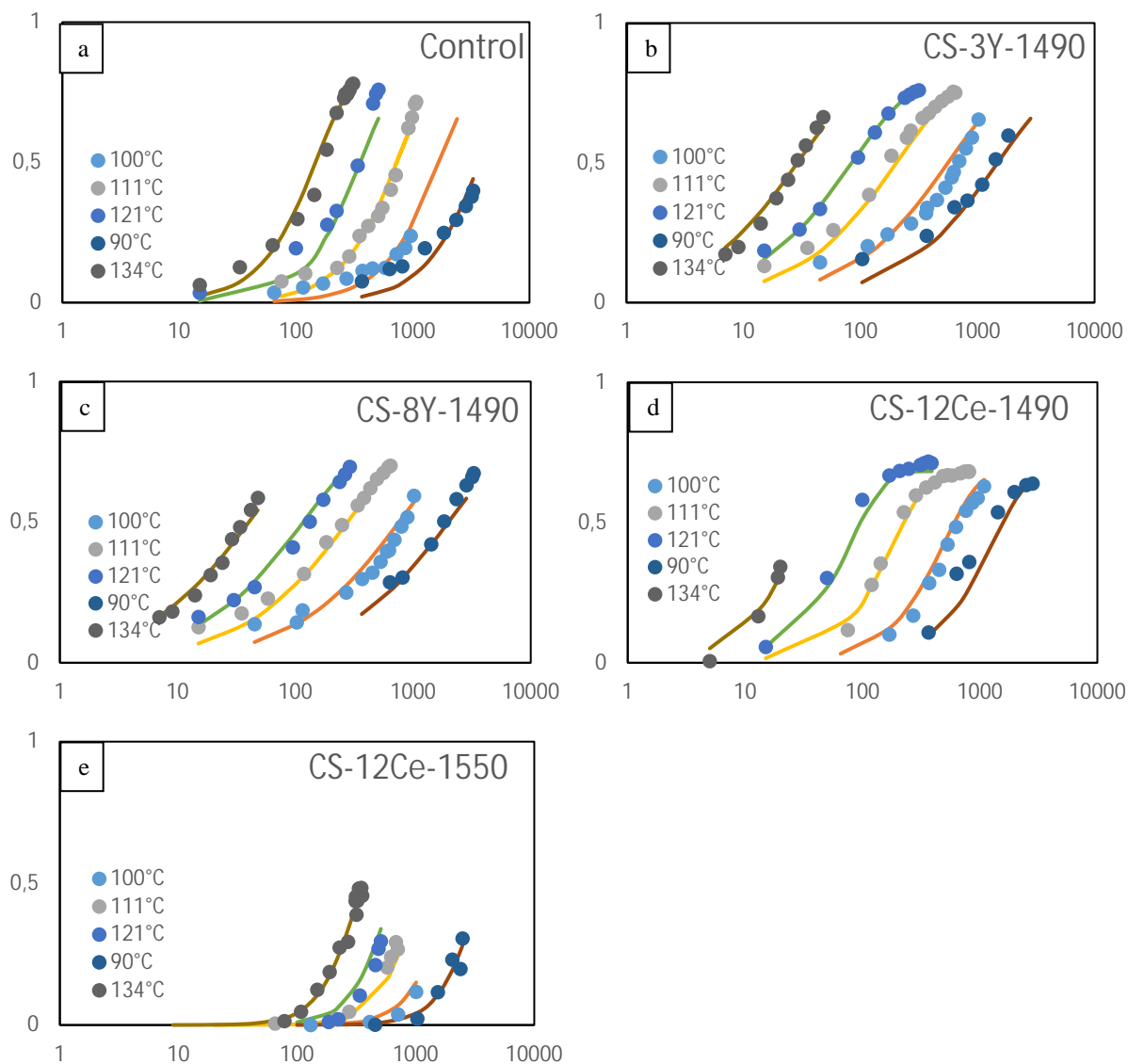


Fig.4-5 Hydrothermal ageing kinetics between 80 and 140°C for samples: a. control, b. CS-3Y-1490, c. CS-8Y-1490, d. CS-12Ce-1490, e. CS-12Ce-1550

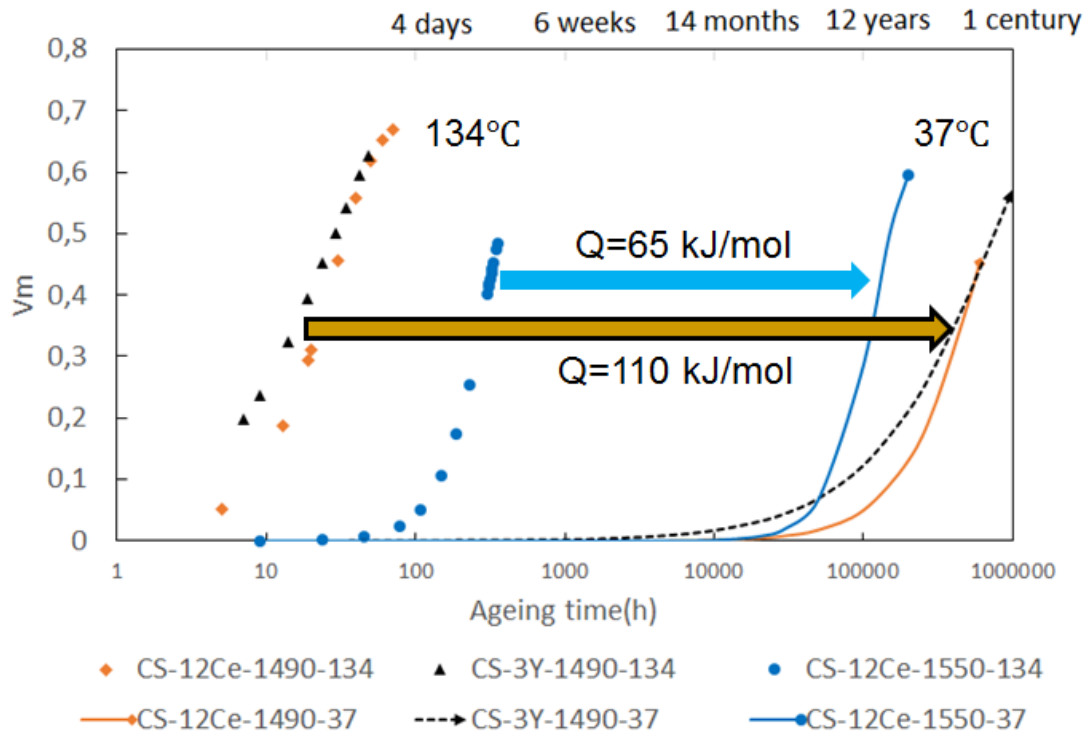


Fig. 4-6 Hydrothermal ageing kinetics at 90°C,134°C for CS-3Y-1490 and CS-12Ce-1550 samples

Table 4-3 Summary of the related ageing parameters

	V_{max}	n	b_0 (h^{-1})	Q (kJ/mol)
Control	0.8	1.55	$2.7 \cdot 10^9$	90.4
CS-3Y-1490	0.8	0.88	$4.43 \cdot 10^{12}$	110
CS-8Y-1490	0.8	0.82	$2.33 \cdot 10^{12}$	109
CS-12Ce-1490	0.68	1.48	$2.07 \cdot 10^{12}$	107
CS-12Ce-1550	0.62	2.42	$7.63 \cdot 10^5$	65.1

4.5 Discussions

4.5.1 The relationship between microstructure and doping with ceria and yttria

This work focuses on the change of the microstructure of zirconia samples placed on powders with different doping elements in post-sintering process. The results show that the grains on zirconia surface treated with CeZ12 powder are growing more during the post-sintering treatment than the one treated with Y-TZP powders, even though some large grains may appear in a small-grained matrix when treating with Y-stabilized zirconia. This is related to the segregation of yttrium at grain boundaries and the solute drag mechanism of dense zirconia grain growth at elevated temperature ($>1200^\circ\text{C}$), which is highest for Y-TZP, and absent for Ce-TZP and moderate for Y, Ce-TZP [14-17]. The results also show that more cubic phase appears on CS-12Ce samples. In the absence of external source of yttrium, the content of Y_2O_3 in the tetragonal phase should be reduced with the increase of the cubic phase content, accompanied by a large amount of yttrium into the cubic phase [18], in accordance with $\text{ZrO}_2\text{-Y}_2\text{O}_3$ phase diagram. However here the TZ8Y powder is an external Y source, thus a significant increase in Y content of both tetragonal and cubic phases take place in CS-8Y-1490 sample.

4.5.2 Influence on ageing kinetic

As the ageing process of Ce-TZP at 134°C is very slow, thermal activation energy of Ce-TZP and Ce-Y-TZP are seldom, if ever, reported. Our results show that the thermal activation energy for ageing of Y-Ce-tetragonal zirconia can be lower than the one of Y-TZP: CS-12Ce-1550 has an activation energy as low as $\sim 65 \text{ kJ}\cdot\text{mol}^{-1}$ while all other materials are around $100 \text{ kJ}\cdot\text{mol}^{-1}$. As a result, Y-Ce-tetragonal phase (in CS-12Ce-1550) exhibits a strong resistance to ageing at 134°C, similarly to what was observed by Marro et al. [19], but this rule may not be applicable at 37°C. For CS-12Ce-1490 samples, the thermal activation energy is not reduced, perhaps because the surface has a very small amount of cerium. Relevant reports pointed out that the yttrium content of the grain boundaries in Y,Ce-TZP is independent of temperature and ceria-concentration[14]. So the reason may be that Ce elements participation in the grain growth process led to the formation of more cubic phase[20], which in turn led to the decrease of yttrium in the tetragonal phase, so that the thermal activation energy can be reduced. In addition, the hydrothermal ageing process is a nucleation and growth process[10], which has a very close relationship with annihilation of oxygen vacancies[21-24], and doping cerium ions can reduce the number of oxygen vacancies. Schubert and Frey [25] found that the penetration depth of water radicals during the ageing process is larger than the size of nucleus for martensitic transformations. The penetration of water radical leads to a lattice contraction, which leads to stress generation, and the stress accumulation is large enough to cause nucleation. For CS-12Ce-1550 samples, Ce ions penetrate into the zirconia lattice. Since the amount of yttria is not changed, this does not result in a significant reduction in the number of oxygen vacancies on the sample surface. The delayed ageing at 134 °C may thus be explained by a combination of the stabilizing effects of Y and Ce, and a globally higher stability of tetragonal phase.

4.5.3 The ageing resistance feasibility of this post-sintering treatment (the surface treatment method of the formation of zirconia containing cerium on the surface of Y-TZP)

In this work, the TSS-12Ce-1430 sample showed the best ageing resistance at 134 °C. Therefore, we have been tracking the ageing behaviour of its surface for longer times. After 2800h at 134°C, very obvious cracks appear on the edges and surfaces of the sample (Fig.4-7). At this time, the surface monoclinic content is about 55%. The emergence of many large cracks in the edge could be due to the uneven composition (since only one side was treated) or to the fact that the t-m transformation may occur below the surface, similarly to what occurred in air in some nitride zirconia[26]: indeed, introducing Ce on the surface may put the surface under compression, thus the sub-surface under tension which may increase the sensitivity to t-m transformation of the sub-surface.

Here it is known that it is very important to ensure the uniformity of the surface composition of the sample during post-sintering process. Our results show that the thermal activation energy of Y-Ce-tetragonal can be lower than Y-TZP, therefore whether it has excellent resistance to ageing at 37 °C is still unknown for us.

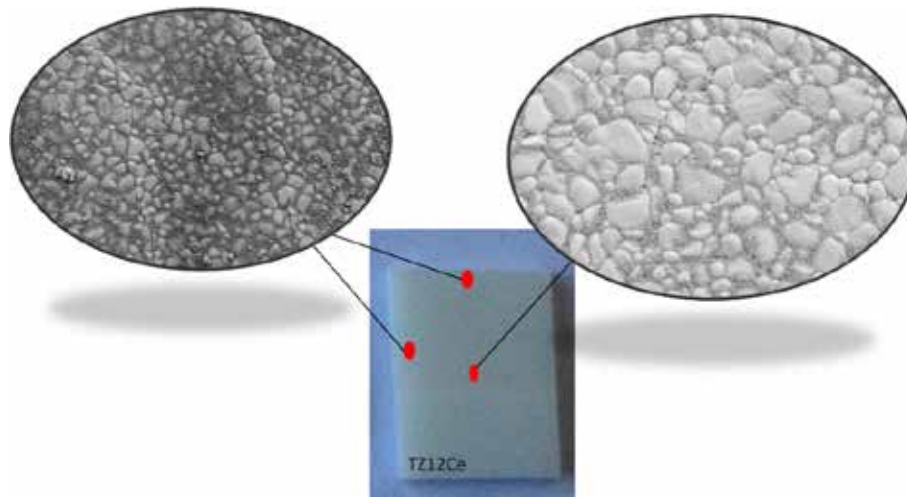


Fig. 4-7. SEM micrographs of TSS-12Ce-1430 sample after ageing at 134°C for 2800h

4.6 Conclusions and future work

This chapter introduced a method to delay ageing: doping the surface of 3Y-TZP samples with cerium (the source of cerium being 12Ce-TZP powder). It shows that ageing at 134°C can be delayed by this treatment, while hardness and crack propagation threshold are mostly preserved. However, the activation energy of ageing is decreased, and that impacts negatively the resistance to ageing at lower temperature. Thus it is very important to qualify ageing not only at 134°C, but also at other temperatures so that the ageing behaviour can be extrapolated at use temperature.

As this chapter is a preliminary work, some data and explanations are still missing. In particular, the microstructures of the different samples should be more carefully studied (grain size profile, diffusion profiles of Ce and Y...). The hypothesis according which TSS-12Ce-1430 could suffer from sub-surface ageing should also be verified (FIB cross-sections could be of help here).

References

- [1] J. Chevalier, J. Loh, L. Gremillard, S. Meille, E. Adolfson, Low-temperature degradation in zirconia with a porous surface, *Acta Biomaterialia* 7(7) (2011) 2986-2993.
- [2] C. Oblak, I. Verdenik, M.V. Swain, T. Kosmac, Survival-rate analysis of surface treated dental zirconia (Y-TZP) ceramics, *Journal of Materials Science: Materials in Medicine* 25(10) (2014) 2255-2264.
- [3] S. Deville, J. Chevalier, L. Gremillard, Influence of surface finish and residual stresses on the ageing sensitivity of biomedical grade zirconia, *Biomaterials* 27(10) (2006) 2186-2192.
- [4] M. Inokoshi, K. Vanmeensel, F. Zhang, J. De Munck, G. Eliades, S. Minakuchi, I. Naert, B. Van Meerbeek, J. Vleugels, Aging resistance of surface-treated dental zirconia, *Dental Materials* 31(2) (2015) 182-194.
- [5] E. Camposilvan, F.G. Marro, A. Mestra, M. Anglada, Enhanced reliability of yttria-stabilized zirconia for dental applications, *Acta Biomaterialia* 17 (2015) 36-46.
- [6] F. Lange, D. Marshall, J. Porter, Controlling Microstructures Through Phase Partitioning from Metastable Precursors The ZrO₂-Y₂O₃ System, *Ultrastructure processing of advanced ceramics* (1988) 519-532.
- [7] H.G. Scott, Phase relationships in the zirconia-yttria system, *Journal of Materials Science* 10(9) (1975) 1527-1535.
- [8] T. Stoto, M. Nauer, C. Carry, Influence of Residual Impurities on Phase Partitioning and Grain Growth Processes of Y-TZP Materials, *Journal of the American Ceramic Society* 74(10) (1991) 2615-2621.
- [9] G. Anstis, P. Chantikul, B.R. Lawn, D. Marshall, A critical evaluation of indentation techniques for measuring fracture toughness: I, direct crack measurements, *Journal of the American Ceramic Society* 64(9) (1981) 533-538.
- [10] J. Chevalier, B. Cales, J.M. Drouin, Low-Temperature Aging of Y-TZP Ceramics, *Journal of the American Ceramic Society* 82(8) (1999) 2150-2154.
- [11] L. Gremillard, J. Chevalier, T. Epicier, S. Deville, G. Fantozzi, Modeling the aging kinetics of zirconia ceramics, *J. Eur. Ceram. Soc.* 24(13) (2004) 3483-3489.
- [12] H. Toraya, M. Yoshimura, S. Somiya, Calibration Curve for Quantitative Analysis of the Monoclinic Tetragonal ZrO₂ System by X-Ray Diffraction, *Journal of the American Ceramic Society* 67(6) (1984).
- [13] R.C. Garvie, P.S. Nicholson, Phase analysis in zirconia systems, *Journal of the American Ceramic Society* 55(6) (1972) 303-305.
- [14] M.M.R. Boutz, A.J.A. Winnubst, A.J. Burggraaf, Yttria-ceria stabilized tetragonal zirconia polycrystals: Sintering, grain growth and grain boundary segregation, *Journal of the European Ceramic Society* 13(2) (1994) 89-102.
- [15] G.S.A.M. Theunissen, A.J.A. Winnubst, A.J. Burggraaf, Effect of dopants on the sintering behaviour and stability of tetragonal zirconia ceramics, *Journal of the European Ceramic Society* 9(4) (1992) 251-263.
- [16] G.S.A.M. Theunissen, A.J.A. Winnubst, A.J. Burggraaf, Surface and grain boundary analysis of doped zirconia ceramics studied by AES and XPS, *Journal of Materials Science* 27(18) (1992) 5057-5066.
- [17] S.-L. Hwang, I.W. Chen, Grain Size Control of Tetragonal Zirconia Polycrystals Using the Space Charge Concept, *Journal of the American Ceramic Society* 73(11) (1990) 3269-3277.
- [18] J. Chevalier, S. Deville, E. Münch, R. Jullian, F. Lair, Critical effect of cubic phase on aging in 3mol% yttria-stabilized zirconia ceramics for hip replacement prosthesis, *Biomaterials* 25(24) (2004) 5539-5545.
- [19] F. Marro, J. Valle, A. Mestra, M. Anglada, Surface modification of 3Y-TZP with cerium oxide, *Journal of the European Ceramic Society* 31(3) (2011) 331-338.
- [20] S.G. Huang, J. Vleugels, L. Li, O. Van der Biest, P.L. Wang, Composition design and mechanical properties of mixed (Ce,Y)-TZP ceramics obtained from coated starting powders, *Journal of the European Ceramic Society* 25(13) (2005) 3109-3115.
- [21] X. Guo, Hydrothermal degradation mechanism of tetragonal zirconia, *Journal of materials science* 36(15) (2001) 3737-3744.
- [22] X. Guo, Property Degradation of Tetragonal Zirconia Induced by Low-Temperature Defect Reaction with Water Molecules, *Chemistry of Materials* 16(21) (2004) 3988-3994.
- [23] G. Pezzotti, M.C. Munisso, A.A. Porporati, K. Lessnau, On the role of oxygen vacancies and lattice strain in the tetragonal to monoclinic transformation in alumina/zirconia composites and improved environmental stability, *Biomaterials* 31(27) (2010) 6901-6908.
- [24] F. Zhang, M. Batuk, J. Hadermann, G. Manfredi, A. Mariën, K. Vanmeensel, M. Inokoshi, B. Van Meerbeek, I. Naert, J. Vleugels, Effect of cation dopant radius on the hydrothermal stability of tetragonal zirconia: Grain boundary segregation and oxygen vacancy annihilation, *Acta Materialia* 106 (2016) 48-58.
- [25] H. Schubert, F. Frey, Stability of Y-TZP during hydrothermal treatment: neutron experiments and stability considerations, *Journal of the European Ceramic Society* 25(9) (2005) 1597-1602.
- [26] A. Feder, J. Alcalá, L. Llanes, M. Anglada, Microstructure, mechanical properties and stability of nitrided Y-TZP, *Journal of the European Ceramic Society* 23(15) (2003) 2955-2962.

General Conclusions

The object of this thesis is to study the influence of stress and structural parameters on the hydrothermal ageing of zirconia-based ceramics.

1. Residual stresses reaching the GPa as an order of magnitude triggers lattice distortion to form a small amount of distorted tetragonal phase easily converted into monoclinic phase, which in turn accelerates the aging process of 3YS and 4YS samples. The effect of applied stresses (both tensile and compressive) due to less than transformation-generated stresses slightly accelerates the aging process. In ZTA composites, the tensile internal stress of zirconia particles increases linearly with the increase of the content of alumina. At the same time, the monoclinic phase content after ageing is closely linked with the average tensile internal stress and alumina content.
2. A phenomenological model can approximate rather precisely the ageing behavior of 3Y-TZP materials (via the parameters n , Q , V_{\max} , V_0 and b_0 of the MAJ law describing ageing kinetics), based on their microstructure in chapter 3. From the model, it was deduced that V_{\max} has a strong linear relationship with both the content of cubic phase and the grain size. b_0 is closely linked with yttria content in the tetragonal phase and grain size.

Finally, a simple method to delay ageing is introduced: doping the surface of 3Y-TZP samples with cerium (the source of cerium being 12Ce-TZP powder), while hardness and crack propagation threshold are mostly preserved. However, the delay may only be at 134°C, not at 37 °C. Therefore, it is very important to qualify ageing not only at 134°C, but also at other temperatures so that the ageing behaviour can be extrapolated at use temperature.

Appendix:

**A fast, stepwise
procedure to
extrapolate
hydrothermal ageing
of zirconia-based
materials to low
temperatures**

Appendix A fast, stepwise procedure to extrapolate hydrothermal ageing of zirconia-based materials to low temperatures

Une procédure incrémentale rapide pour mesurer l'équivalence temps-température lors du vieillissement hydrothermal de matériaux à base de zircon.

This work was published in the Journal of the European Ceramic Society:

L. Gremillard, C. Wei, J. Chevalier, K. Hans, T. Oberbach, *A fast, stepwise procedure to assess time-temperature equivalence for hydrothermal ageing of zirconia-based materials*, Journal of the European Ceramic Society, 2018, 38 (1) pp. 181-86, <https://doi.org/10.1016/j.jeurceramsoc.2017.08.018>

Abstract

Hydrothermal ageing is one lifetime-limiting phenomenon of zirconia-based ceramics and composites for many applications, from biomedical implants to ferrules and watches. Predicting hydrothermal ageing at use-temperature implies a set of accelerated ageing experiments conducted under water vapour at several, high temperatures (usually between 100 °C and 140 °C). From these data, the activation energy of ageing can be determined, and thus ageing can be predicted at any temperature. However, obtaining precise extrapolations with this procedure requires the use of lower temperatures (70 or 80 °C), leading to a rather long procedure (up to a few thousand hours), and should involve at least one specimen for each test temperature. This article presents a new procedure that allows the determination of all ageing parameters and the estimation of kinetics at use-temperatures with the use of a single specimen within a shorter time, accurate enough for fast screening of new materials.

Résumé

Le vieillissement hydrothermal est un phénomène limitant la durée de vie des céramiques et composites à base de zircon utilisés dans de nombreuses applications (implants biomédicaux, férules, pièces de montre...). Prédire le vieillissement hydrothermal aux températures d'usage nécessite la mesure de cinétiques de vieillissement sous vapeur d'eau à plusieurs températures relativement hautes (typiquement entre 100 et 140°C). À partir de ces données, une énergie d'activation peut être calculée, et le vieillissement peut donc être calculé à n'importe quelle température (entre l'ambiante et 150°C). Mais pour obtenir des extrapolations précises il faut faire des mesures à des températures basses (typiquement 70 ou 80°C), ce qui mène à des procédures longues (plusieurs milliers d'heures en autoclave) et nécessite au moins un échantillon par température.

Ce chapitre présente une nouvelle procédure qui permet la détermination de tous les paramètres de vieillissement d'un matériau, et donc l'estimation des cinétiques de vieillissement aux températures d'usage, à partir de mesures à plusieurs températures sur un seul échantillon. Cette procédure est assez rapide et précise pour un criblage rapide ou une comparaison de nouveaux matériaux.

Introduction

Zirconia ceramics can exist in three crystallographic phases at atmospheric pressure: cubic, tetragonal and monoclinic. The phase transition temperatures depend on many parameters, among which one of the most important is the nature and amount of stabilising oxides present in the ceramics. 3Y-TZP (tetragonal zirconia polycrystal stabilized with 3 mol.% Y_2O_3) is the most used monolithic zirconia ceramic for biomedical applications, thanks to a combination of interesting properties: high toughness and strength (up to 6 MPa·m^{1/2} and 1200 MPa respectively), perfect biocompatibility, white colour and translucency. These good mechanical properties mainly come from Phase Transformation Toughening (PTT) that involves the tetragonal-to-

monoclinic (t-m) phase transformation around the tip of propagating cracks, the resulting volume increase acting to close the cracks and slow them, reinforcing the material[1]. However, the same t-m transformation can occur on surfaces in contact with water, and lead to roughening and microcracking[2]. This degradation phenomenon is called hydrothermal ageing (or Low Temperature Degradation) and is responsible for the decline of 3Y-TZP components in orthopaedics in the 2000s. To prevent it, several strategies exist. In particular alumina-toughened zirconia (ATZ) presents similar mechanical properties, while being less sensitive to ageing[3]. ZTA (standing for zirconia-toughened alumina) is also highly developed because of a higher resistance to ageing[4].

Ageing may occur at any temperature where tetragonal phase is metastable (for 3Y-TZP, anywhere below ~500 °C). Over a certain temperature range (for 3Y-TZP between room temperature and more than 150 °C) it is a thermally activated phenomenon, thus faster at high temperature and slower at low temperature. To assess ageing at room (or body) temperature, it is thus convenient to extrapolate it from experiments made at higher temperature (typically in water and in autoclave, between 80 and 150 °C). The typical procedure thus consists in measuring the evolution of monoclinic fraction with time of the surface of samples exposed to water (or steam) at different temperature, one sample being exposed to only one temperature until saturation of the monoclinic fraction. Then, from the ageing kinetics measured at (at least) two temperatures, an extrapolation to the temperature of interest can be conducted.

Any procedure to extrapolate ageing kinetics at low temperature is based on the fact that hydrothermal ageing is cumulative, and on two hypotheses:

- 1- Hydrothermal ageing is thermally activated in the temperature range used for the tests
- 2- The ageing exponent, n , is constant vs temperature

If these hypotheses are satisfied, the hydrothermal ageing kinetic can be expressed as the evolution of the monoclinic volume fraction (V) vs time by:

$$V(t, T) = 1 - \exp\left[-\frac{b(T) \cdot t^n}{b_0}\right] \quad \text{with} \quad b(t) = b_0 \exp\left[-\frac{Q}{RT}\right] \quad \text{eq. 1}$$

Thus the knowledge of the three ageing parameters b_0 , n and Q allows the calculation of $V(t, T)$ for any ageing time and temperature.

The usual method [5] requires the determination of $V(t, T)$ at different temperatures, and determines analytically b_0 , n and Q . Indeed, one can write equation 1 as:

$$\ln(1 - V(t, T)) = -\frac{b(T) \cdot t^n}{b_0} \quad \text{or} \quad \ln\left[\frac{1}{1 - V(t, T)}\right] = n \ln(b(T)) + n \ln(t) \quad \text{eq. 2}$$

Thus, after Eq. 2, for each temperature, plotting $\ln\left[\frac{1}{1 - V(t, T)}\right]$ vs $\ln(t)$ gives a straight line of slope n .

Then a common value of n is chosen for all temperatures (usually the average of the values obtained at each temperature), and for each temperature a value of $b(T)$ is determined after the intercept of

$\ln\left[\frac{1}{1 - V(t, T)}\right]$ vs $\ln(t)$ (this intercept is: $n \cdot \ln(b(T))$). Then plotting $\ln(b(T))$ vs $1/T$ gives again a straight

line of intercept $\ln(b_0)$ and of slope $-Q/R$. This is a well-established method that gives correct results, but suffers from a few limitations that make it not always easy to use. In particular, it was shown [6] that n may vary during a same kinetic. Thus the determination of n and b may depend on the person who makes the calculations.

Another, numerical, method starts from the same data ($V(t,T)$ at different temperatures), but minimizes the global error function e between the measured values and the ones predicted by eq. 1 by optimizing the parameters b_0 , n and Q .

$$e = \sum_i \frac{\sum_j \left(1 - \exp\left(-\frac{b_0}{t_j} \exp\left(-\frac{Q}{RT_j}\right)\right) \right)^n - f_{ij}}{n_j} \quad \text{Eq.3}$$

Equation 3 presents such an error function, in which each kinetic is given the same weight whatever the number of time points. In eq. 3, i relates to the number of temperatures tested and j to the number of time points for each temperature; f_{ij} are the measured monoclinic fraction at temperature T_i and time t_j . Many other error functions can be used, the other most frequent one being the one in which each experimental point is given the same weight. Optimization of b_0 , n and Q can be conducted numerically using a solver. This method presents the advantage to optimize all three parameters at once, and is less sensitive to measurement uncertainties. On the other hand, it must be considered with care since it will not directly reveal potential deviations from eq. 1, contrary to the analytical method.

We propose here a new, stepwise method to extrapolate ageing kinetics to room temperature. It is based on ageing measurements at different temperature on a single sample, and can largely reduce the time necessary for correct extrapolations. In its principle it is similar to Locati procedure for the determination of mechanical fatigue limit[7], in that that it calls on different levels of stress applied on a single sample (the “level of stress” being here a temperature) and on a “theoretical shape” of the physical quantity to characterize (fatigue limit follows a Wohler curve for Locati procedure, and here monoclinic content follows a Mehl Avrami Johnson law (Eq. 1) for hydrothermal ageing). There are of course some differences between the method we propose here and Locati procedure. The main difference is that fatigue tests only rely on one single measurement: the number of cycles to fracture; they don’t allow the evaluation of the damage parameter during the test. On the contrary, our procedure allows, and necessitates, the evaluation of the monoclinic fraction at every step of the test.

Materials and methods

Materials

Experiments were conducted on alumina-toughened zirconia balls (Ceramics®, Mathys Orthopaedie, Moersdorff, Germany) in their machined / polished state.

Ageing procedure

To assess the ageing procedure proposed here, hydrothermal ageing was conducted in autoclave (Wolf Sanoclav, Germany), in water vapour at different temperatures between 70 and 141°C, according to the schedules shown in Table 1. Schedules 1 and 2 are used to apply the stepwise procedure (thus each sample is submitted to the whole schedule), whereas the Usual schedule refers to one single temperature per sample until saturation of the monoclinic fraction.

The monoclinic fractions were determined using X-Ray Diffraction (D8-Advance, Bruker, Germany) at every time point of the same schedule. XRD diagrams were acquired between 26 and 33 deg. 2θ , exposing the (-111) and (111) monoclinic peaks, and (101) tetragonal peak. The volume monoclinic fraction (f_m) was deduced from these peaks intensities using Garvie and Nicholson’s equation[8] modified by Toraya[9]:

$$f_m = \frac{1.311X_m}{1 + 0.311X_m}, \text{ with } X_m = \frac{I_{-111}^m + I_{111}^m}{I_{-111}^m + I_{111}^m + I_{101}^t} \quad \text{Eq. 4}$$

All ageing schedules were performed on 3 samples. All measurements of the monoclinic fraction were performed on two locations (pole and equator) of each sample.

Table 1 : ageing kinetics schedules for the stepwise (SW) extrapolation procedure; Schedule SW1 and schedule SW2: all samples undergo the whole schedule; Usual schedule: three samples for each temperature.

Schedule 1 :		Schedule 2 :		Usual Schedule :	
SW1		SW2A, SW2S		UA, US	
T _i (°C)	D _{t_i} (h)	T _i (°C)	D _{t_i} (h)	T (°C)	Total time (h)
141	4	141	6	134	150
134	7	134	7	111	650
121	15	111	35	90	3200
111	40	75	500		
100	120	90	100		
85	400	85	200		
75	1000	100	150		
		121	80		
		134	20		
TOTAL	1586		1098		4000

Theory/ calculation

Extrapolation procedures

The usual extrapolation procedures are described in the introduction. Here they are referred to as UA (usual schedule, analytical determination of the ageing parameters using Eq. 2) and US (usual schedule, determination of the ageing parameters by global error minimisation using Eq. 3).

The stepwise procedure presented here does not rely anymore on complete kinetics measured at different, constant temperatures. Instead, a single piece of zirconia-based material is submitted successively to different ageing temperatures. The single ageing kinetics obtained this way allows the determination of all three ageing parameters.

The method is based on a set of three equations obtained from eq. 1, and on preliminary approach used to describe ageing at two alternating temperatures [10]. It is developed below.

Let's assume a completely tetragonal material before hydrothermal ageing ($V(0, T_0) = 0$ whatever T_0). Then a first accelerated ageing in autoclave is conducted at temperature T_1 during time D_{t_1} . The resulting monoclinic fraction is V_1 and could be calculated by Eq. 1. Then the temperature is changed to T_2 and the material is aged again for a duration D_{t_2} . The resulting monoclinic fraction is V_2 . One cannot represent the points (D_{t_1}, V_1) and $(D_{t_1} + D_{t_2}, V_2)$ on the same curve, since they were obtained at different temperatures. Instead, one can estimate the "virtual time" t_2 that would have been necessary to reach the monoclinic fraction V_1 at the ageing temperature T_2 . This time is given by:

$$t_2 = \frac{\sqrt[n]{-\ln(1 - V_1)}}{b_2}, \text{ with } b_2 = b_0 \exp\left(\frac{Q}{RT_2}\right) \quad \text{Eq. 5}$$

Then, V_2 could be calculated with equation 6:

$$V_2 = 1 - \exp\left[-\frac{Q}{RT_2} (b_2 (t_2 + Dt_2))^n\right] \quad \text{Eq. 6}$$

This leads to an iterative procedure, in which the state of the material after the i^{th} iteration (ageing at T_i during Dt_i) is described by the following set of equations:

$$V_i = 1 - \exp\left[-\frac{Q}{RT_i} (b_i (t_i + Dt_i))^n\right] \quad \text{Eq. 7(a)}$$

$$\text{with } t_i = \frac{\sqrt[n]{-\ln(1 - V_{i-1})}}{b_i} \quad \text{Eq. 7(b)}$$

$$\text{and } b_i = b_0 \exp\left[\frac{Q}{RT_i}\right] \quad \text{Eq. 7(c)}$$

Note that for a material that retains a non-zero monoclinic fraction after sintering (V_0) and whose monoclinic fraction saturates at a fraction V_M the set of equations 7 can be changed to the set of equations 8:

$$V_i = V_0 + (V_M - V_0) \left\{ 1 - \exp\left[-\frac{Q}{RT_i} (b_i (t_i + Dt_i))^n\right] \right\} \quad \text{Eq. 8(a)}$$

$$\text{with } t_i = \frac{1}{b_i} \sqrt[n]{\ln\left[\frac{V_M - V_0}{V_M - V_{i-1}}\right]} \quad \text{Eq. 8(b)}$$

$$\text{and } b_i = b_0 \exp\left[\frac{Q}{RT_i}\right] \quad \text{Eq. 8(c)}$$

The result of an ageing experiment following this procedure is thus a list of $[(T_i, Dt_i, V_i), i=1,2,\dots]$ (list in which all T_i are not necessarily different). From this list one can extract n , Q and b_0 (and V_0 and V_M if necessary) either using a solver or analytically.

Indeed, if one use twice the same temperature ($T_2 = T_1$) for the two first iterations ($t_1=0$), it follows that $b_2=b_1$, and the situation can be described by:

$$V_1 = 1 - \exp\left[-\frac{Q}{RT_1} (b_1 (Dt_1))^n\right] \quad \text{and} \quad V_2 = 1 - \exp\left[-\frac{Q}{RT_2} (b_1 (Dt_1 + Dt_2))^n\right] \quad \text{Eq. 9}$$

Which leads to the knowledge of n by:

$$n = \frac{\ln\left[\frac{1 - V_1}{1 - V_2}\right]}{\ln(Dt_1) - \ln(Dt_1 + Dt_2)} \quad \text{Eq. 10}$$

Moreover, incorporating a time increment Dt_i of 0 in equation 6(a) leads to:

$$V_i = V_{i-1} = 1 - \exp\left(-\frac{b_i}{t_i}\right)^n \quad \text{Eq. 11}$$

Combined with equation 7(a):

$$\frac{1 - V_{i-1}}{1 - V_i} = \frac{\exp\left(-\frac{b_i}{t_i}\right)^n}{\exp\left(-\frac{b_i}{(t_i + D_i)}\right)^n} = \exp\left(\frac{b_i}{t_i} - \frac{b_i}{(t_i + D_i)}\right)^n \quad \text{Eq. 12(a)}$$

$$\text{or } \ln\left(\frac{1 - V_{i-1}}{1 - V_i}\right) = n \left(\frac{b_i}{t_i} - \frac{b_i}{(t_i + D_i)} \right) \quad \text{Eq. 12(b)}$$

If D_i is small enough as compared to t_i , then V_i is very close to V_{i-1} , then a first order limited development of the exponential, a classical equivalent of the logarithm and a combination with equation 7(c) give:

$$\frac{1}{D_i} \ln\left(\frac{1 - V_{i-1}}{1 - V_i}\right) = n b_i \left(\frac{1}{t_i} - \frac{1}{t_i + D_i} \right) \approx n b_0 \exp\left(-\frac{Q}{RT_i}\right) \quad \text{Eq. 13(a)}$$

$$\ln\left(\frac{1}{D_i} \ln\left(\frac{1 - V_{i-1}}{1 - V_i}\right)\right) = \ln(n b_0) - \frac{Q}{RT_i} \quad \text{Eq. 13(b)}$$

Thus plotting $\ln\left(\frac{1}{D_i} \ln\left(\frac{1 - V_{i-1}}{1 - V_i}\right)\right)$ versus $\frac{1}{RT_i}$ between two close points (small D_i as compared to t_i) gives a straight line of slope $-Q$ and intercept $\ln(n b_0)$, thus b_0 can be calculated thanks to the previous knowledge of n .

Results

Fig. 1 shows the determination of n , b_0 and Q using the classical, analytical approach (three complete kinetics measured at 90, 111 and 134°C, analysed using eq.2). It confirms that n is almost independent on the temperature. Here a value of 0.94 was chosen for n (average of the three slopes reported on Fig. 1(a)). From these parameters (reported in Table 2 in the column ZTA-UA) one can calculate the ageing kinetics at the same temperatures and extrapolate at 37°C. The result is shown on Fig. 2(a). Using the same set of experimental points, one can minimize the error function described in eq. 3 to obtain directly another set of parameters (reported in Table 2 in the column ZTA-US). The kinetics calculated using this new set are reported in Fig. 2(b). In both cases, a good fit of all experimental data is obtained.

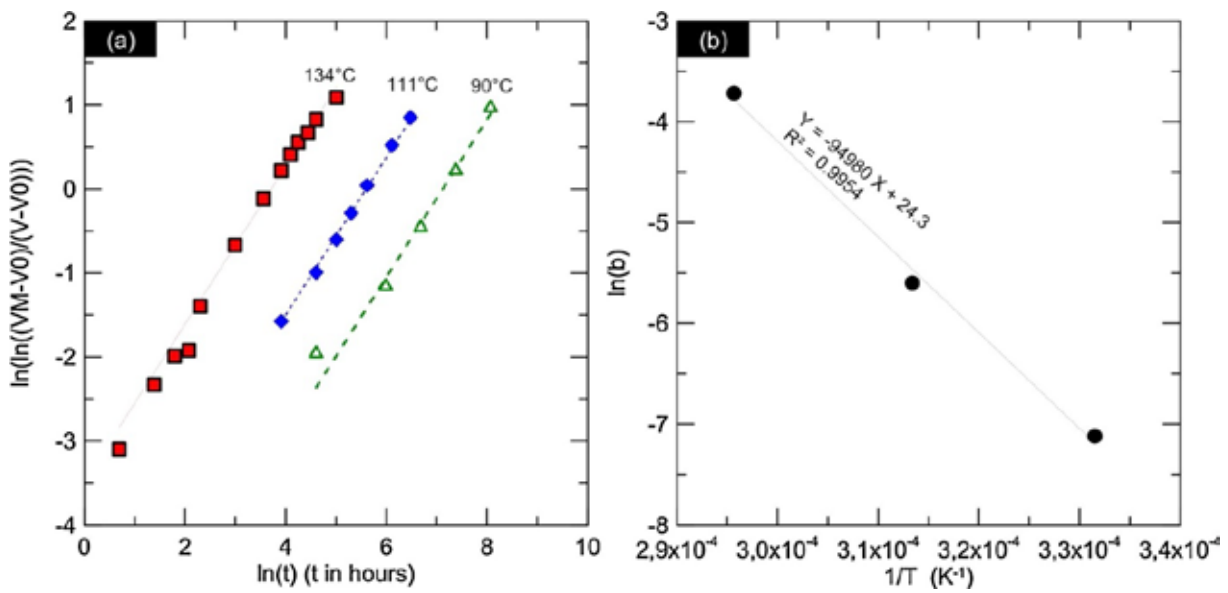


Fig. 1 : calculation of n , b_0 and Q according to the analytical procedure

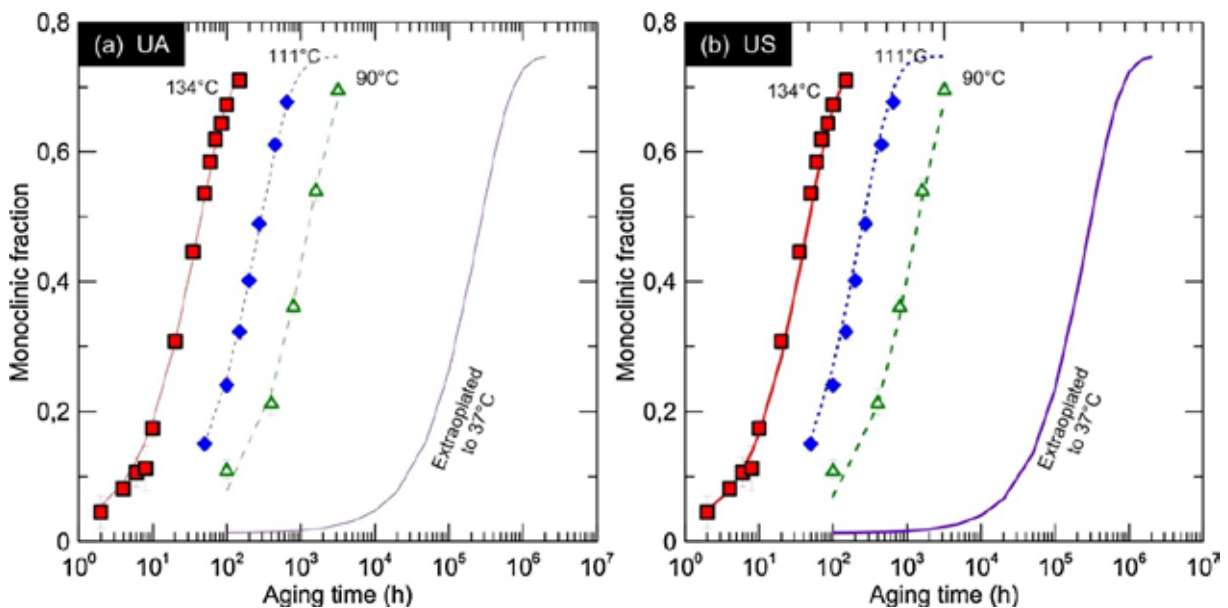


Fig. 2 : Ageing kinetics of ATZ using the classical procedure. Left: parameters derived from an analytical approach (UA); right: parameters derived from a global error minimization (US) Data For Article.xlsx, ATZ US and ATZ UA

Fig. 3 shows the results obtained from the schedule 1 of the stepwise procedure (see SW1 on Table 1). The calculation of the ageing kinetics parameters was conducted using a solver, and minimizing the difference between the experimental values of the monoclinic fraction and the calculated ones. A very good agreement is reached. However, since only one point was used for each temperature, an analytical determination of the ageing parameters was not possible. The values of n , b_0 and Q found for the best fit are reported in Table 2 (column SW1).

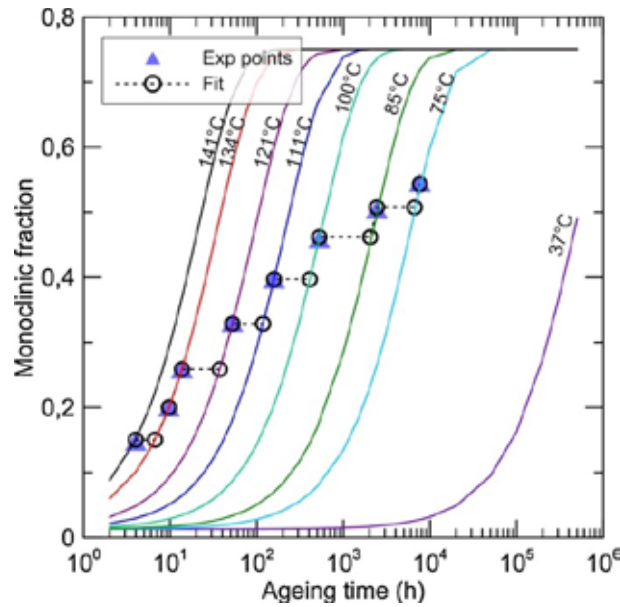


Fig. 3 Ageing kinetics of ATZ calculated after the SW1 procedure, using schedule 1

Schedule 2 (see Table 1, SW2) was devised so that the measurements at lower temperatures occur during the fastest increase of monoclinic fraction with ageing time (above 30% monoclinic fraction). This decreases again the total ageing time by a factor of almost 1.5 as compared to schedule 1. Moreover, an analytical determination of n , b_0 and Q was made possible by incorporating intermediate time points at several temperatures. The results are shown on Fig.4 and were exploited using two procedures.

In the first one, n was determined from the two first points at 141°C according to Eq. 10. Knowing n , it was

possible to plot $\ln \frac{1 - V_i}{1 - V_{i-1}} \ln \frac{1 - V_{i-1}}{1 - V_i} \frac{1}{RT_i}$ versus $\frac{1}{RT_i}$ at the different temperatures (Fig.4(b)) to determine the

activation energy (100 kJ/mol) and b_0 according to equation 13(b). However it can be seen that the agreement between measured and calculated monoclinic fractions is not that good. These results are reported in the column SW2A of Table 2.

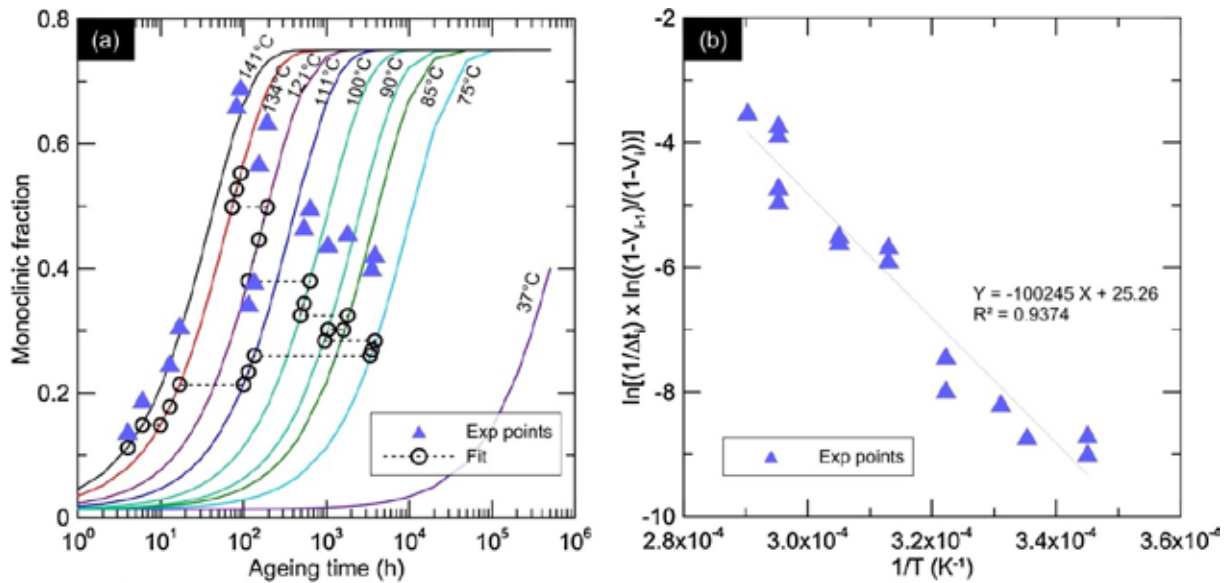


Fig.4 : Ageing kinetics calculated after the stepwise procedure (schedule 2, analytical)

Using the same dataset the second procedure called upon a numerical solver minimize the global error by adjusting b_0 , Q and n . The resulting kinetics are displayed on Fig. 5, and show a much better agreement between calculations and experiment. Once again the ageing kinetics parameters are reported in Table 2 (column SW2S).

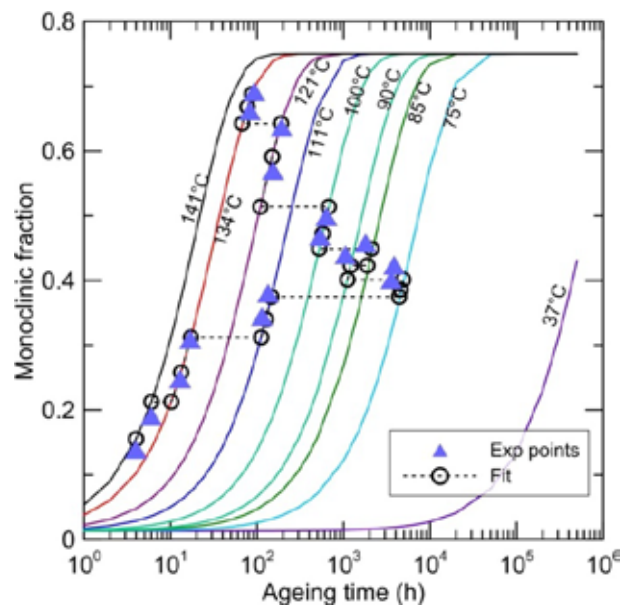


Fig. 5 : ageing kinetics calculated after the stepwise procedure, schedule 2

Table 2 : parameters for ageing of ATZ according to the different ageing procedures

	Analytical (UA)	Solver (US)	Step-wise Schedule 1 solver (SW1)	Step-wise Schedule 2 Analytical (SW2A)	Step-wise Schedule 2 solver (SW2S)
V₀	0.013	0.013	0.013	0.013	0.013
V_M	0.75	0.75	0.75	0.75	0.75
b₀ (h⁻¹)	3.6·10 ¹⁰	3.6·10 ¹⁰	4.5·10 ¹¹	1.1·10 ¹¹	1.1·10 ¹²
Q (kJmol⁻¹)	95.0	95.3	102.8	100.2	105.7
b at 37°C	3.5·10 ⁻⁶	3.1·10 ⁻⁶	2.1·10 ⁻⁶	1.4·10 ⁻⁶	1.7·10 ⁻⁶
n	0.94	0.98	0.95	0.84	0.96
Overall error	5.3·10 ⁻³	1.2·10 ⁻²	1.2·10 ⁻⁴	2.2·10 ⁻¹	2.8·10 ⁻³
Error / point	1.9·10 ⁻⁴	4.4·10 ⁻⁴	1.3·10 ⁻⁵	1.4·10 ⁻²	1.8·10 ⁻⁴
time in autoclave (h)	4000	4000	1586	1098	1098
Nb of XRD measurements	28	28	9	16	16

From the parameters reported on Table 2, it is possible to extrapolate all the measured kinetics at 134°C and at body temperature (37°C) (Fig.6). At 134°C, all (but one) extrapolated kinetics agree reasonably well with the measured kinetics. Only SW2A set of parameters results in an incorrect extrapolation that underestimate the ageing kinetics.

At 37°C no experimental determination of the ageing kinetics of ATZ is possible in a reasonable timeframe. Taking as a reference the extrapolation realized using the classical, analytical procedure (UA), it can be seen that all other extrapolations lie below although they are in the same order of magnitude. For example, at 200 000 hours (23 years) the calculated monoclinic fractions lie between 0.23 (SW2A) and 0.39 (US). Conversely the times necessary to reach 40% monoclinic fraction lie between 200 000 hours (23 years, UA) and 500 000 hours (57 years, SW2A). All other extrapolations lie between UA and SW2A.

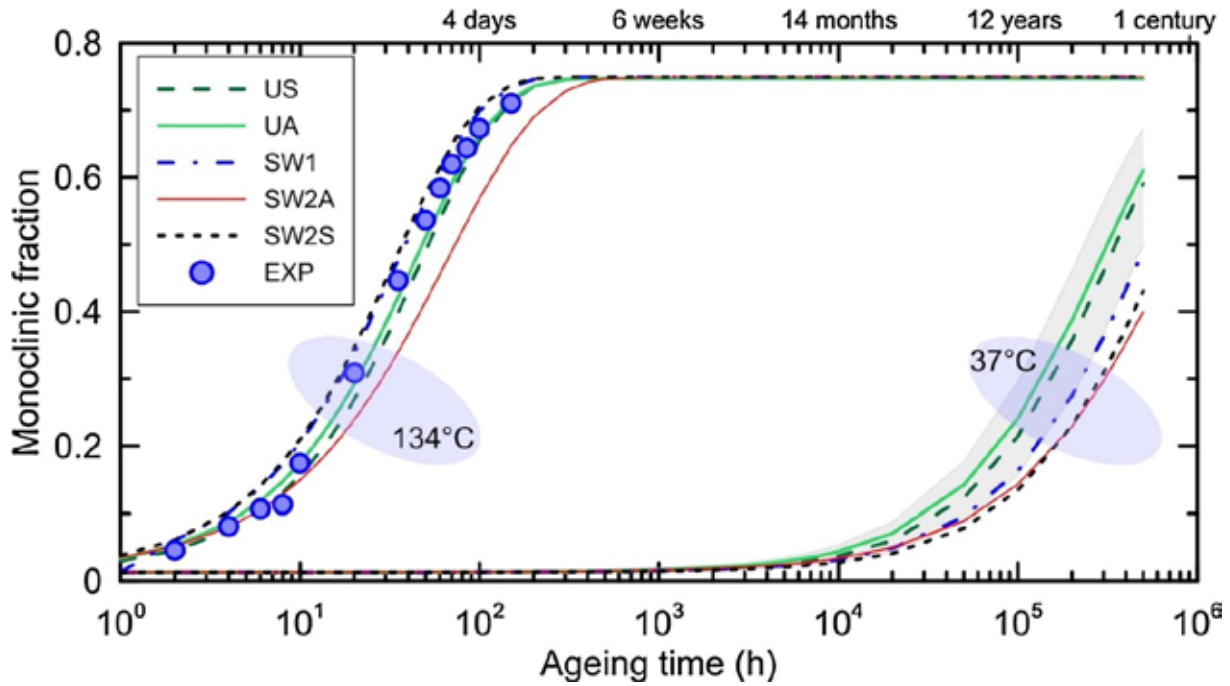


Fig.6 : calculations of the monoclinic fraction vs time at 134°C and at 37°C using the different ageing procedures.

Discussion:

The parameters shown in Table 2 reveal some interesting findings:

- First, all values of V_0 and V_M are identical (resp. 0.013 and 0.75) whatever the fitting procedure.
- Second, the values of n are also very close: from 0.94 to 0.98, with one exception (SW2A for which $n=0.84$).
- Third, there is more scattering in the values of the activation energy and of b_0 . However, when using b_0 and Q to calculate b at 37°C, all values of b are in the same range ($1.4 \cdot 10^{-6}$ (SW2A) to $3.5 \cdot 10^{-6}$ (UA)).

In fact, since n is the same for all extrapolation procedures (except SW2A), the parameter b (at 37°C) directly controls the speed of ageing at 37°C. This explains why the values of b (at 37°C) are ordered in the same way as the ageing kinetics extrapolated at the same temperature: $SW2A < SW2S < SW1 < US < UA$ (where the sign “<” indicates a smaller value of b and a slower kinetic). On Fig.6, the grey band indicates an interval of confidence calculated from the data of the classical procedure. Except for SW2A and SW2S, all extrapolation procedures lead to equivalent ageing kinetics at 37°C (all kinetics fall inside the interval of confidence).

This leads us to wonder why the two SW2 procedures are outside this band. SW2A proves to be the least precise. It is probably related to the way n is calculated (Eq. 10), taking into account only the two first experimental points. Moreover, ensuring that Dt_i is small enough as compared to t_i means that V_i and V_{i-1} are similar. Thus small, unavoidable errors on the measurement of V_i will cause large relative errors on $V_i - V_{i-1}$, thus a large imprecision on Q and $n \cdot b_0$ obtained by Eq. 13(b) if one tries this analytical approach. In conclusion the SW2A procedure should not be used alone; however it can prove useful to provide initial parameters for the global error minimization of SW2S.

The difference between SW2S and the other procedures (UA, US, SW1) may be attributed to the less important weight given in this procedure to the lowest temperatures: in SW2S (and SW2A) 15% of the total increase of the monoclinic fraction during ageing can be attributed to temperatures equal to or lower than 100°C. In SW1, this figure rises to 27%, and to 32% in UA and US. On the other hand, schedule 1 does not lead to saturation of the monoclinic fraction.

SW1 and SW2 procedures present several advantages over the classical ones:

- 1- They are faster: SW1 requires around 1600 h to test ageing at 7 different temperatures, covering here a 75 – 141°C temperature range; SW2 requires less than 1100 h to cover the same temperature range. UA and US necessitate 4000 hours to establish the full kinetics at 3 different temperatures (90, 111, 134°C); this time would go up to 12 000 h to measure whole kinetics at the same 7 temperatures. SW2 represents then a gain of time by a factor of 4 to 11.
- 2- They necessitate less XRD measurements (28 for UA and US, 9 for SW1, 16 for SW2)
- 3- They require much less samples: a single sample is enough for SW1 and SW2, whereas UA and US necessitate at least one sample per temperature (here at least 3).

It is rather difficult to decide what extrapolation procedure gives the most precise results. One might decide on choosing the worst case. But it is doubtful that the worst case will always be given by the UA procedure.

In our opinion, the UA procedure may prove to be the most accurate, provided it's conducted at both low (down to 80 or 70°C) and high (up to 150°C) temperatures, which is not the case here. On the other hand, this procedure will be so long that it cannot be used to assess numerous new materials. In the framework of zirconia-based materials development, schedule SW1 may be a good option to compare relatively quickly between several materials. Of course, the schedules presented here are not the only ones possible, and further developments could be implemented in the case of completely unknown materials (for example, start with a few hours at 134°C, and change the ageing temperature after each 10% increase of the monoclinic fraction).

Finally, it is worthy to point out that although the measurements of monoclinic fraction after each ageing step are mandatory, X-ray diffraction is not the only method available. The stepwise procedure presented here should give similar results when using Raman spectroscopy [11, 12] or any other 'evolution indicator' to measure the monoclinic fractions.

Conclusion

This work presents a stepwise procedure to determine the parameters of hydrothermal ageing of zirconia-containing ceramics. This procedure relies on ageing at different temperatures applied on a same sample. It is shown to be faster than usual ones (relying on a single temperature per sample) and less costly (necessitating less time, only one sample and fewer measurement of the monoclinic fraction). The extrapolation to 37 °C realised using both usual and stepwise procedures lie in the same order of magnitude. However, they are not exactly alike. It is suggested that the stepwise procedure should be used for fast screening of new materials, while a more precise extrapolation may be provided by the usual procedure extended to lower temperatures.

References

- [1] J. Chevalier, L. Gremillard, A.V. Virkar, D.R. Clarke, The Tetragonal-Monoclinic Transformation in Zirconia: Lessons Learned and Future Trends, *J. Am. Ceram. Soc.*, 92 (2009) 1901-1920.
- [2] J. Chevalier, L. Gremillard, S. Deville, Low-temperature degradation of Zirconia and implications for biomedical implants, *Annu. Rev. Mater. Res.*, 37 (2007) 1-32.
- [3] J. Schneider, S. Begand, R. Kriegel, C. Kaps, W. Glien, T. Oberbach, Low-Temperature Ageing Behavior of Alumina-Toughened Zirconia, *J. Am. Ceram. Soc.*, 91 (2008) 3613-3618.
- [4] J. Chevalier, S. Grandjean, M. Kuntz, G. Pezzotti, On the kinetics and impact of tetragonal to monoclinic transformation in an alumina/zirconia composite for arthroplasty applications, *Biomaterials*, 30 (2009) 5279-5282.
- [5] J. Chevalier, B. Cales, J.M. Drouin, Low-Temperature Ageing of Y-TZP Ceramics, *J. Am. Ceram. Soc.*, 82 (1999) 2150–2154.
- [6] L. Gremillard, J. Chevalier, T. Epicier, S. Deville, G. Fantozzi, Modeling the ageing kinetics of zirconia ceramics, *J. Eur. Ceram. Soc.*, 24 (2004) 3483-3489.
- [7] L. Locati, *La Metallurgia Italiana*, 47 (1955) 301-308.
- [8] R.C. Garvie, P.S. Nicholson, Phases analysis in zirconia systems, *J. Am. Ceram. Soc.*, 55 (1972) 303-305.
- [9] H. Toraya, M. Yoshimura, S. Somiya, Calibration curves for the quantitative analysis of the monoclinic-tetragonal ZrO₂ system by X-ray diffraction, *J. Am. Ceram. Soc.*, 67 (1984) C119-C121.
- [10] L. Gremillard, L. Martin, L. Zych, E. Crosnier, J. Chevalier, A. Charbouillot, P. Sainsot, J. Espinouse, J.L. Aurette, Combining ageing and wear to assess the durability of zirconia-based ceramic heads for total hip arthroplasty, *Acta Biomater.*, 9 (2013) 7545-7555.
- [11] D.R. Clarke, F. Adar, Measurement of the crystallographically transformed zone produced by fracture in ceramics containing tetragonal zirconia, *J. Am. Ceram. Soc.*, 65 (1982) 284–288.
- [12] G. Pezzotti, K. Yamada, S. Sakakura, R.P. Pitto, Raman Spectroscopic Analysis of Advanced Ceramic Composite for Hip Prosthesis, *J. Am. Ceram. Soc.*, 91 (2008) 1199-1206.

FOLIO ADMINISTRATIF

THESE DE L'UNIVERSITE DE LYON OPEREE AU SEIN DE L'INSA LYON

NOM : WEI

20.10.2017

(avec précision du nom de jeune fille, le cas échéant)

DATE de SOUTENANCE :

Prénoms : CHONG

TITRE : Influence of stress and structural parameters on the hydrothermal aging of zirconia-based ceramics

NATURE : Doctorat

Numéro d'ordre : 2017LYSEI091

Ecole doctorale : Matériaux de Lyon

Spécialité : Matériaux

RESUME :

Cette thèse explore l'influence des contraintes et des paramètres structuraux sur la sensibilité au vieillissement de la céramique à base de zircon. Il traite d'abord de l'influence des contraintes externes (appliquées) et des contraintes internes (résiduelles). Des contraintes extérieures sont appliquées par des tests de flexion in situ, tandis que des contraintes internes sont obtenues en contrôlant la microstructure des composites d'alumine durcis à la zircon. Le comportement de vieillissement de différents matériaux (3Y-TZP, 4Y-TZP et ZTA) est étudié par diffraction des rayons X (XRD) et spectroscopie Micro-Raman. Le résultat principal est l'influence principale des contraintes résiduelles sur les contraintes appliquées, principalement dans les matériaux de zircon.

Il détruit alors l'effet de différents paramètres microstructuraux sur la cinétique du vieillissement. 3Y-TZP échantillons de même composition nominale mais différentes microstructures (caractérisées par leur taille de grain, la teneur en Y_2O_3 en phase tétragonale et la proportion de phase cubique) sont obtenues en utilisant différents procédés de frittage (frittage en deux étapes ou frittage normal pour différents temps et à différents moments Températures). En utilisant deux modèles semi-empiriques, on peut d'abord quantifier la relation entre la microstructure et les paramètres de traitement, puis la relation entre la cinétique du vieillissement et la microstructure.

Enfin, il qualifie différents traitements de surface pour améliorer la résistance au vieillissement de 3Y-TZP. Les échantillons 3Y-TZP sont recuits sur des poudres de différentes compositions (TZ3YE, TZ4YS, TZ12Ce) et leur comportement de vieillissement est comparé. Les résultats montrent qu'une amélioration significative de la résistance au vieillissement peut être atteinte à 134 °C, sans compromettre la ténacité, mais ce gain n'est pas toujours valable à température ambiante ou corporelle.

Étant donné que cette thèse traite de nombreux matériaux et des temps de vieillissement très long (jusqu'à plusieurs milliers d'heures), il était essentiel d'accélérer les tests de vieillissement et de réduire le nombre d'échantillons. Ainsi, nous avons mis en place une méthode rapide permettant d'accéder à l'énergie d'activation du vieillissement, avec une réduction de dix fois de la durée des études vieillissantes (présenté en annexe).

MOTS-CLÉS : zircon; vieillissement; alumine-zircon; taille de grain; phase tétragonale; phase cubique.

Laboratoire (s) de recherche : Matériaux, Ingénierie et Science (MATEIS)

Directeur de thèse: Laurent Gremillard (MATEIS, INSA Lyon)

Co-directrice de thèse:

Président de jury : Hanlin Liao

Composition du jury : Marc Anglada, Jérôme Chevalier, Elisabeth Djurado, Laurent Gremillard, Hanlin Liao, Jozef Vleugels.